Upgrading a Broad Area Illuminating Integrating Sphere and Solar Transmittance Measurement of a Sheer Blind

by

Victor Halder

A thesis
presented to the University of Waterloo
in fulfilment of the
thesis requirement for the degree of
Master of Applied Science
in
Mechanical Engineering

Waterloo, Ontario, Canada, 2007

I hereby declare that I am the sole author of this thesis. This is a true copy of the thesis, including any required final revisions, as accepted by my examiners.

I understand that my thesis may be made electronically available to the public.

Abstract

Shading devices are frequently used to control solar gain through windows. Solar optical properties are very important in the energy analysis of windows. Transmittance, absorptance and reflectance are required to quantify solar heat gain through complex fenestration systems, which consist of combinations of glazing and shading layers.

In this research the solar transmittance of a sheer blind was measured using a Broad Area Illuminating Integrating Sphere (BAI-IS). More specifically, the spectral directional-hemispherical transmittance was measured in the wavelength range of 0.4 μm to 2.0 μm.

A "sheer blind" consists of soft fabric vanes, similar to a venetian blind, suspended between two vertical layers of sheer fabric. This arrangement is popular because it is attractive and it has potential application for daylighting. The vertical sheer fabric reduces the solar intensity and diffuses incident radiation; generally reducing solar gain and producing soft, natural illumination. The fabric vanes control the amount of light entering the room.

Shading devices such as venetian blinds, sheer blinds and drapes have spatially non-uniform and light scattering surfaces. Hence, measurement error occurs if the solar optical properties are measured by traditional narrow-beam measurement techniques typically used in commercial spectrophotometers. To reduce this error, a BAI-IS is recommended.

The BAI-IS apparatus consists of a 20-inch diameter integrating sphere, sample mounting system, monochromator, radiant source, lock-in-amplifier, photo sensor, optical chopper and various auxiliary devices. In order to improve reliability of the measurement the BAI-IS has recently been upgraded by replacing most of the key control and measurement equipment.

The refurbishment of the BAI-IS apparatus was successful. The directional-hemispherical transmittance of a sheer blind from BAI-IS measurement was found to agree well with an analytical model.

Acknowledgments

I would like to thank my supervisor, Professor J. L. Wright, for his guidance, encouragement and patience throughout this research. It has been a rewarding learning experience for me to work with him. I would like to express my deepest gratitude and appreciation to him. I would also like to thank Professor Michael Collins for sharing his insight and experience on the experimental apparatus.

I am grateful to Andy Barber, James Merli and Al Hodgson as well as the employees of the engineering student and machine shop. Their technical assistance and constructive ideas were key inputs for the successful experimental study.

Special appreciation to my lab colleagues at the University of Waterloo for making the work enjoyable and interesting. I would like to express my recognition to Bart, Chris, Martin, Nathan, Neil, Omid, Sohel and Vivek for creating a friendly environment at the Solar Lab. I am specially thankful to Nathan for his guidance and academic discussion on the topic of the research. I am grateful to my office-mate, Veronique, for her encouragement and support everyday.

I dedicate this work to my parents, my wife, Sandra and daughter, Viola for their inspiration, patience and understanding at every stage of the research.

Finally, special acknowledgement to the Canadian Solar Building Research Network and Solar Thermal Research Laboratory at the University of Waterloo for the financial support and the opportunity to do the research.

Dedication

This is dedicated to the study of energy conservation and solar energy.

Contents

List of Figures

List of Tables

Nomenclature

Abbreviation

AC	Alternating current
BAI-IS	Broad area illuminating-integrating sphere
BTU	British thermal unit [1 BTU = 252 Calorie]
CaGBC	Canada Green Building Council
C.I.	Confidence interval
CIE	Commission Internationale de Eclairage
cm	Centimeter
DAQ	Data acquisition
DC	Direct current
ESR	External Sample Reflectance
GHG	Green house gas
HVAC	Heating, ventilation and air-conditioning
IEA	International Energy Annual
IFF	Inward flowing factor
ISR	Internal Sample Reflectance
LEED	Leadership in Energy and Environmental Design
M	Signal recorded with the sample over the inlet port
mm	Millimeter
N	Index of refraction
N	Number of samples
NIR	Near infra red
NZEH	Net Zero Energy Home
SAI	Small area illuminating
SHGC	Solar heat gain coefficient
S/N	Signal to noise ratio of the photo-detector
T	Slat thickness [mm]
UV	Ultra violet
V	Voltage reading from DAQ system
VIS	Visible

Symbols

100_λ	100 % baseline reading on Cary 5000 spectrophotometer
A	Area occupied by the fenestration system
A_1, A_2	Finite area on the integrating sphere
$A_{i\square}^f$	directional front absorptance of the i-th glazing layer in the fenestration system
A_{in}	Area of inlet port of integrating sphere
A_d	Active area of the photo-detector
$A_{measurement}$	Area of measuring port of integrating sphere
A_i	Fraction of the incident solar radiation absorbed at the
A_s	Integrating sphere area
A_{slit}	Exit slit area of the monochromator
B_i	Beam flux at the i-th layer
dA_1, dA_2	Infinitesimal area of integrating sphere.
D_i	Diffuse flux at the i-th layer
d	Integrating sphere diameter
$dF_{dA_1-dA_2}$	Exchange factor between area dA_1 and dA_2
d_λ	Linear dispersion $\left[\frac{\mu m}{mm}\right]$
f	Port fraction of integrating sphere
f	Focal length of a lens or mirror [mm]
G_s	Solar irradiance $\left[\frac{W}{m^2}\right]$
Hz	Frequency [Hertz]
$I_R(\lambda)$	Reference reading [Voltage]
$I_S(\lambda)$	Sample reading [Voltage]
N_i	Inward flowing fraction (IFF) at the i-th layer
q_{net}	Net energy flow through multi-layered fenestration system
R	Radius of integrating sphere
R_t	Thermal resistance of the fenestration system $\left[\frac{W}{m^2-K}\right]$
s	Slat separation, [mm]
S	Distance between area dA_1 and dA_2
S_S	Standard deviation
$SHGC(\theta, \phi)$	SHGC for multi-layer fenestration system.

Symbols (Continued)

T_{in}	Inside temperature [K]
T_{out}	Outside temperature [K]
T_H^f	hemispherical front transmittance of shading device
U	Thermal transmission, U-value
w	slat width, mm
$W_{slit-\text{minimum}}$	Minimum slit width of the monochromator
Z_λ	Zero baseline reading on Cary 5000 spectrophotometer

Greek Letters

β	Solar altitude angle [rad]
γ	Wall-solar azimuth angle [rad]
$\Delta\lambda_{\text{min}}$	Spectral resolution [μm]
ϕ	Slat angle [rad]
Φ	Radiation flux $\left[\frac{\text{Watt}}{m^2}\right]$
Φ_∞	Radiation flux at integrating sphere wall $\left[\frac{\text{Watt}}{m^2}\right]$
θ	Incidence angle [rad]
λ	Wavelength [μm]
μm	Micron
ρ	Reflectance [%]
τ	Transmittance [%]
$\tau(\lambda)$	Spectral transmittance [%]
Ω	Profile angle [rad]

Subscript

b	Effective back property of blind layer
b	Beam property
bb	Beam to beam property
bd	Beam to diffuse property
d	Diffuse property
dd	Diffuse to diffuse property
f	Effective front property of blind layer
R	Reference reading
S	Sample reading
solar	Effective property
t	Total property
λ	Spectral quantity

Chapter 1

Introduction

1.1 Scope

The solar transmittance and reflectance of glazing / shading materials are important optical properties to evaluate energy performance of a building envelope. The solar optical properties of thin, non-scattering samples are measured by commercial spectrophotometers. The measurement is taken by passing a beam of light through the sample and collecting the transmitted or reflected portion by a detector. To measure the optical properties of spatially non-uniform and scattering samples, however, the above-mentioned apparatus is not suitable, because (1) the smaller inlet port and the narrow beam are not broad enough to irradiate a representative sample area, and (2) outscattering loss will occur for thick and scattering samples.

The primary objective of this research is to refurbish a custom-designed spectrophotometer, which was built in 1994. Since a broad area beam and an integrating sphere are used, this custom-made spectrophotometer is called a broad area illuminating integrating sphere (BAI-IS) apparatus. The BAI-IS is capable of measuring solar transmittance and absorptance of thick, scattering samples, such as shading devices (venetian blind, sheer blind) and advanced glazing materials (honeycomb insulation, patterned glass). This instrument will then be used to measure the solar transmittance of a sheer blind in the wavelength range from 0.4 μm to 2.0 μm.

1.2 Background

According to an International Energy Annual (IEA) report, globally 6.2 billion human beings consumed about 132 trillion KWH (450 quadrillion BTU) of energy in 2001 (1 trillion = 10^{12} and 1 quadrillion = 10^{15}). The energy requirement of buildings represents approximately 33% of this total energy consumption which contributes roughly 100 million tons of greenhouse gas (GHG) emissions per year. In Canada buildings account for about 30% of total energy consumption, about 50% of total electricity consumption and roughly 28% of total GHG emissions. These energy flows and GHG emissions which are associated with heating, cooling, ventilation and lighting of buildings have the potential to be substantially reduced. This large amount of energy consumption lead to over-use of resources, climate change and depletion of natural resources and impact environment, economy, health and productivity.

To counterbalance this adverse situation, in recent years, designers, architects, builders, corporations and home owners are showing keen interest in adopting green or sustainable buildings. Currently, the rapid membership growth (approximately 10% per month) of the Canada Green Buildings Council (CaGBC) reflects the expansion of green buildings in the market. Green Building entails an integrated approach to building design and management, with emphasis on energy efficiency (Canada Green Building Council 2007 and U.S Green Building Council 2007). Some buildings currently are being designed as net-zero energy users. The net zero energy home (NZEH) can produce as much energy as it consumes over a year, by adopting an energy efficient building envelope integrated with renewable energy sources (NZEH Coalition 2005)

The primary intent to design, build and own a green building or NZEH is to maximize economic, environmental and social performance and attain superior indoor ambiance. With these goals, the Leadership in Energy and Environmental Design (LEED) has established a Green Building rating system that encourages and accelerates global adoption of sustainable building construction. LEED is developed through an open, consensus-based process by the U.S. Green Building Council and adapted for Canada by CaGBC. LEED is the benchmark for the

design, construction and operation of high performance green buildings. LEED promotes sustainability by recognizing performance in five key areas of human and environmental health: sustainable site planning and development, water savings, energy efficiency and atmosphere, materials and resource conservation and indoor environmental quality. According to the LEED rating system, on a total scale of 70 merit points, 17 points are allocated for the "Energy and Atmosphere" category, giving this category the highest priority (U.S Green Building Council 2008).

1.2.1 Thermal Insulation of the Building Envelope

For energy efficiency, a common strategy is to use more thermal insulation in the building envelope, which reduces envelope heat gain and loss. However, due to the presence of insulation, the building acts as furnace with the heat trapped inside - heat given off by occupants, internal lighting, appliances and solar gain. This heat increases cooling load and energy consumption. It is known that over half of the total energy required for building operation is used in space heating and cooling, which are directly impacted by the building envelope.

For heating dominated buildings, it is easy to fulfill the occupants' need if the building has a low level of insulation. The comfortable thermal condition is achieved by adding more heat to the building or reducing heat as required. As soon as the insulation level is increased the internal generation of heat becomes important. When heating is required this internal gain offsets the heat requirement to warm the space. However, when cooling is required the internal gain adds to the cooling load. Therefore, for a well insulated building, it is complicated to synchronize the heating and cooling in different parts of the building and at different times of the year.

1.2.2 Windows in Building Envelope

Windows are primarily incorporated in building envelopes to connect people physically and/or visually with the outdoors. A window has a strong effect on

human behavior, health and productivity. In the USA, as a general rule, the minimum window area is considered to be 20% of floor area for day-lighting consideration (ASHRAE 1989). Windows therefore comprise a large area of opening in the building structure.

Good window design provides control over daylighting, views to the exterior and ventilation. A good design minimizes traffic noise and solar heat gain when cooling is required and at the same time does not allow too much heat loss when heating is required.

In practical situations, the solar gain through windows represents the largest peak heat gain. Windows also account for as much as 25-30% of the heat loss in a building because window glazing is a poor insulator. Therefore, windows have a strong effect on the heating and cooling requirements, energy costs and the comfort level experienced by its occupants. Windows are, by far, the weakest link in a building envelope for heat gain in the summer time and heat loss in the winter time.

The solar gain through windows varies from one day to another throughout the year and also depends on building surroundings, location and orientation as shown in Figure 1.1. Solar gain also varies from day-to-day and even minute-to-minute.

Generally, during summer, the highest solar gain occurs on eastern and western exposure in the early morning and late afternoon respectively but the lowest solar gain occurs on northern exposure. On the southern exposure the solar gain is low at low latitude but maximum at high latitude at solar noon as shown in Figure 1.2. Therefore, the window design should also vary from one facade to another.

Due to hourly variation of solar radiation, intermittent cloud cover, random change in weather conditions and seasonal variation in solar elevation, solar gain represents the most 'dynamic' heat gain of the indoor space. Glazing strategies for cooling-load dominated buildings are different from the strategies that allow solar gains to offset winter heating requirements. The critical design issue is to control the variable solar gain to meet personal comfort and achieve energy efficiency. It is clearly beneficial to have a dynamic and adjustable barrier to block incoming radiation when cooling is required and allow solar gain when heating is required.

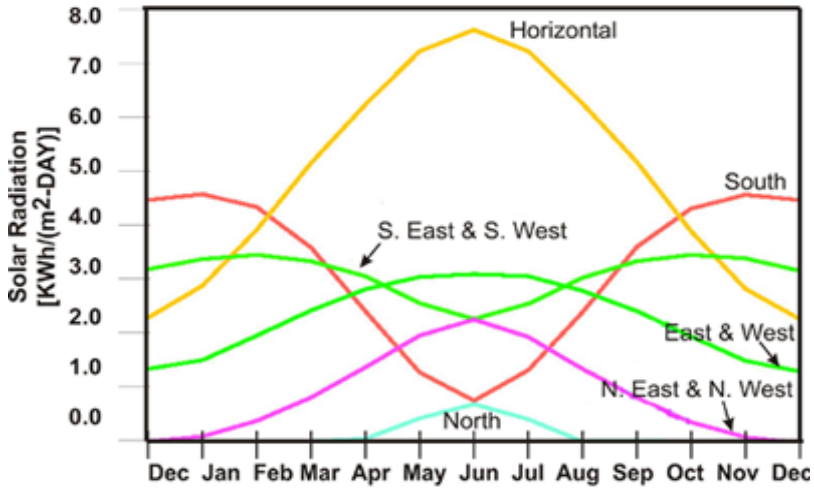

Figure 1.1: Average Monthly Solar Radiation in Various Directions (LEARN London Metropolitan University 2004)

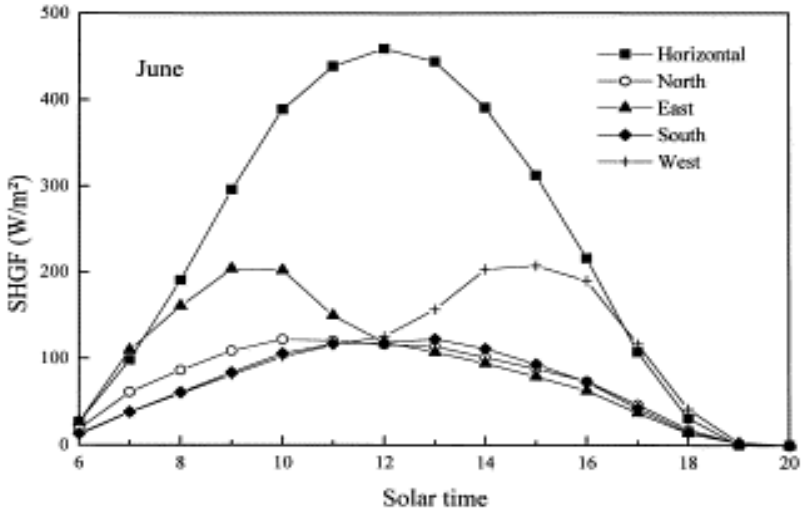

Figure 1.2: Average Solar Heat Gain Factor (SHGF) at 22.3 Deg. N Latitude (Li and Lam 2000)

The following options can be considered to achieve switchable glazing strategy.

Outdoor shading devices such as awnings and overhangs provide the most effective means of solar control because they prevent sunlight from striking the windows. The main disadvantage is that their design must account for daily and seasonal variation of the sun's path and they cannot be adjusted easily.

High-performance glazing systems can significantly reduce solar heat gain. For example, low-emissivity coated glazing with visible light transmissivity greater than 0.6 and solar transmissivity less than 0.4 can be used in commercial buildings where cooling load is critical. For residential buildings in a cold region, the glazing should admit solar radiation as well as visible light. Tinted or reflective glass can also be used to reduce solar heat gain.

To offset the variable nature of solar gain, smart switchable glazing can be used which changes the optical or thermal properties of windows to adjust solar gain at will. It is the chromogenic phenomenon of these glazing materials that changes their reflectivity and absorptivity.

Thermo-chromic glazing changes optical properties in response to temperature change. Electro-chromic glazing changes optical properties when an electric charge is applied. Low-voltage current drives ions between the layers, causing the window to change color. Photo-chromic materials change their properties in response to light (Elmahdy and Cornick 1990).

Currently, these smart switchable window technologies are primarily prototype products. They are very expensive and require high technological support for maintenance and operation. Moreover, their optical and thermal properties are not generally available. It is very difficult to estimate the dynamic performance of such devices with variable insolation.

1.2.3 Shading Devices

Solar gain through windows causes heat to enter buildings. In the summertime, to maintain human comfort, this additional heat is removed by a cooling system which requires additional investment and accounts for high electricity consumption

and greenhouse gas (GHG) emission. Installing a shading device is a simple and cost effective strategy to control solar gain through windows. Indoor shading devices are primarily used for privacy, solar gain control and retaining view. The most popular shading devices are venetian blinds, curtains and roller shades. The use of sheer blinds has also become popular in the design of daylighting systems.

Among all types of shading devices, indoor louvered blind such as venetian blinds and sheer blinds are effective and popular because of their flexibility in daylight control, peak cooling load reduction, privacy and easy operation. For louvered blinds, dynamic solar and day lighting control is achieved by changing the angle of the slats. Solar gain and light control can also be achieved by varying the width, thickness, curvature, color and type of slat material. So, the louvered blind acts as a switchable, mecha-chromic glazing layer. Moreover, these devices are inexpensive, easy to install and maintain and add architectural appeal.

A venetian blind consists of a set of opaque horizontal slats or vanes, usually of aluminium, connected with string in such a way that they can be rotated about the horizontal axis at different angles to allow light to pass between the slats or rotated to a closed position to block the light. The blind can also be retracted.

It is planned to measure the solar transmittance of sheer blind in this research. A sheer blind is a modified version of venetian blind. The sheer blind is made of soft fabric with a more complex geometry. A number of soft fabric vanes or slats are suspended between two layers of vertical sheer fabric facings as shown in Figure 1.3. The sheer fabric is usually made from white, knitted, translucent polyester and the vanes are made of heavier woven fabric. Sheer blinds are popular for daylighting because the transmitted sunlight is largely diffuse.

The sheer blind can easily control light and privacy with light filtering or room darkening fabrics. The blind layer filters light in daytime and offers privacy as required with the vanes closed. The sheer materials offer a muted view to the outdoors at the open position. At night light filtering vanes, in the closed position, reveal silhouettes of people and objects. The room darkening vanes, in the closed position, provide complete privacy at night. They also add a clean and contemporary look to the room and offer directional solar control by reducing passive solar gain and cooling load on a hot day.

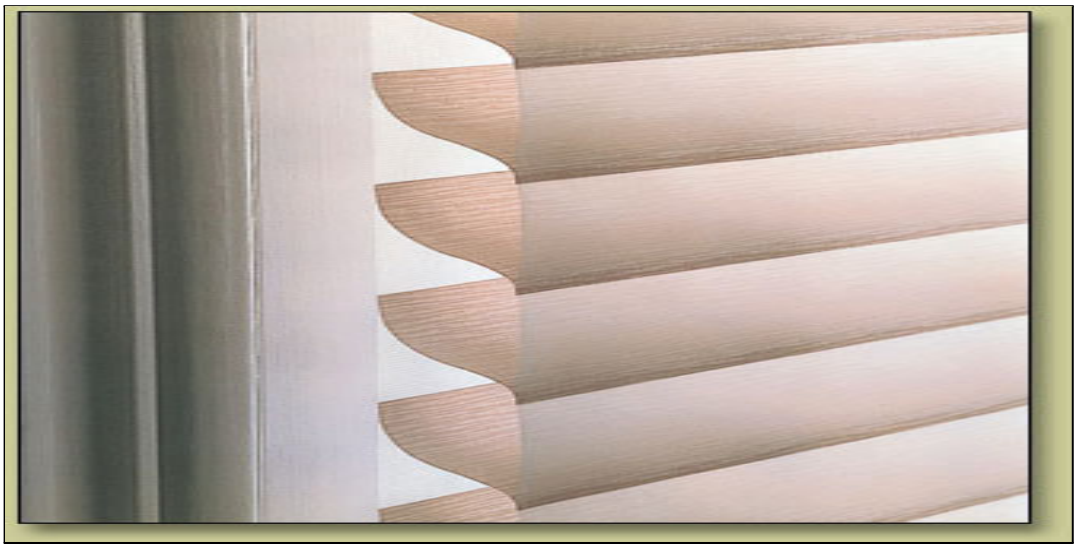

Figure 1.3: Sheer Blind

The vanes of a sheer blind can be rotated to different angles to allow sunlight inside the room and can also be retracted but can not be used to block the light completely since the fabric transmits light to some extent.

In the past, a lack of data, limited modeling capability and lack of confidence in solar gain control strategy for building envelopes, research of shading devices was largely neglected. With the recent technological advancement in transparent building envelopes and need for implementing energy efficient features, it is necessary to predict accurately the dynamic energy performance of building facades. This is why building energy simulation programs need improved models for shading devices. The building energy simulation will ensure proper control of shading devices to synchronize lighting, heating, ventilation and air-conditioning (HVAC) components. Energy consumption can be reduced by lowering peak and total cooling loads, while simultaneously maintaining comfort.

To estimate total energy impact in response to solar radiation, the optical characteristics of shading layers are required. The effective solar optical properties of louvered blinds are the function of geometry of the blind layer, the angular specification of incident and transmitted / reflected solar radiation and solar optical

properties of individual component of the blind assembly (e.g., slat and sheer material for sheer blind).

The louvered blinds are specified by blind geometry and angular parameters.

The geometry of a louvered blind is comprised of (1) slat angle, ϕ (2) slat width, w (3) slat spacing, s and (4) radius of curvature, r, as shown in Figure 1.4. When $\phi = 0$, the blind is fully open and $\phi = 90$, the blind is fully closed. The support strings prevent the slats from being closed beyond $\phi \simeq \pm 75^0$. Venetian blind slats often have curvature for strength. In this case it is also necessary to know the radius of curvature, r. Usually $r \simeq 2w$.

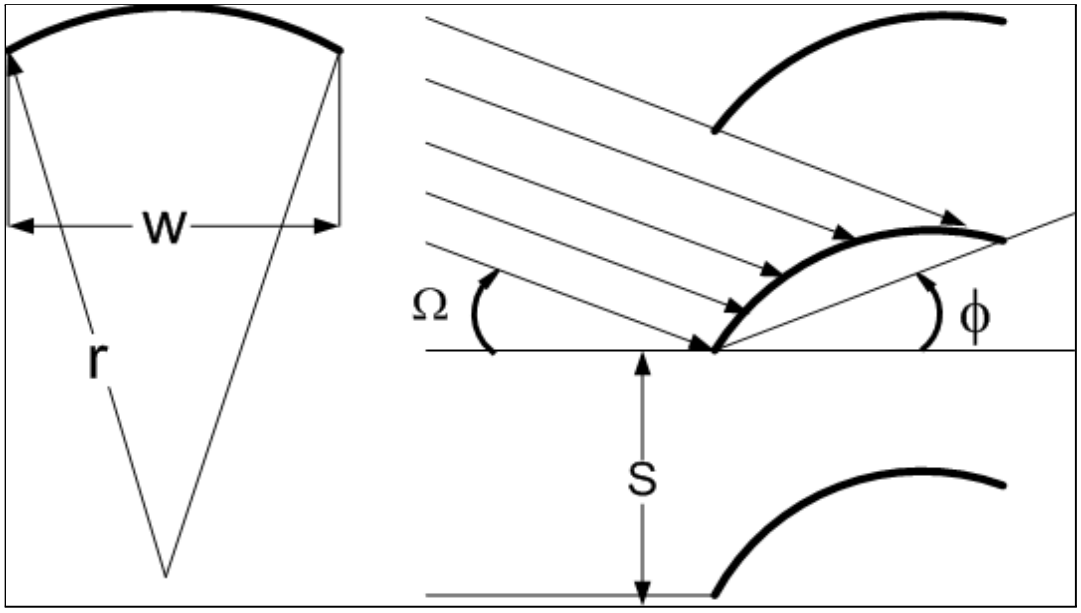

Figure 1.4: Radius of Curvature of a Slat (Kotey et al. 2007)

The angular direction of the incident solar radiation is specified as the projected solar altitude angle, Ω,as shown in Figure 1.5. This angle is also known as the profile angle which is defined as the angle between the normal to the blind assembly and the projection of the solar ray on a vertical plane normal to the same surface. The geometric parameters are summarized in Table 1.1.

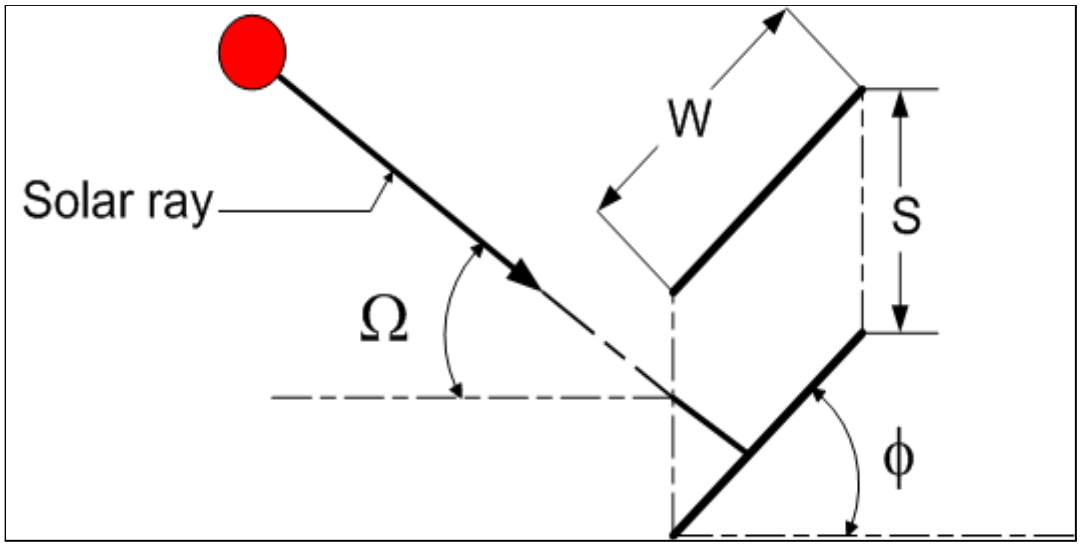

Figure 1.5: Blind Geometry and Solar Profile Angle, Ω

Table 1.1: Geometric Data

Symbol	Item description	Unit	Limit
w	Width of the slat	mm	$w > 0$
s	Distance between adjacent slats	mm	$s > 0$
ϕ	Slat tilt angle	Deg	$-90^0 \leq \phi \leq 90^0$
r	Radius of slat curvature	mm	$r > \frac{w}{2r}$

1.2.4 Need for Spectrophotometer

Effective optical properties of shading devices are obtained by averaging spectral measurements. The louvered blinds have non-planar, spatially non-uniform and light scattering surfaces. This is why, when a beam of light strikes the blind surface at a single incidence angle, the reflected and/or transmitted light gets scattered and diffused in numerous directions. Therefore, an integrating sphere spectrophotometer is used to obtain directional integration over the hemisphere of outgoing radiation. A spectrophotometer is an instrument that can determine the optical characteristics of the test specimen as a function of the wavelength.

The primary component of a spectrophotometer is an integrating sphere. An integrating sphere is a hollow sphere coated internally with near-perfectly diffusing material and has at least two ports; an inlet port and a measurement port. Integrating spheres function as light collectors. The basic principle of operation is that the transmitted or reflected radiation from the sample enters the integrating sphere, goes through multiple reflections on the diffusely coated interior surface where it is scattered uniformly. The spherical shape and the special coating spatially integrate the collected radiation and transform it into a uniform field of diffused radiant flux. The radiant flux available at the measurement port is proportional to the rate at which radiant energy enters the inlet port. Photo-detectors can then convert this flux to electrical signals for measurement as shown in Figure 1.6. This is a measure of the rate at which energy arrives at the inlet port - integrated both spatially and with respect to incident direction.

Selection of inlet port size entails a design trade-off. A larger inlet port lets more radiation inside the sphere, and ensures a stronger signal. A larger inlet port is also preferable because it can sample a broader area. However, some of the reflected light escapes through the inlet port. This reduces the signal strength and the precision of the measurement. To have optimum integration with sufficiently strong signal, the ratio of port area to the sphere area is kept as small as possible. For high accuracy measurements it is recommended to keep this ratio less than 0.05 (Labsphere Inc. 2005). The BAI-IS has less than 1 % port area with respect to the total reflecting surface area.

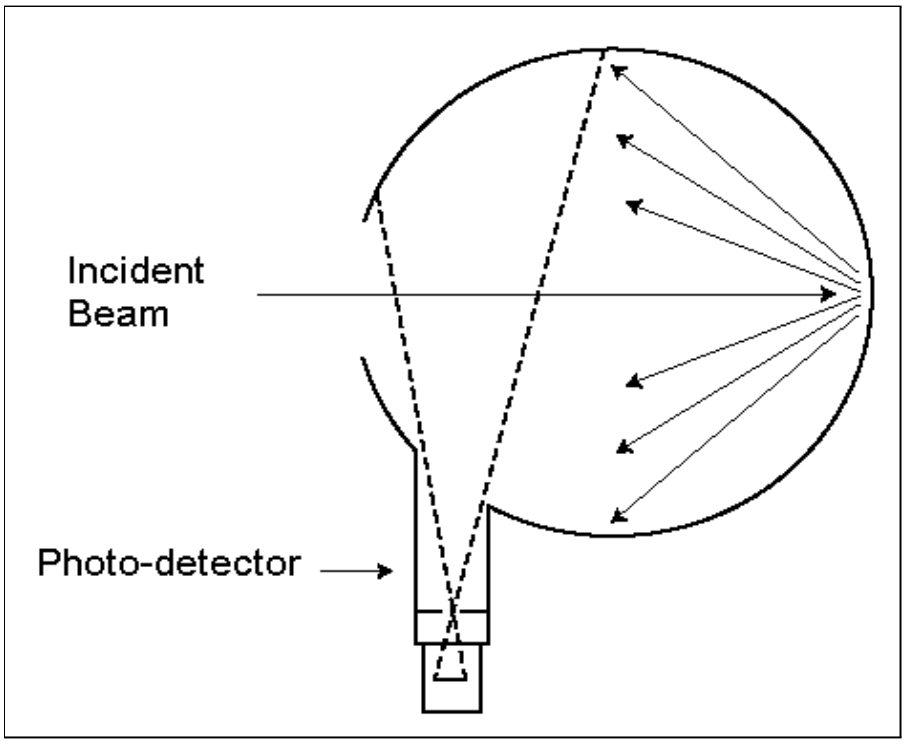

Figure 1.6: Integrating Sphere (Labsphere Inc. 2005)

With an integrating sphere-based spectrophotometer, the spectral reflectance / transmittance is measured from the ratio of the reflected / transmitted flux by the specimen to that of a reference standard under identical geometric and spectral conditions. For transmittance measurement, the reference standard is air (i.e., an open inlet port) and for reflectance measurement, the reference standard is usually a surface having the same, known optical property as the integrating sphere coating.

For traditional spectrophotometers, the integrating sphere is smaller in size ($d < 100$ mm), and uses two narrow beams of light for measurement. Here d is the diameter of an integrating sphere. The BAI-IS has a larger integrating sphere ($d > 200$ mm) and uses only one broad beam of light. The principle of operation is further discussed in Chapter 3.

In a dual beam configuration, the incident beam is split into two parts with a moveable mirror. One beam illuminates the sample and the other beam illuminates the reference standard. In this technique, the sample and reference readings are taken alternately without moving the sample, as shown in Figure 1.7.

In the single beam technique, the light illuminates the sample and the reference standard alternately. For measurement accuracy, the light source, detector and electronics must be quite stable over time. The single beam process requires more time than dual beam configuration since the sample is moved for each measurement as shown in Figure 1.8. However, single beam system entails a simpler and compact construction than the dual beam system.

Traditional spectrophotometers use small integrating spheres and dual beam illumination. Only thin, non-scattering and spatially uniform materials can be measured. A narrow beam of light is sufficient because a small sampling area on the specimen can be representative of the overall material. On the other hand, the BAI-IS uses a larger integrating sphere and a single beam of light, illuminating a broad area on the test specimen. In the BAI-IS, the single beam is preferred over the dual beam configuration due to the fact that it is difficult to design dual radiant sources with adequate collimation and uniformity over both reference and measuring ports at the same time.

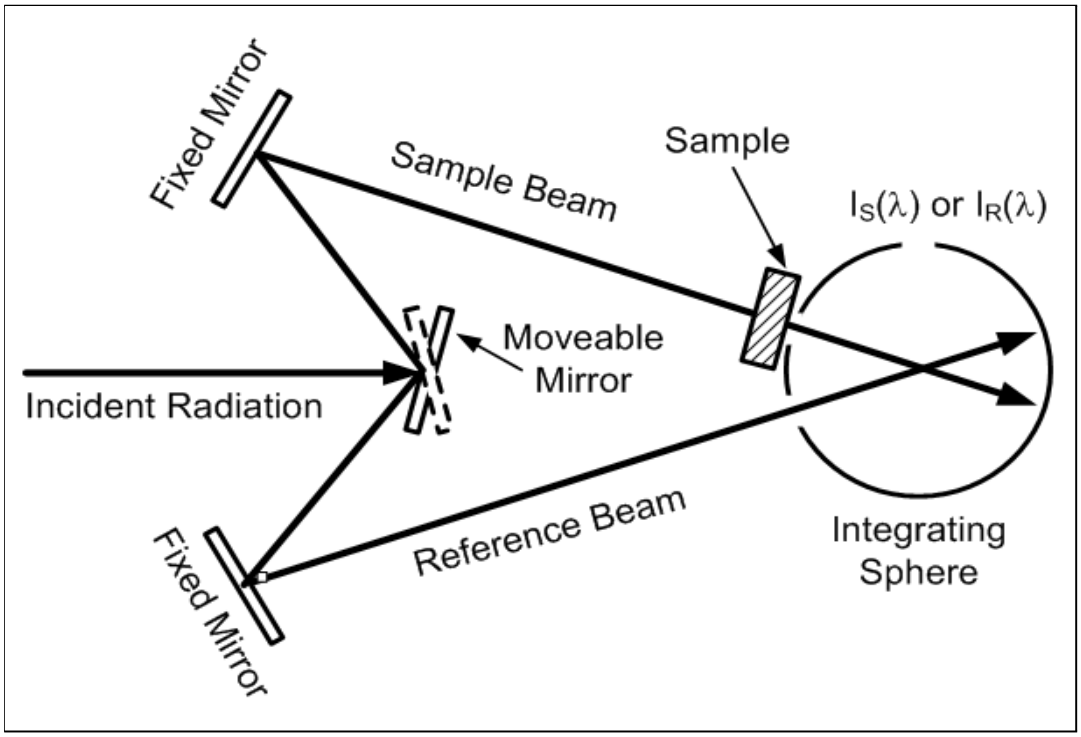

Figure 1.7: Dual Beam Configuration (Milburn 1994)

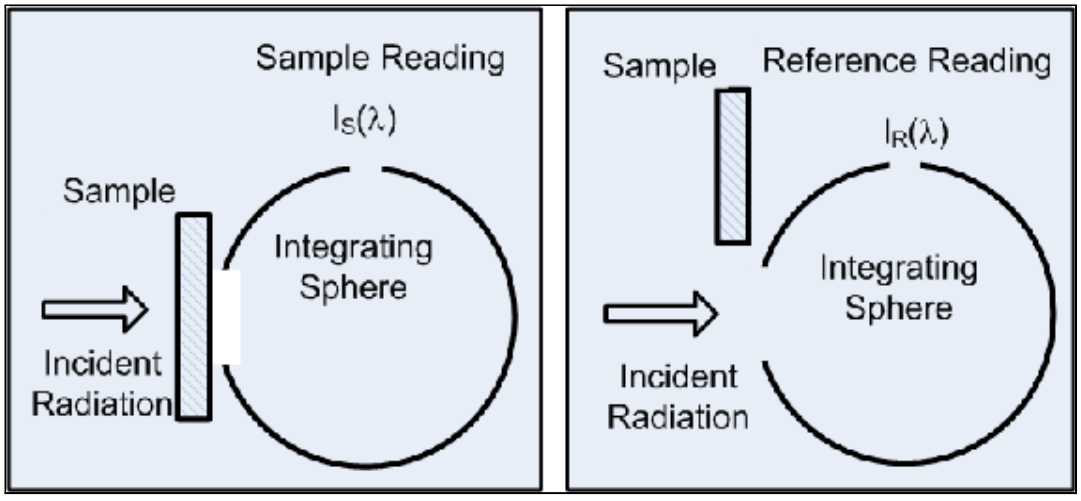

Figure 1.8: Single Beam Configuration (a) Sample Reading (b) Reference Reading

The BAI-IS is used to measure optical properties of spatially non-uniform and scattering specimens. Broad area illumination has two significant advantages:

It samples a representative area to characterize the overall material; and it collects scattered light in such a way that the inscattered light compensates for the out-scattered light.

This way, measurement errors are minimized. Out-scattered light is discussed further below.

For thick, scattering samples, with a narrow beam of incident light, some portion of the light will be scattered at some point across the thickness of the sample. The non-scattering part will leave the other side of the sample covering a small area at the back of the sample. Due to the finite thickness of the sample, the scattered portion of the incident light will be transmitted through the back of the sample after being shifted laterally. If the inlet port area is not large enough to pick up this transmitted ray, this shifted, scattered ray will be lost from the detector reading and an erroneous transmittance reading will be recorded. This is known as out-scattering loss or flux loss due to scattering as shown in Figure 1.9.

For broad area illumination, since the sample will collect uniform radiation over a larger area it will compensate out-scattered flux from one area of the sample by in-scattered flux coming from another part of the sample as shown in Figure 1.10.

Type, size, geometry, application and optical characteristics of the material are important factors to consider when selecting the appropriate spectrophotometer. This is why Milburn (1994) built the BAI-IS to measure optical properties of honeycombs. The BAI-IS can also be used to measure solar transmittance of shading devices such as venetian blinds, tip-to-tip sheer fabric blinds and drapes or any other non-homogeneous, thick and light scattering samples and advanced glazing materials.

1.2.5 BAI-IS Description

The BAI-IS, which was designed and built at the University of Waterloo (Milburn 1994), was being re-furbished to improve accuracy and reliability.

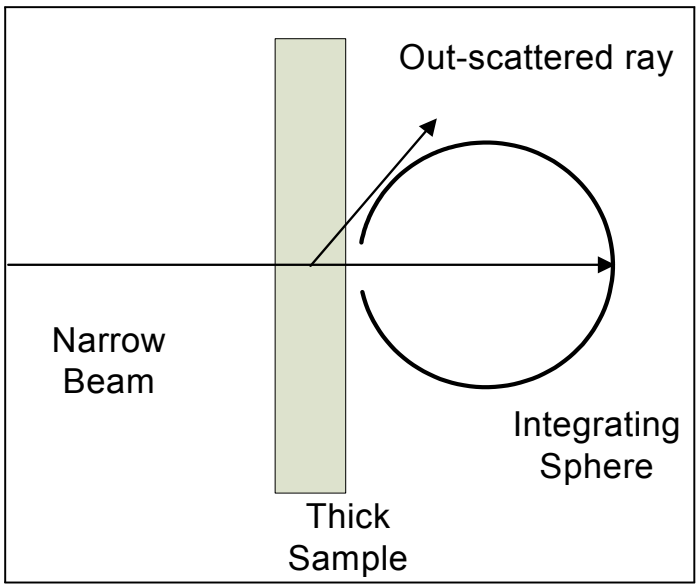

Figure 1.9: Narrow Beam with Thick Scattering Sample

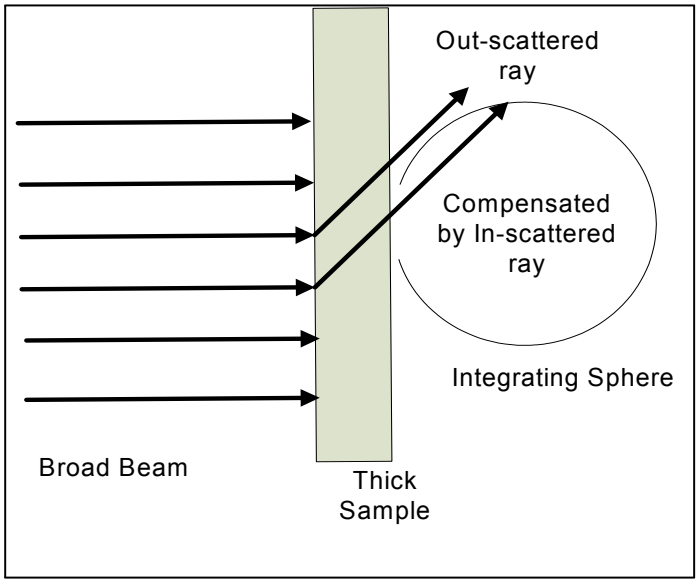

Figure 1.10: Broad Beam with Thick Scattering Sample

The apparatus uses a 50 cm diameter integrating sphere and a single broad beam of incident radiation as shown in Figure 1.11. While measuring non-planar,

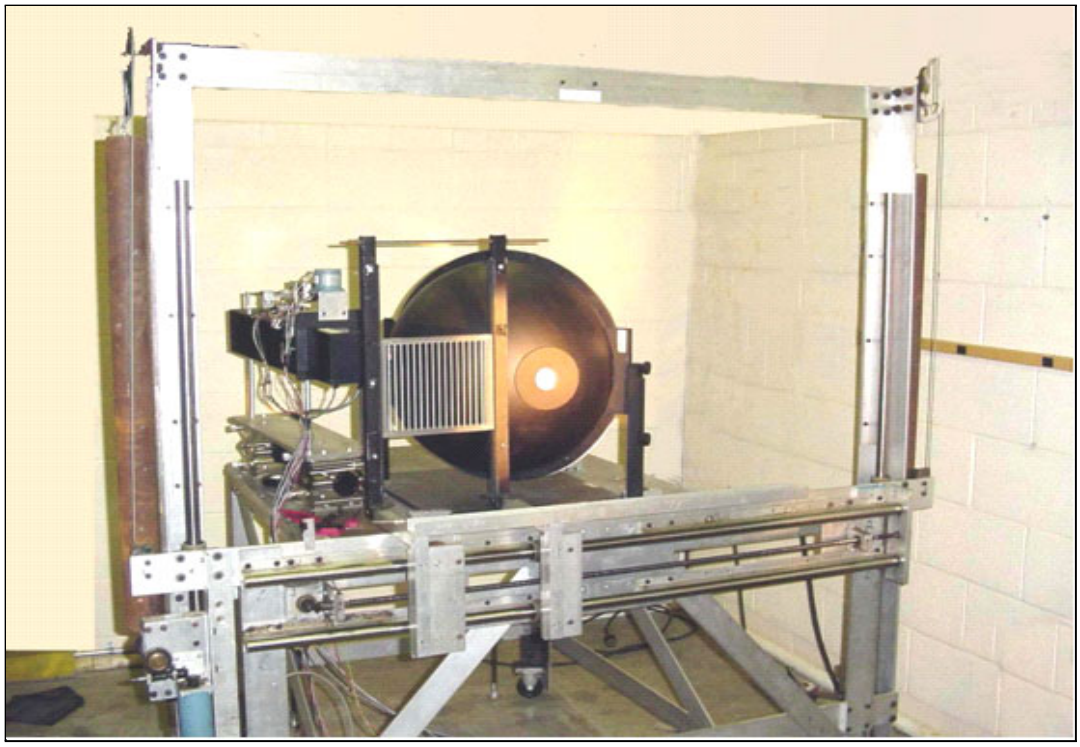

Figure 1.11: Integrating Sphere with Sample Mounting Rig

scattering, thick samples with uniform irradiation, the flux loss due to out-scattering near the sample is offset by the in-scattering from other parts of the sample, as described above.

The radiant source irradiates the sample and the transmitted radiation enters the inlet port of the integrating sphere. The incoming radiation experiences multiple reflections at the wall and then the hemispherically integrated uniform radiation leaves through the measurement port of the sphere and is conveyed to a monochromator. The radiant flux, Φ_∞ is sampled by the monochromator as shown in Figure 1.12, where a prism spreads the radiation by wavelength. This enables the detector to make spectral readings. The radiation of desired wavelength exits the monochro-

mator through a slit, which can be adjusted by changing its width. A wider slit allows more radiant energy to pass through and strike the detector but reduces spectral resolution. The outgoing radiation is then focussed to strike the active area of a photo-detector.

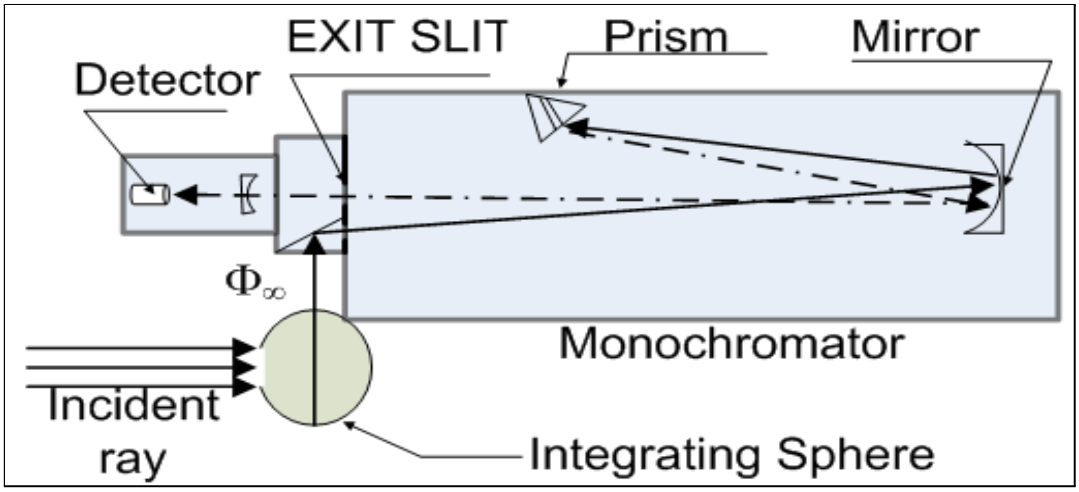

Figure 1.12: Typical Quartz Prism Monochromator

1.2.6 Solar Optical Property Measurement

The BAI-IS built by Milburn (1994) is used to obtain solar optical properties of shading devices. To calculate the solar gain and/or heat loss through window glazing and shading devices they need accurate and reliable information regarding thermal and solar optical properties. The solar-optical properties are used to quantify the amount of transmitted, absorbed and reflected solar radiation through each layer in complex fenestration system (Jiang 2005). Longwave properties (emissivities) and convective heat transfer coefficients are needed to perform the energy balance at each layer in the system. The properties in the range of long wavelengths can easily be analyzed separately with independent models because there is no appreciable interference between these two radiation bands as shown in Figure 1.13.

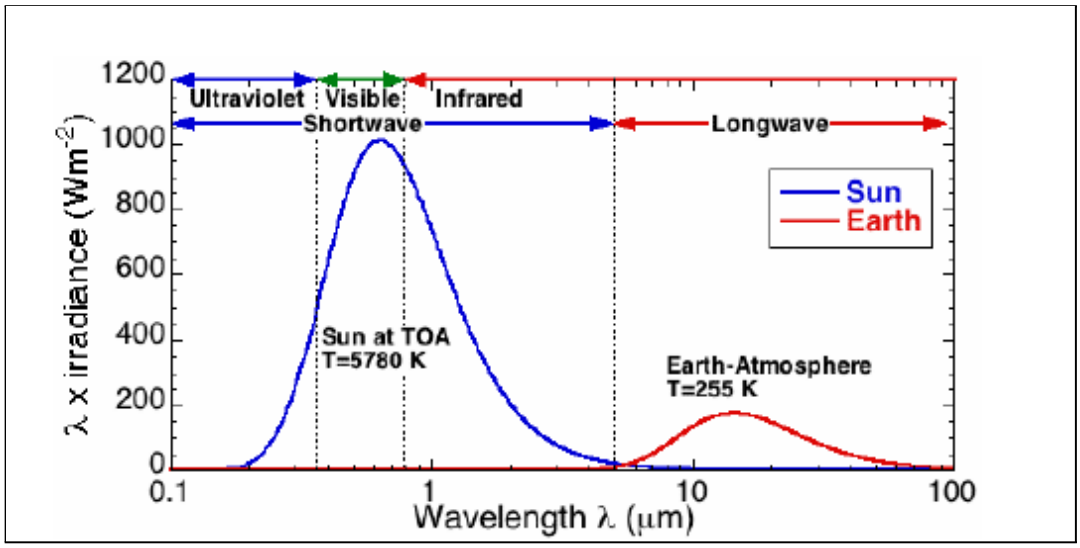

Figure 1.13: Spectra for Solar and Black-Body Radiation. (Broeke and Reijmer 2006)

For energy consideration the key performance characteristics of a shading device can be categorized as its thermal insulating ability or U-value and solar heat gain coefficient (SHGC) which is related to solar radiation transmitted through the fenestration system. Heat transfer through the building envelope varies for different shading devices at different parametric conditions such as orientation, climate, window size and type. Net energy flow through the multi-layered fenestration system can be shown to be the sum of heat flux and directly transmitted solar energy, such that

$$q_{net} = U \times (T_{out} - T_{in}) + SHGC \times G_s \tag{1.1}$$

Here, G_s is the solar irradiation and and U is the heat transfer coefficient. The U-value and SHGC for the fenestration system play an important role to control heating and cooling load for the building (Hunn et al. 1993, Reilly and Hawthorne 1998). U-value varies as the inverse of the thermal resistance of the fenestration system, R_t.

$$U = \frac{1}{AR_t} \tag{1.2}$$

Here, A is the effective heat transfer area occupied by the system. The U-value is a measure of thermal transmission. It is used to calculate the heat transfer caused by temperature differential between the indoor (T_{in}) and outdoor (T_{out}) space. So U-value indicates how much heat is going to be retained inside the room. A smaller U-value usually results in lower peak cooling loads.

By definition, SHGC is a measure of solar gain. Low SHGC reduces cooling load and high SHGC reduces the heating load.

SHGC is the sum of transmitted solar radiation, τ, and the inward-flowing fraction, N_i, of the portion of incident solar radiation absorbed in each layer of the system:

$$SHGC = \tau + \sum N_i \times A_i \tag{1.3}$$

As mentioned earlier, shading devices can act as switchable layers for optimum energy performance by controlling SHGC as required and lowering U-value for the overall fenestration system. They also help to reduce cold draft near the windows and raises the radiation temperature of the room in a cold winter night (Shurcliff 1980).

For plane specular surfaces, (i.e., glass) it is easy to quantify directional solar properties. Moreover, it is to be noted here that each optical property changes with the direction of incident radiation for any material used to fabricate shading devices. A directional-directional property specifies a quantity for single incident angle having only a single direction of transmitted or reflected radiation. But in reality, for non–specular, non-planar items, (i.e., shading devices), for any incident radiation, some radiation is absorbed by the material but the transmitted and the reflected components are scattered in numerous directions. As a result their optical properties and solar heat gain are dependent on both incidence angle and angle of transmission or reflection. The corresponding directional-directional quantities must be obtained with numerous measurements.

Consider the directional-hemispherical transmittance. It can be defined as the ratio of transmitted radiant energy collected over the entire hemisphere (2π) to the collimated incident radiant energy coming from the specified incidence angle θ and azimuthal angle ϕ as shown in Figure 1.14. Therefore, the expression for solar heat gain coefficient of a fenestration system having "n" layers is written as:

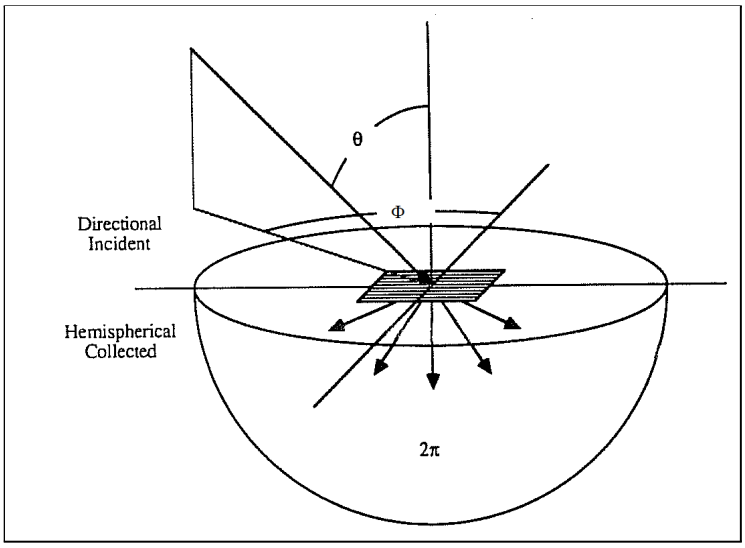

Figure 1.14: Directional-Hemispherical Transmittance (Papamichael and Selkowitz 1987)

$$SHGC(\theta,\phi) = T_H^f(\theta,\phi) + \sum_{i=1}^{n} N_i \times A_i^f(\theta,\phi) \tag{1.4}$$

Here the directional-hemispherical transmittance, $T_H^f(\theta,\phi)$, and directional absorptance, $A_i^f(\theta,\phi)$,are optical properties and independent of individual layer temperature and its longwave emissivity. Since the shading layers are not uniform, "spatially-averaged" or "effective" solar optical properties are assigned (Klems 1994a, 1994b, Van Dijk and Goulding 1996, Rosenfeld et al. 2000, Yahoda et al. 2005, Jiang 2005). To estimate spatially averaged solar properties of a sheer blind multi-layer solar calculations were used (Wright and Kotey 2006).

The inward-flowing fraction (IFF), N_i, is the fraction of energy absorbed at layer i, that reaches the indoor space. N_i is a thermal quantity that depends on heat transfer properties of the assembly and is independent of wavelength. The value of N_i is usually calculated from heat transfer models.

Therefore, if all the terms in Equation 1.4 are known, then a simplified one-dimensional energy analysis can be carried out to estimate net heat flow through any fenestration system with louvered blind. With this end in view, the scope of this research is limited to the measurement of the directional-hemispherical transmittance of shading devices by using the BAI-IS apparatus, because this property is required as a first step to estimate solar heat gain as well as to estimate daylighting performance of the fenestration system (Kessel and Selkowitz 1984). The directional-hemispherical transmitted solar radiation over the photopic range is required to assess the lighting quality and illuminance distribution in the room interior. Similarly, Papamichael and Selkowitz (1987) have also emphasized that it is appropriate to measure only the directional-hemispherical solar-optical properties to simulate the luminous and thermal performance of a complex fenestration system.

1.3 Research Objectives and Motivation

This thesis mainly introduces the concept of a spectrophotometer whose basic component is an integrating sphere and deals with the measurement of solar transmittance of sheer blind. It also summarizes the refurbishment plan of the apparatus and discusses contributions of individual components on overall performance.

This research is divided into five parts:

(1) refurbishing an existing spectrophotometer,

(2) measurements to check accuracy,

(3) measurement of solar transmittance of a venetian blind and a sheer blind ,

(4) comparison of experimental results with the results of analytical models and

(5) uncertainty analysis of the experimental results.

It is evident that the BAI-IS apparatus is one of the most useful and practical tools for measuring directional-hemispherical solar optical properties for spatially non-uniform, scattering, thick samples. Milburn (1994) designed and built the BAI-IS with custom made measuring and control devices at the University of Waterloo. Most of these devices are now outdated and unreliable. Now, components are available which are more accurate, easy to use and maintain. Refurbishment was undertaken by replacing the primary measuring and control components of the BAI-IS, which include photo-detector, optical chopper, lock-in-amplifier, data acquisition system, stepper motor drive and control interface software. Following this upgrade, the apparatus was calibrated to verify measurement accuracy

The BAI-IS was used to measure weighted average solar transmittance of a venetian blind and "tip-to-tip sheer fabric blind" at different slat and profile angles. The optical properties of aluminium slat of venetian blind and fabric slat, sheer fabric of sheer blind were measured using a commercial UV-VIS-NIR spectrophotometer, Cary-5000, at different incident angles. Measurements were compared to the solar-optical models for venetian blinds developed by Wright and Kotey (2006) and Kotey et al. (2007).

Since solar transmittance and reflectance are the key inputs to quantify heat gain through different elements in a fenestration system these data are useful to engineers and designers for selection of glazing materials and building energy analysis. As a result, many building materials require measurement for product specification and standardization. The solar transmittance data of a shading device is essential to evaluate the building envelope performance characteristics and to carry out energy simulation for assessing different design options to achieve energy efficiency.

Chapter 2

Literature Review

2.1 Introduction

This chapter describes previous research regarding :

1. integrating sphere theory,
2. various standards for transmittance measurement of thick, scattering samples,
3. chronological development of the BAI-IS,
4. measurement error of the BAI-IS and gradual development of different stages of apparatus design to improve overall performance and accuracy,
5. various window glazing and shading layer models

2.2 Integrating Sphere Theory

Integrating sphere theory was first stated by Sumpner (1892) based on the multiple reflections of light inside a hollow cavity. The theory states that the radiance from a diffusely reflecting spherical surface is independent of angle of view and its intensity is proportional to the projected surface area (Rosa and Taylor

1922). Jacquez and Kuppenheim (1955) formulated an integral equation to quantify integrating sphere efficiency and measurement error as a function of sphere geometry. The equivalent function is presented by Hisdal (1965a, 1965b) to quantify reflectance for diffuse and specular samples using matrix relations. Goebel (1967) described the fundamental principle of the integrating sphere by developing general algebraic equations for sphere efficiency as a function of wall-coating reflectance. Tardy (1991) used matrix methods to model integrating sphere irradiance for perfectly spherical systems, non-spherical systems and systems with non-uniform irradiance.

The integrating sphere with its spherical shape and diffuse coating produces a spatially integrated, uniform field of light following multiple reflections. The flux measured by the photo-detector is proportional to the incident flux entering the integrating sphere. An integrating sphere is an ideal tool to average the radiation flux that comes from a spatially non-uniform source.

2.3 Apparatus

The standard description of a spectrophotometer with a small integrating sphere is found in ANSI/ASHRAE Standard 74-1988. ASTM E903-96 also represents a standard method for measuring optical properties of thin, homogeneous sheet materials by using a small integrating sphere. Both of these standards are unable to handle spatial non-uniformity or thick scattering samples. ASTM E424-71, Method A, provides a standard test method for measuring solar transmittance of thin, scattering samples in sheet form but it does not support spatially non-homogeneous samples. ASTM E1175-87 provides a standard test method where a large diameter integrating sphere is used for measuring solar or photometric optical properties of scattering samples made of spatially non-uniform material. This method uses broad-area-irradiation, where the size of the beam is larger than the disparities of the sample being tested. In this way the spatial non–uniformities of the sample are averaged out, but still it is not suitable for thick scattering samples.

Milburn (1994) mentioned that there is no standard method available to measure directional-hemispherical optical properties of thick, scattering and spatially

non-uniform samples. In 1900 Ulbricht first designed a simple hollow sphere with diffusely reflecting interior walls to integrate light for general purposes. Krochmann (1979), E. Krochmann and J. Krochmann (1983) first suggested the use of broad area illumination for measuring transmittance of thick, scattering samples. Symons (1982) and Symons et al.(1982) first described an apparatus for measuring directional-hemispherical transmittance of non-planer scattering samples. Kessel and Selkowitz (1984) described a 2-m diameter integrating sphere used to measure the directional-hemispherical transmittance of window systems including geometrically complex shading devices. They used a photopic sensor to measure visible transmittance to characterize the daylighting properties of the fenestration system. Zerlaut and Anderson (1984) also mentioned a very large, solar illuminated, 8-ft diameter integrating sphere for measuring solar optical properties of non-planar, light scattering samples. Later, Platzer (1992) described a larger integrating sphere with broad area irradiation and a single beam of radiant light to minimize error due to out-scattering loss. In this method, the out-scattering flux near the sample can be offset by the in-scattering flux coming from other parts of the sample surface. Milburn (1994) first attempted to standardize the optical-property measurement process using a 50-cm diameter integrating sphere with broad-area-illuminating technique which is capable of spectral measurements.

Integrating sphere manufacturers discuss design attributes in terms of very few basic parameters : sphere diameter, physical characteristics, quantity and size and location of port openings and baffles, and sphere coatings for different operating spectral ranges. Signal intensity at the photo-detector is proportional to the radiation entering through the inlet port of the sphere. It can be shown that sphere throughput is inversely proportional to sphere diameter and directly proportional to wall reflectance for the same port fraction. Sphere response decreases with the increase in port size due to loss in flux. See Section 2.4.1 and 2.4.2. A larger ratio of measurement port area to sphere surface area can also increase throughput to the detector (Lovell 1984). A larger sphere ensures improved integration ability of radiant energy. Hence for optimum throughput as well as uniform spatial performance a larger sphere is traded off with smaller port fraction and highest possible wall reflectance (Labsphere Inc. 2005 and Sphere Optics 2005).

2.4 Measurement Error

The BAI-IS was developed in the 1980s. Since then there have been many studies to analyze its error in measuring different optical properties for different kinds of samples. As per ASTM E-903-96, random errors arise from signal detection, electronic data processing, inherent error associated with the geometry and coating of integrating sphere system and distribution of scattered or reflected radiation. It is known that a high degree of accuracy is difficult to achieve and depends on operator skill, experience, care, equipment design and maintenance.

Three stepper motors including sets of gears, lead screws and linkages are used in the BAI-IS to move sample traversing mechanism, adjust slit width of the monochromator and control wavelength. According to Milburn and Hollands (1994) uncertainty in wavelength selection arises due to precision error which is caused by the fact that, the stepper motor, lead screw, small gears and relevant mechanical linkages may not return to the same point consistently every time because of backlash. Gear and lead screw mechanism are shown in Figure 2.1. Error due to backlash and tolerance are applicable for all stepper motor sub-systems. In addition, Edwards et al. (1961) and Clarke et al. (1986) have listed a set of systematic errors for any integrating sphere apparatus that may arise from geometric imperfections. They have identified the probable causes and summarized corrective actions to improve accuracy and reliability of measurement. Moreover, imperfect calibration will cause systematic bias error.

Roos et al. (1988) discussed the error in measurement due to flux loss through open ports of the sphere, where reflectance is assumed to be zero. Hanseen (1989) researched detector field-of-view. Milburn (1994) showed that the typical dual beam small area illuminating method with a smaller integrating sphere is suitable for measuring transmittance of thin, planar homogeneous specimens but for thick, scattering, spatially non-uniform samples, lower transmittance values are obtained due to out-scattering loss. Since the BAI-IS apparatus was designed to minimize this out-scattering loss it is important to examine this error in detail.

Milburn (1994) also noted that the BAI transmittance measurement involves

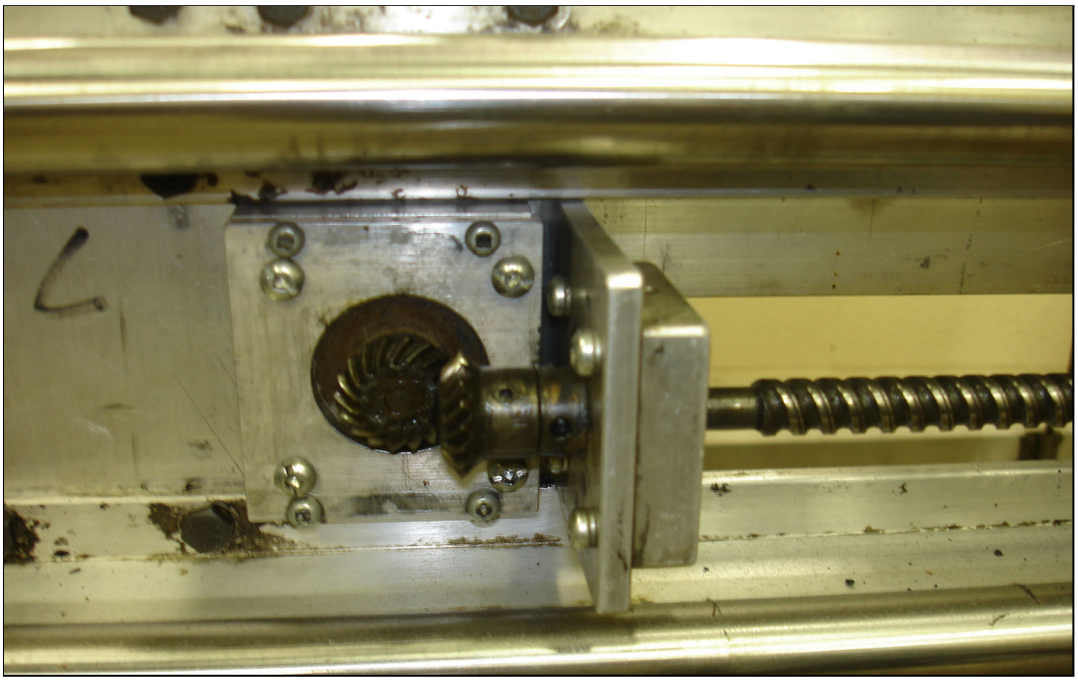

Figure 2.1: Lead screw and gear arrangement for Sample Mount

error due to two specific factors which are caused by sample reflectance. The two factors are :

1. External Sample Reflectance (ESR)
2. Internal Sample Reflectance (ISR)

Milburn and Hollands (1995) derived expressions to evaluate ESR and ISR factors and discussed schemes to minimize ESR errors and to eliminate ISR errors.

2.4.1 External Sample Reflectance Error

The sample surface as well as the exterior surface of the sphere have reflective properties. When the sample is brought in front of the inlet port almost all of the radiation entering the sphere gets inside directly after passing through the sample.

There may be a few paths in which radiation passing through the sample reflects off the exterior surface of the integrating sphere or any surrounding structure and then reflects back from the rear portion of the sample and then gets inside the sphere indirectly. This distorted transmitted radiation leads to ESR error which is shown in Figure 2.2. The best way to minimize ESR error is to paint the exterior surface of the integrating sphere with black paint having reflectance as low as possible.

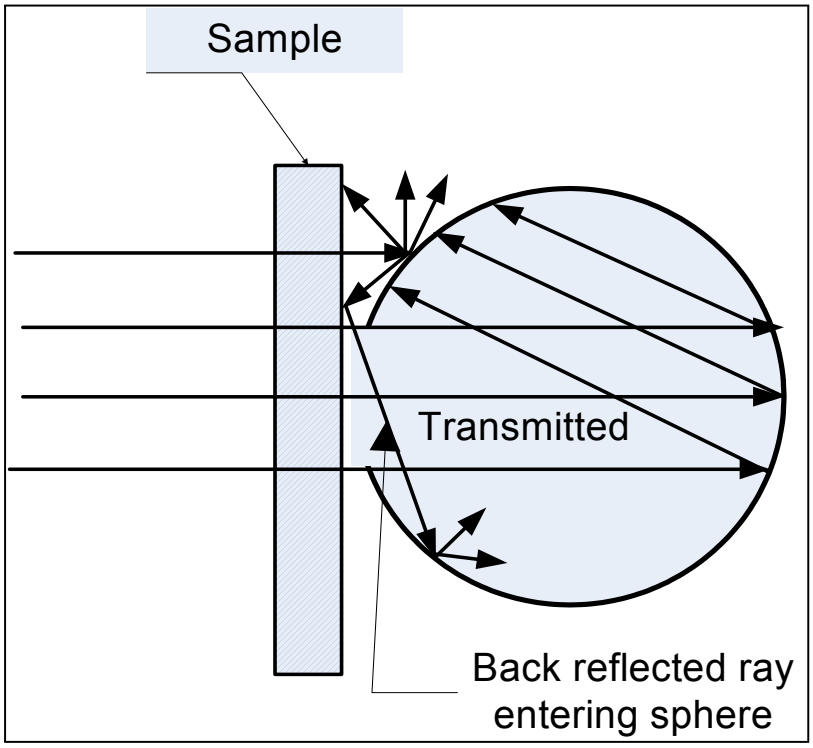

Figure 2.2: External Sample Reflectance Error

2.4.2 Internal Sample Reflectance Error

Internal Sample Reflectance is related to the radiation that has already entered through inlet port of the sphere. Some rays leave the sphere through the inlet port. For the reference reading, when there is no sample placed in front of the sphere,

none of this radiation returns to the sphere. For the sample reading, when the sample is mounted in front of the inlet port, some of the rays get reflected back from the sample surface and re-enter the sphere. This reflected portion from the sample surface is responsible for ISR error which results in a higher, erroneous sample reading. The ISR error is shown in Figure 2.3.

To eliminate ISR the best result is obtained if the size of the entrance port can be minimized so that little radiation can leave the sphere. However this reduction in port size is a trade-off with the fact that the port should let in enough radiation to have an acceptable signal-to-noise ratio. Fendley (1985) proved that proximity of the sample to the sphere wall affects the transmittance measurement, especially for scattering and thick samples. For non-scattering, thin samples there is apparently no difference in transmittance readings if the samples are mounted at different distances from the sphere wall. Errors may arise due to smaller sample size, or

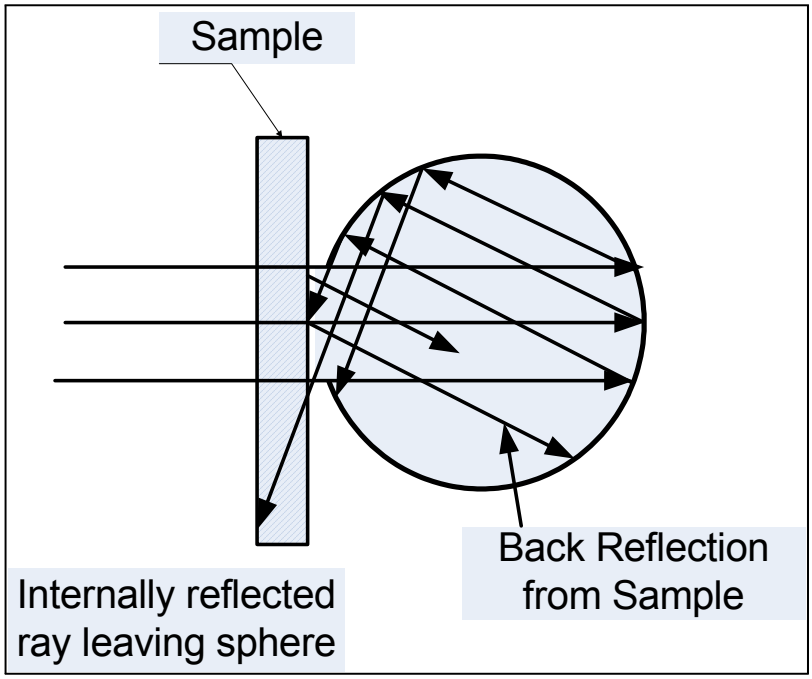

Figure 2.3: Internal Sample Reflectance (ISR) Error

smaller beam size or spatial non-uniformity of sample or irradiation. In order to

improve irradiation uniformity over the entire sample it is better to keep the radiant source further from the sample but this is a trade-off with the required intensity of light. Accordingly, measurement errors are expected to increase with the increase in incidence angle.

2.4.3 Uncertainty Analysis

Uncertainties are associated with any experimental procedure. Therefore, it is important to present the outcome of any experiment by mentioning the estimated uncertainties. Experiments can be classified into two types: single-sample and multiple-sample experiments.

The single sample experiments are those where uncertainties are not reduced by repeated sampling. The basic framework for single-sample uncertainty analysis was first illustrated by Kline and McClintok (1953). Moffat (1982, 1985, 1988) discussed techniques of single-sample uncertainty analysis as a decision making tool for planning, executing and reporting experiments.

The uncertainty of experiments using repeated measurements is evaluated by statistical tools. Techniques for multiple-sample uncertainty analysis are discussed by Abernethy et al. (1985) and by ANSI/ASME PTC 19.1 (1983).

Milburn and Hollands (1996) compared the broad area illuminating (BAI) and small-area-illuminating (SAI) methods and estimated errors caused by out-scattering of radiant flux while measuring transmittance for thick samples for different incidence angle ranging between, $0^0 \leqslant \theta \leqslant 70^0$ (Milburn and Hollands 1995, 1996). It was found that the outscattering loss is significant for SAI measurement, which is strongly dependent on the nature of the sample and incident angle. For a low-scattering, thick material (Teflon large-celled honeycomb), spectral transmittance (at λ =0.5 μm) from the BAI-IS was found to be 2.6% higher than the SAI measurement, at normal incidence (i.e., at $\theta = 0^0$). At θ =70^0, the difference increased due to outscattering losses in the SAI measurement with the BAI-IS result 50% higher than the SAI measurement.

The ANSI/ASHRAE standard 74-1988 explains the root causes of errors and uncertainties of measurement and quantifies the precision and accuracy of a com-

mercial spectrophotometer. Various uncertainties in spectral measurement arise due to the fact that detector's signal-to-noise (S/N) ratio varies with wavelength. At λ =0.85 μm, the S/N ratio is maximum but decreases in the near infra red portion of the spectrum. Measurement uncertainty is inversely proportional to the S/N ratio of the detector. This type of uncertainty can be reduced by slow or stepwise scanning and averaging over a longer time span for each wavelength.

2.5 Analytical Models for Slat Type Shading Devices

Louvered blinds are used extensively as shading devices because of their simplicity in design and effective thermal and daylighting performance. Moreover, louvered blinds are inexpensive, easy to install, operate and maintain, attractive, durable, and safe with respect to fire and mechanical hazard. There have been many analytical, numerical and experimental studies on louvered blinds to determine their optical properties.

Louvered blinds are spatially non-uniform, possess non-planar surfaces and scatter light. Specular optical properties do not characterize such blind layers. Due to scattered radiation, the specular and diffuse properties exhibit complex angular dependency. The directional properties of such non-uniform layers are averaged spatially to represent the overall blind layer as a thin, homogeneous, specular layer. The spatially averaged property of such a blind layer is known as an "effective" property (Wright and Kotey 2006).

2.5.1 Aubele and Parmelee Model (1952, 1953)

An analytical model was developed to determine solar absorptance, reflectance and transmittance of the shading device and window glass combination. The shading device has a set of uniformly spaced opaque, flat slats. In this model the shading layer was considered to be infinitely large and slat curvature was neglected but a

correction factor for slat thickness was incorporated. The model treats both beam radiation and diffuse radiation (ground diffuse and sky diffuse).

The model is based on a 2-dimensional ray tracing technique with infinite inter-reflection at the slat surfaces. For a specularly reflecting, opaque, slat surface having a certain value of absorptance, the incident beam radiation can be divided into three parts:

(1) Some portion will be reflected back to the outdoors after reflection on the slat surface.

(2) The transmitted portion may be sub-divided as follows:

(a) Reflected-through portion : This radiation is transmitted through the blind layer by multiple reflections on the slat surface and enters the indoor space. The effective transmittance of the blind layer depends on slat geometry, profile angle, reflectance or absorptance of the slat surface.

(b) Straight-through portion: This part of the radiation is directly transmitted through the slat array without striking any slat surface. The transmittance value is purely a geometric factor and can be obtained from slat geometry and profile angle.

(3) The remaining portion is absorbed by the slat surface.

The reflected radiation at the blind layer can be calculated by considering two extreme cases:

(i) slat surfaces are purely specular,

(ii) slat surfaces are purely diffuse.

Note that the transmittance is function of three major factors:

(I) Irradiation geometry : (a) profile angle (b) direction of incident solar radiation (i.e., location of the sun).

(II) Slat geometry: (a) Slat width (b) Slat spacing (c) Slat Angle (d) Slat thickness (e) Slat curvature.

(III) Slat absorptivity.

For specular slat surfaces the effective optical properties of the blind assembly can be calculated from geometry while accounting for beam radiation absorbed and reflected at each specular reflection. For diffuse surfaces the slat which is illuminated directly by beam radiation is divided into illuminated and shaded portions. Then the view factors are to be computed between the openings, the two elements (shaded and illuminated) and the adjacent shaded surface from beam radiation. The effective optical properties of the blind assembly can be calculated from the beam radiation that is directly transmitted and from the transmitted and reflected radiation that occurs due to diffuse reflections on slat surfaces.

For diffuse solar radiation, the sky is treated as a quarter of a sphere, which is divided into 81 patches. The diffuse transmittance is the ratio of the transmitted radiant energy through the shade to the sum of the radiant energy from the patches incident on the shade.

In their second paper (Parmelee and Aubele 1953) experiments were carried out to measure the solar transmittance and absorptance of a shade-glass combination. The solar optical properties were measured for four different types of slat-type shading devices combined with window glass by using a solar calorimeter. The calorimeter was set in a vertical position exposed to direct sunlight (for incident beam radiation) or facing away from the sun (for incident diffuse radiation). The experimental results and the results from the analytical model were compared but due to lack of accurate solar-optical property data for the slat material, unstable weather conditions, unaccountable diffuse radiation from surroundings and significant effect of the heat absorbing glass, the validation was not conclusive.

2.5.2 Pfrommer et al. (1996) Model

The Pfrommer Model was developed on the basis of four paths of transmitted and reflected solar beam radiation and is applicable to any incidence angle. The four paths are as follows:

1. Direct transmittance : This portion is calculated from blind geometry and direction of beam radiation.

2. Direct-reflected transmittance : This portion is either pure diffuse, or pure specular or any combination. It has two components:

   (a) Diffusely reflected portion.

   (b) Specularly-reflected portion.

3. Diffuse transmittance : This is obtained by integrating the transmitted radiation from each slice of the sky or ground across the vault between the cut-off angles and dividing it by the total radiation.

4. Diffuse-reflected transmittance : This is derived from an analytical solution with an assumption that the slat surfaces are purely diffuse.

To characterize the diffuse nature of the slat surface, a "Shining Factor" was introduced. The shining factor is set equal to unity for diffuse reflection or zero for specular reflection.

Pfrommer found that the influence of slat curvature decreases as the radius of curvature increases. For most of the cases where, slat width, (w) $\simeq$ slat spacing, (s), the influence of curvature is small but for highly curved slats (slat radius of curvature, r <w) then the influence of slat curvature becomes important.

2.5.3 Rosenfeld et al. (2000, 2001) Simple Model

Rosenfeld et al. (2000) developed a simple model to analyze the thermal and optical performance of double glazing units combined with a venetian blind. In the model, each component of the complex glazing system was treated as one of 'n' layers. A complex glazing system contains one or more non-specular optical elements in the glazed area of the window. Slats were assumed to be flat. The optical properties of the slat surface were held constant, independent of incidence angle. It was also assumed that the specular and diffuse reflectance components of the slats are independent of incidence angle. For specular reflections, the fraction of incident light that undergoes multiple reflections between slats and is ultimately transmitted through the shading layer can be determined from geometry. At each reflection, some fraction is lost due to absorption. Some fraction of incident light is

also transmitted directly without hitting any slat surfaces depending on slat angle and direction of the incident beam. For diffuse reflection the reflected part of the transmittance was treated as quasi-specular. This treatment was based on the assumptions discussed below.

For radiation that emerges from the shading device following two or more reflections :

1. At each reflection a fraction, F, of the diffusely reflected light would transmit through the blind in the same way as the specular component.

2. The remaining fraction (1-F) is reflected backwards and retraces its path as if it is specularly reflected to emerge on the illuminated side of the blind with a fraction being absorbed by the slat surface at each reflection.

This model has an input parameter F, which shows how closely the diffuse reflections are concentrated at the angles close to the specular direction. For example, it is set at F=0.5 for a Lambertian distribution and F=0.7 to 0.9 for double glazed unit with venetian blind. However, the results are not very sensitive to the choice of F (Breitenbach et al. 2001). The fractions of incident light reflected and absorbed due to multiple reflection ultimately yield the effective transmittance, absorptance and reflectance of the blind layer. This model is applicable to normal incidence of light only. This is a significant limitation.

Rosenfeld et al. (2001) described an experimental procedure to study the thermal and optical performance of complex glazing systems. The experiment used a double glazed window combined with venetian blind. The spectral bidirectional transmittance of the specimen was measured with a Cardiff goniospectrometer at different incident angles. The Rosenfeld et al. (2000, 2001) model is in good agreement with the experimental result at lower slat angles, $\phi < 60^o$.

2.5.4 WIS Model (2000)

The WIS (Advanced Window Information System) is a software package that is based on a model for calculating effective solar optical properties of slat type shading devices. The fenestration system with an attached louvered blind is modeled

as having multiple layers. The slat-type blind is considered as a layer with effective optical properties which are functions of slat properties, slat geometry and the incidence angle of beam solar radiation. In this model the representative slat-type blind unit is represented by two adjacent parallel slats and two virtual closing surfaces at two ends of slats which have 100% transmittance. WIS assumes that slats are flat and their reflectance is purely diffuse. In this model the direct-hemispherical reflectance value of slats is used throughout and these properties are measured at normal incidence.

The beam radiation that is transmitted by the blind has two parts :

1. The directly transmitted fraction that emerges from the blind assembly without interacting with slat surfaces. This can be easily calculated from the geometry.

2. The other part is transmitted to the indoor space following multiple diffuse reflection at slat surfaces.

Diffuse radiation is calculated by dividing each slat into five equal parts. The blind enclosure is formed by two adjacent slats and two fictitious closing surfaces that act as blackbodies as shown in Figure 2.4. According to the WIS model, a view factor matrix must be determined between the twelve segments of the blind enclosure. The view factor matrix is converted into a configuration matrix by using slat reflectance. These two steps are carried out for all required wavelengths (ISO/FDIS 15099: 2003) to estimate diffuse transmittance and reflectance of the blind layer.

2.5.5 Yahoda Model (2002, 2005)

This model can determine effective solar optical properties of slat type shading layers at various solar profile angles. The model inputs are slat geometry, slat surface reflectance and the beam-diffuse split of the incident radiation. The beam-diffuse split, F is defined as the ratio of diffusely reflected radiation to the total

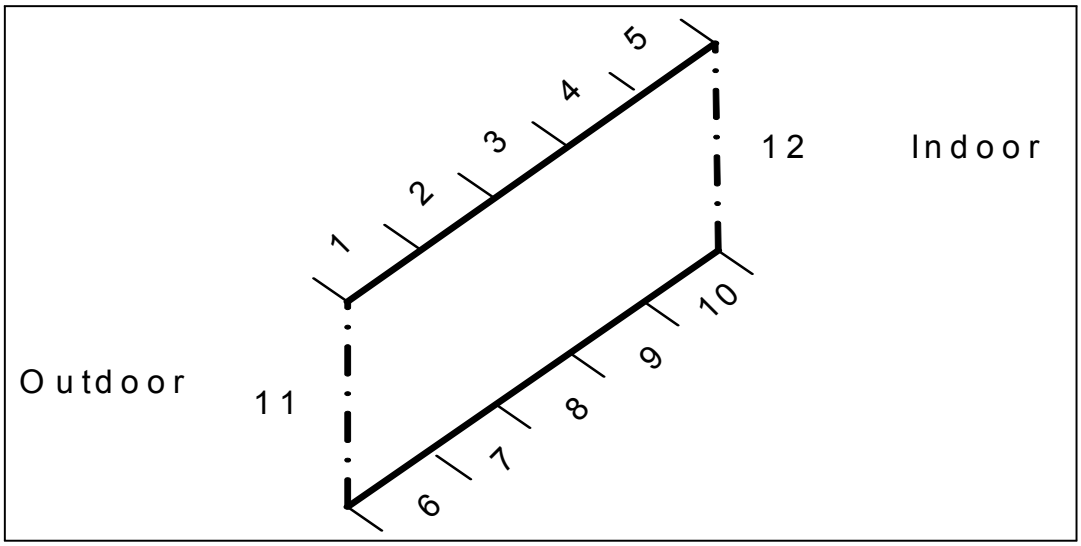

Figure 2.4: 12-Surface Enclosure for WIS Model

incident beam radiation at the slat surface. F=1 for purely diffuse reflection and F=0 for purely specular reflection.

Since the slats can be either specular or diffuse, the model needs two separate techniques to deal with solar beam radiation and solar-diffuse radiation. The incident beam radiation on a shading layer is modelled as transmitted or reflected radiation through five paths:

1. Directly transmitted beam radiation (beam-to-beam);

2. Indirectly transmitted beam radiation by specular reflection by slat surfaces (treated as beam-to-diffuse);

3. Indirectly transmitted diffuse radiation by diffuse reflection by slat surfaces (beam-to-diffuse);

4. Reflected beam radiation by specular reflection on slat surfaces which reflects to the outdoor environment (treated as beam-to-diffuse); and

5. Reflected diffuse reflection on slat surfaces which reflects to the outdoor environment (beam-to-diffuse).

For incident beam radiation this model provides the effective beam-to-beam transmittance and beam-to-diffuse transmittance of the shading layer for different irradiation geometry (Ω), slat geometry (w/s, ϕ) and solar optical properties of the slat.

The beam-to-beam model uses an entrance height algorithm and ray tracing technique with infinite reflections to determine direct transmittance and reflectance. The shading layer is represented by an enclosure consisting of two adjacent slat surfaces with two virtual surfaces at the front and back openings having 100% transmittance. For given values of w, s, Ω and ϕ the fraction of incident beam radiation that will undergo transmission through n-reflections can be found if the corresponding upper and lower entrance heights are known.

This model deals with diffusely reflected beam radiation (Item 3 and 5 listed above). The beam-diffuse model also assumes that the top and the bottom slat surfaces are not uniformly irradiated. In this model, the above mentioned enclosure is divided into 8 surfaces (three on each slat and two virtual surfaces) as shown in Figure 2.5. Regarding the slat separation, Van Dijk and Goulding (1996) suggested division of each slat into five equal parts, Parmelee (1952) and Pfrommer et al. (1996) considered only diffuse radiation resulting from directly intercepted beam radiation. Yahoda separated each slat surface according to the location of direct beam or specularly reflected direct beam solar radiation. It was also assumed that reflected beam radiation results in diffusely reflected radiation.

In Yahoda's model, the slat thickness and slat curvature were neglected. BAI-IS experiments (Jiang 2005) clearly demonstrated that the effective solar transmittance of a venetian blind was over-predicted in the analytical model with respect to the experimental measurement when the incident beam was aligned with the slats. The model predicts 100% transmission when the incident radiation is parallel to the slats but showed good agreement with experimental results otherwise. The difference was as high as 12 %. The discrepancy between model and experiment is associated with the assumption of neglecting slat curvature as shown in Figure 2.6.

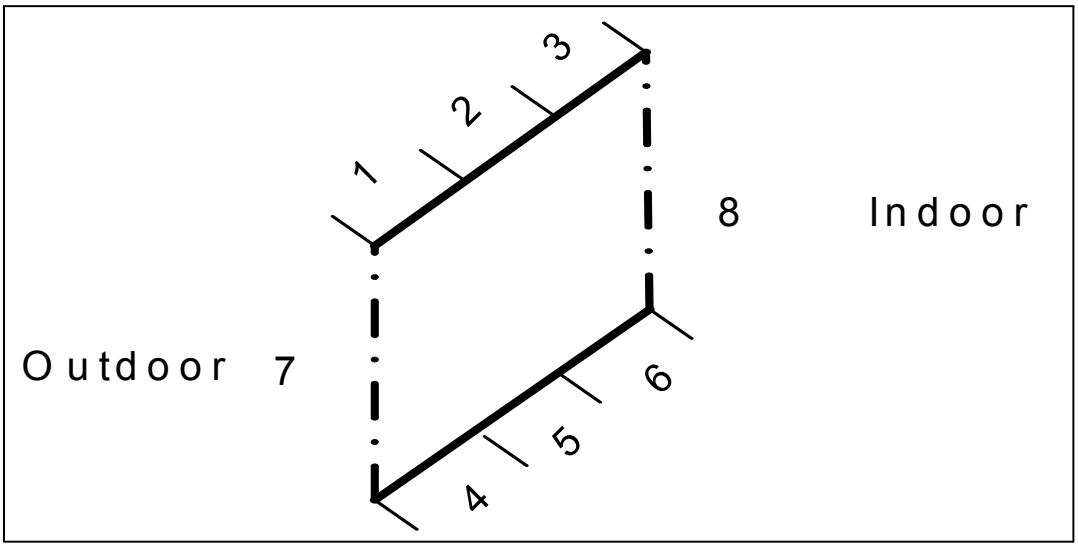

Figure 2.5: 8-Surface Enclosure for Beam-Diffuse Model (Yahoda 2005)

2.5.6 Kotey et al. (2007) Simplified Solar Optical Model

This model for louvered blinds estimates effective optical properties as functions of slat geometry, optical properties of slat surface and profile angle of incident beam radiation. The main assumption is that the slats are diffuse in nature so that any incident beam radiation will result in diffusely transmitted and/or reflected radiation. This assumption is supported by observation. Slat surfaces reflect diffusely more than 90% of total reflected radiation (Parmelee et al. 1953, Breitenbach et al. 2001). Moreover, if the slats are considered to be translucent (in case of fabric or vinyl slats) only diffuse transmission through the slats is expected. This simplifies the model by eliminating the ray tracing technique which is computationally complex as seen in Yahoda's model. This model also shows that the slat curvature can have a significant effect on transmittance. With the assumption of flat slats and zero thickness there is 100% transmission when beam radiation aligns with the slats (i.e., as $\Omega + \phi \approx 0$).

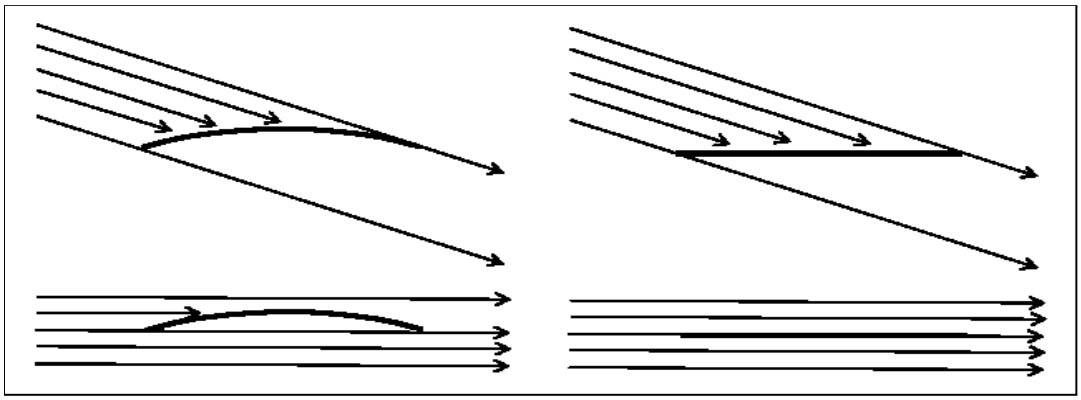

Figure 2.6: Effect of Slat Curvature on Blocking Radiation (Kotey et al. 2007)

This model, with a curvature correction applied, agreed very well (Kotey et al. 2007, Jiang and Collins 2007) with the measurements of Jiang (2005).

2.5.7 Wright and Kotey (2006) Multi-Layer Calculation

This model (Wright and Kotey 2006) is a general form of computational technique for predicting solar optical properties of any complex fenestration system having multiple layers. Here, the existing solar-optical model of Edwards (1977) for specular glazing layers is extended to accommodate the effect of light-scattering properties of shading layers (i.e., diffuse reflection and transmission). Effective beam-beam, beam-diffuse and diffuse-diffuse properties are needed for each layer in the system. Algorithms were formulated to determine all reflected, transmitted and absorbed fluxes within the shading/glazing array due to incident diffuse and /or beam solar radiation. The results provide beam and diffuse fluxes from which the reflected, transmitted and absorbed radiation in each layer can be calculated.

For the sheer blind, the effective transmittance values measured by the BAI-IS were compared with the result calculated using an analytical model. With this end in view, the tip-to-tip sheer fabric blind was modelled as a multi-layer glazing/shading array.

In summary, regarding venetian blinds, Aubele and Parmelee (1952, 1953) formulated a flat slat model and accounted for the first specular reflection with the assumption that it is the only significant inter-reflection for most cases. They did not examine situations at high incidence angle. They considered corrections for slat thickness. Pfrommer et al. (1996) considered all higher order specular reflections. They considered slat curvature as well. Yahoda and Wright (2005) also developed a comprehensive model to obtain effective solar optical properties for venetian blinds. This model involved ray tracing technique which was rigorous and complex. Kotey et al. (2007) eliminated the ray tracing technique by assuming that slats diffusely transmit and reflect solar radiation. This simplified model is useful for fast computation and hence valuable for use in building energy simulation. In the current study, the effective solar optical properties of a sheer blind were obtained by using multi layer array calculation established by Wright and Kotey (2006).

Chapter 3

Experimental Apparatus

3.1 Introduction

In this chapter, integrating sphere theory and the description of a single beam broad area illuminating-integrating sphere are presented. A brief description of a dual-beam, small area illuminating spectrophotometer (Cary-5000) is also presented. The Cary-5000 spectrophotometer was mainly used for calibration in this research. The sample specification and testing procedure are also briefly described for both pieces of equipment.

3.2 Integrating Sphere Theory

Integrating sphere theory is based on the following assumptions:

1. The integrating sphere is a perfect sphere;
2. The sphere coating has uniform reflectance over the entire inner surface;
3. The coating is a Lambertian reflecting surface; and
4. Diffusely reflected radiation reaches the detector after at least two reflections from the sphere wall.

The integrating sphere is a hollow sphere with a highly reflective diffuse coating on its interior surface. In the ultraviolet, visible and near-infra-red spectral region this special coating is Lambertian, which means purely diffuse reflectance.

Integrating sphere theory has been used for many years in spectrophotometry. In its simplest form, the theory states that, if a lamp is located inside a hollow sphere whose internal surface is coated with diffusing material, then the radiation flux, leaving the sphere wall at any location is proportional to the energy emitted by the lamp. A small measurement port in the sphere wall provides a measure of useful lamp output (Lovell 1984).

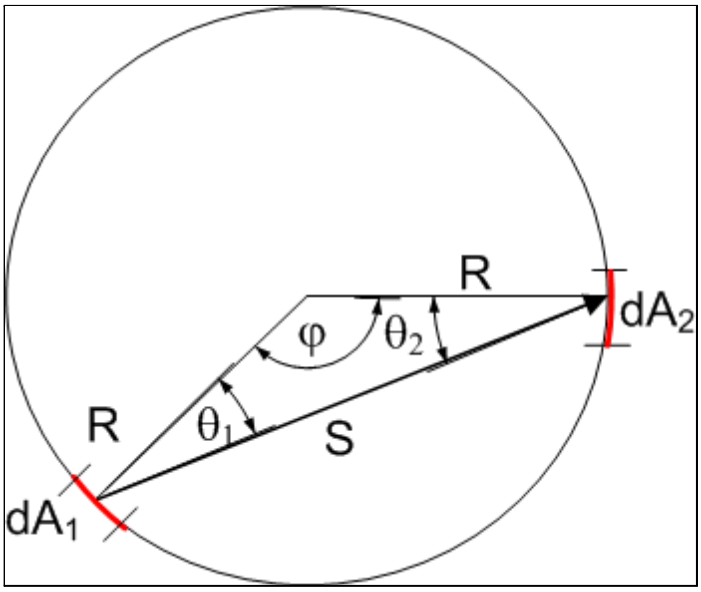

Figure 3.1: Radiation Exchange Within a Spherical Enclosure

The Lambertian surface in combination with a spherical enclosure ensures that every part of the sphere receives the same radiant flux of light following the first reflection. It can be stated that, after the first reflection, the incoming light loses its directional characteristics (Labsphere Inc. 2005 and Sphere Optics 2005).

Consider radiation exchange between two infinitesimal elements dA_1 and dA_2, as shown in Figure 3.1. The radius of the sphere is R and distance between these

two elements is S. The fraction of diffuse radiation that leaves dA_1 and arrives at dA_2 , which is known as the exchange factor, $dF_{dA_1-dA_2}$, will be equal to (Hollands 2004):

$$dF_{dA_1-dA_2} = \frac{dA_2}{4\pi R^2} \tag{3.1}$$

It is evident that the exchange factor is independent of the locations of the two elements, the viewing angle and the distance between the elemental areas. The fraction of radiant energy leaving dA_1 and received by dA_2 is not influenced by the location of dA_1 and dA_2.

If the differential area dA_1 exchanges radiation with a finite area A_2, then Equation 3.1 becomes,

$$\int dF_{dA_1-A_2} = \frac{1}{4\pi R^2} \int_{A_2} dA_2 \tag{3.2}$$

Now, noting that total sphere area is A_s=$4\pi R^2$, we can re-write Equation 3.2 as

$$F_{1-2} = \frac{A_2}{A_s}$$

It is seen that the fraction of the radiant energy received by any area is equal to the fraction of the surface area it occupies within the sphere. After the first reflection on element A_1 light strikes area A_2. Therefore, after the first reflection the sphere produces a uniform field of radiation irrespective of the fact that the incoming radiation from source is spatially and directionally asymmetrical. If we have a perfect sphere, and a lamp is placed at the centre of the sphere, then from pure symmetry we can reach the same conclusion. By ignoring the radiation prior to the first reflection symmetry is not necessary, provided the sphere interior has a Lambertian coating.

3.2.1 Lambertian Wall Flux Measurement

Let us assume that a radiant source, having flux Φ, irradiates the inlet port of an integrating sphere. With reference to Figure 3.2, radiant energy enters the sphere through the inlet port area, A_{in}, at the rate of $G_{in} = \Phi A_{in}$. If the sphere wall

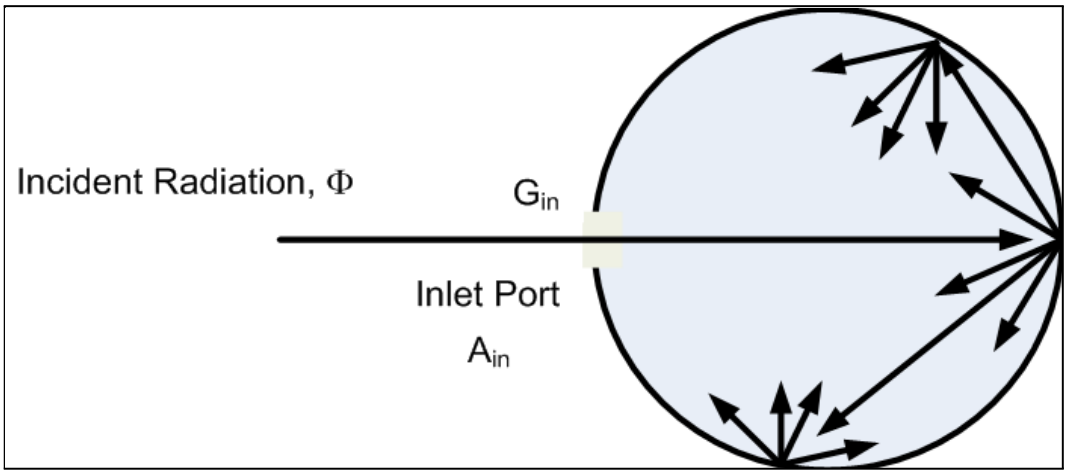

Figure 3.2: Integrating Sphere with Inlet Port.

reflectance is ρ, then fraction ρ of this incoming radiant energy will be reflected. The flux at the first reflection can be treated as a source inside the sphere delivering energy at the rate of $\Phi A_{in}\rho$. The radiation will be spread uniformly over the area of the sphere as shown in Figure 3.3.

Therefore, ignoring the inlet port, the radiant energy leaving the wall after the second reflection can be written as:

$$\Phi_2 = \frac{\Phi A_{in}\rho^2}{A_S} \tag{3.3}$$

Including an infinite series of subsequent reflections, the flux leaving the wall is:

$$\Phi_\infty = \Phi\frac{A_{in}}{A_S}\left(\rho^2 + \rho^3 + \rho^4 + ...\right) \tag{3.4}$$

It is possible to account for the radiation lost through ports, say inlet and measurement ports as shown in Figure 3.4. Let the the port fraction f is defined as:

$$f = \frac{A_{in} + A_{measurement}}{A_s}$$

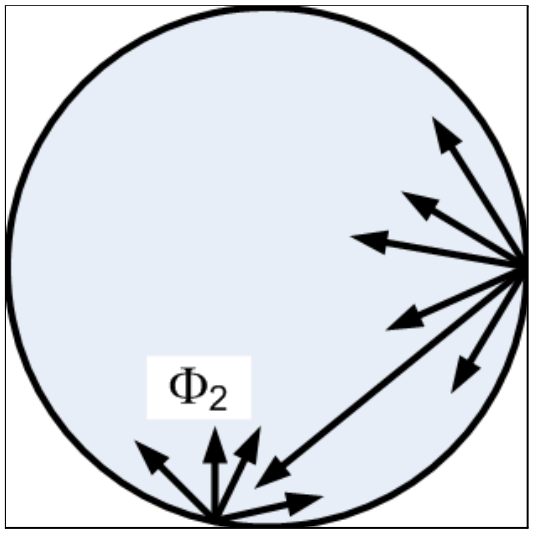

Figure 3.3: Integrating Sphere with No Port

The amount of flux leaving the sphere surface, excluding the ports can be expressed as

$$\Phi_\infty = \Phi\left[(1-f)^2\rho^2 + (1-f)^3\rho^3 + (1-f)^4\rho^4 + ...\right] \tag{3.5}$$

At each reflection, the fraction f of the reflected flux will leave the sphere through the ports. It can be shown that the flux leaving the wall, given by Equation 3.5, is

$$\Phi_\infty = \Phi\frac{\rho}{[1-\rho(1-f)]} \tag{3.6}$$

It can be concluded that:

(1) the incoming flux is spatially and directionally integrated;

(2) the flux sensed by the photo-detector is proportional to the flux entering through the inlet port; and

(3) the ratio $\frac{\Phi_\infty}{\Phi}$ is called the "response of the integrating sphere" or the "sphere multiplier". The Equation 3.6 shows that at $\rho = 1$ and f=0, the wall flux becomes infinity. This highlights the idea that a high value of ρ and a low value of f are essential to achieve $\Phi_\infty > \Phi$ for effective operation of an integrating sphere.

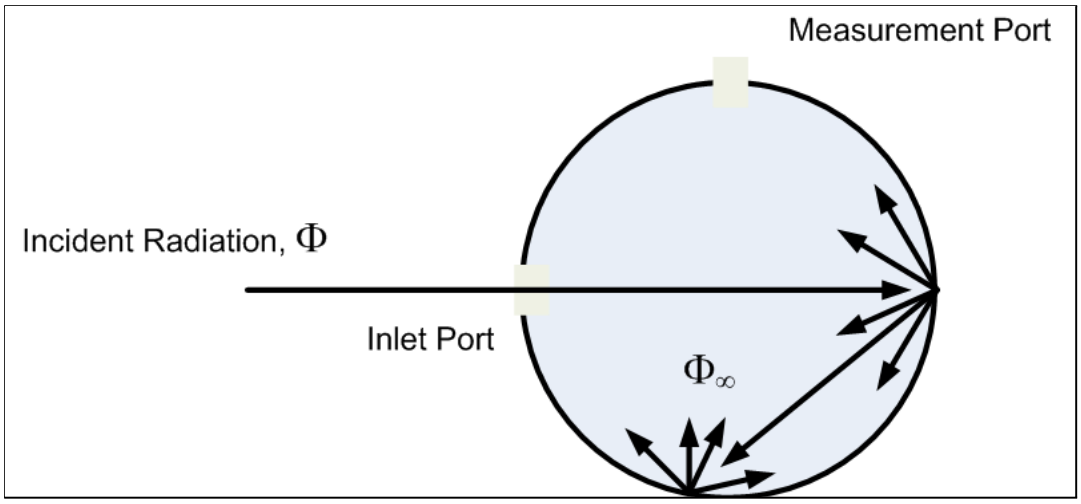

Figure 3.4: Integrating Sphere Wall Flux

3.2.2 Detector Signal Measurement

A measurement port is used to measure Φ_∞. As shown in Figure 3.5, some of the radiation reaching the measurement port area ($A_{measurement}$) of the sphere goes into the monochromator, where it is split into different wavelengths. The measuring port is shielded from the inlet port to ensure that only radiation following the second reflection enters the monochromator.

Only a small portion of flux from sphere wall leaves the exit slit area (A_{slit}) of the monochromator and is focussed on the active area (A_d) of a photodetector. The amount of radiant energy passing through the exit slit will depend on the width of the slit opening, the flux from the integrating sphere wall and the amount of radiation that is gathered within the field of view of the detector.

3.3 Broad Area Illuminating Integrating Sphere

The major part of the research comprises upgrading the existing apparatus which was designed and built at the Solar Thermal Research Laboratory of the

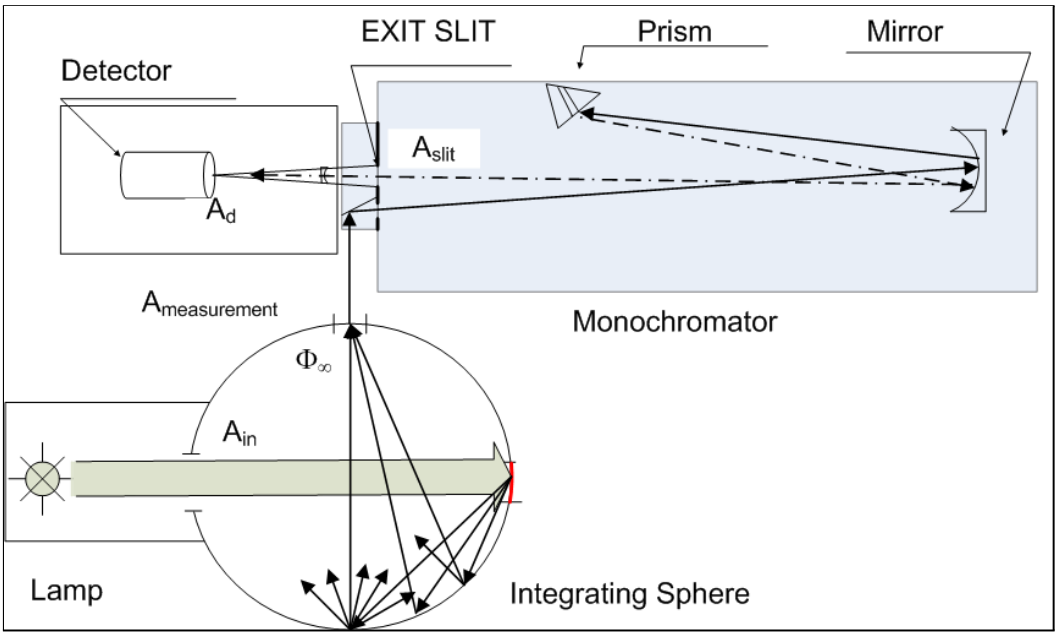

Figure 3.5: Integrating Sphere with Monochromator

University of Waterloo (Milburn 1994). This apparatus is a single beam instrument that illuminates a broad area on the sample surface and is generally used to measure solar transmittance and absorptance of thick, scattering samples.

3.3.1 Test Procedure

The apparatus was used to measure transmittance of shading devices. For transmittance measurement the sample is mounted in front of the inlet port outside the sphere wall, which is also known as a wall-mounted arrangement. In the alternative, known as the Edwards arrangement, the sample is placed inside the sphere for absorption and reflectance measurement.

Spectral Dependency

The sample reading, $I_S(\lambda)$, is taken by the detector when the transmitted radiant flux passes through the sample. The reference signal, $I_R(\lambda)$, corresponds to the total incident radiant flux which is recorded after removing the test sample. The ratio of these readings is a measure of the transmittance. It is to be noted here that the optical properties are spectral quantities so the above pair of readings are taken at specific wavelengths. More specifically, spectral transmittance $\tau(\lambda)$ indicates "that the property was evaluated at wavelength λ within a small wavelength interval $\Delta\lambda$ about λ (NFRC 300 2001), such that

$$\tau(\lambda) = \frac{I_S(\lambda)}{I_R(\lambda)} \times 100\% \tag{3.7}$$

From the spectral values, the solar transmittance was computed by using a 50-point selected ordinate method (ASTM E 903-96).

$$\tau_{Solar} = \frac{1}{50}\sum_{i=1}^{50}\tau(\lambda_i) \tag{3.8}$$

The 50 values of λ_i are specified such that the solar spectral irradiance is divided into 50 equal-energy wavelength intervals.

Angular Dependency

The optical properties of louvered blinds are dependent on blind geometry as well as the incidence angle, θ, or profile angle, Ω, of the incident beam radiation. To define profile angle we have to define the incidence angle, solar altitude angle and wall-solar azimuth angle. The incidence angle subtends the incident ray and the normal to the surface of interest. Now this incident ray can be resolved on either the horizontal plane or the perpendicular plane to the window plane The window plane is the plane of interest.

The projection of the incident ray on the horizontal plane subtends angle γ with the normal to the surface which is also know as the wall-solar azimuth angle. On

the other hand, the projection of the incident ray on a vertical normal plane (this normal plane is perpendicular to the plane of interest) subtends angle Ω with the normal to the surface of interest, which is known as the profile angle as shown in Figure 3.6. Profile angle can also be defined as a function of solar altitude, β, and wall-solar azimuth angle, γ, as follows:

$$\Omega = \tan^{-1}\left(\frac{\tan\beta}{\tan\gamma}\right)$$

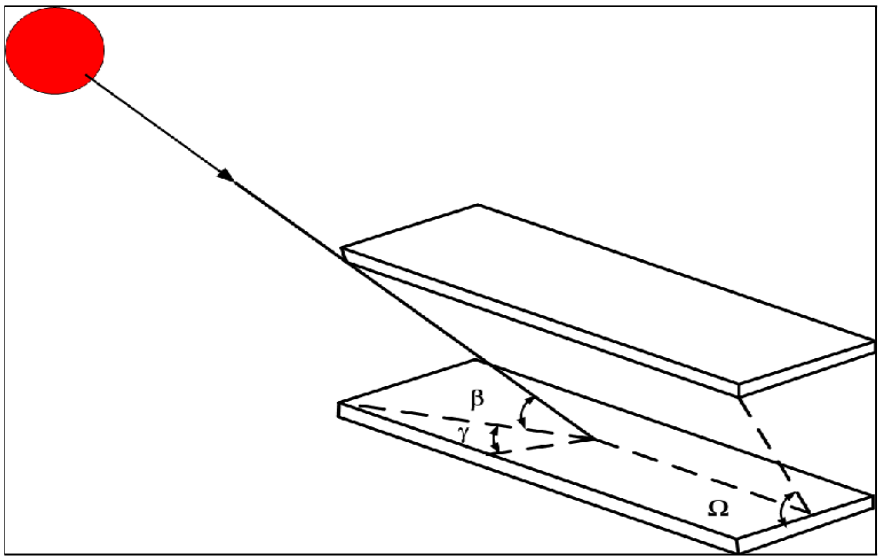

Figure 3.6: Profile Angle Ω, Wall-Solar Azimuth Angle γ and Solar Altitude β for Solar Radiation (Yahoda 2005)

Profile angle and wall-solar azimuth angle determine the length of shadow cast by barriers in front of window glazing. For horizontal louvers, profile angle is important, whilst, for vertical louvers, the wall-solar azimuth angle is important to calculate the length of the respective shadows. This research focusses on horizontal louvered blind, so the optical properties were measured as a function of Ω with the wall-azimuth angle held at zero. In this case the profile angle coincides with solar altitude and incidence angles. The profile angle was adjusted by swivelling

the working-table around the vertical axis. The working table contains the sample blind with the slats placed vertically in front of the integrating sphere. Figure 3.7 describes the sign conventions for Ω and ϕ.

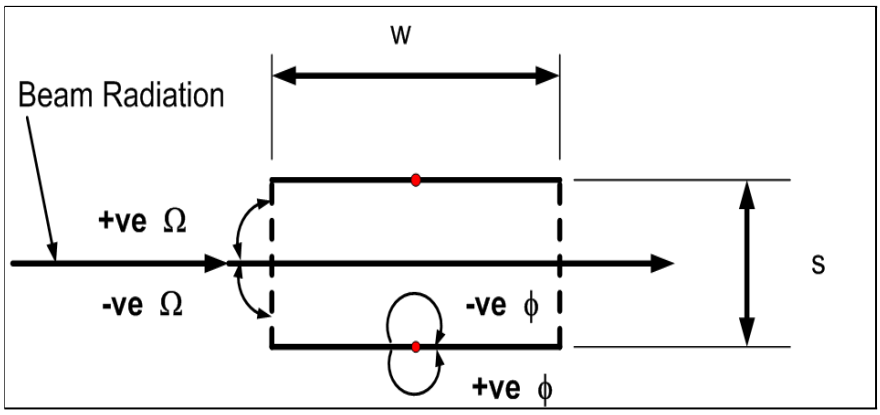

Figure 3.7: Sign Convention for Profile and Slat Angle (Yahoda 2005)

3.3.2 Equipment Description

The apparatus has four main sub-systems: the radiant source; the sample mount; the detector system; and the control system. A 50-cm diameter integrating sphere and a monochromator are the most critical components.

Radiation from lamp travels through a kaleidoscope, fresnel lens, integrating sphere and monochromator. Radiation leaving the monochromator is detected by a photo-detector. The photo-detector produces a proportional electrical signal which is compared and filtered through the optical chopper and lock-in-amplifier and then a useful signal is recorded by a data acquisition system and Labview and stored in a computer data file. The optical path and the electrical signal flow are shown in Figure 3.8

The research involved replacement of many components which are shown in the highlighted areas in Figure 3.9. The replaced components include: (1) Optical chopper control unit (2) Lock-in amplifier (3) Photo-detector (4) Noise free power

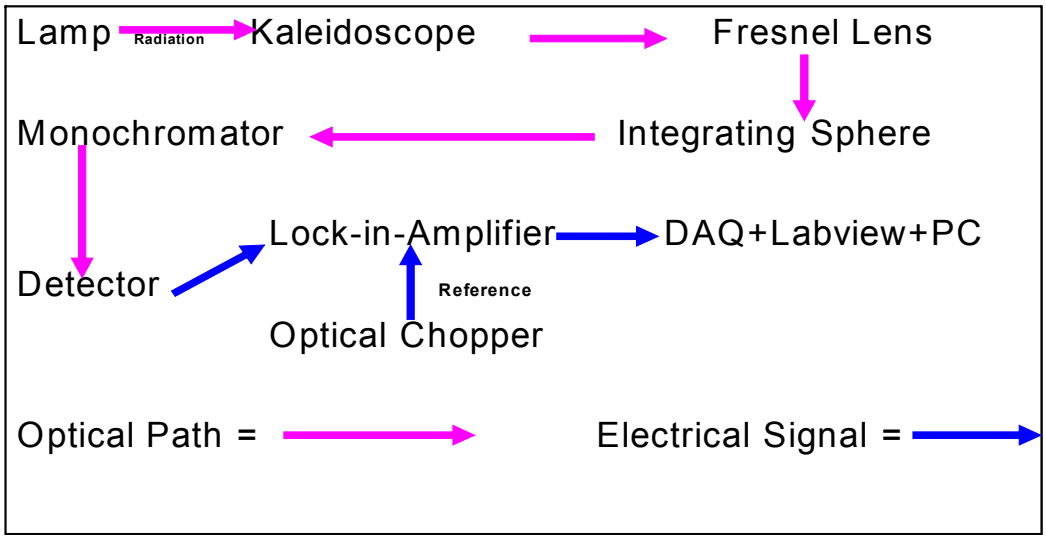

Figure 3.8: The BAI-IS Flowchart

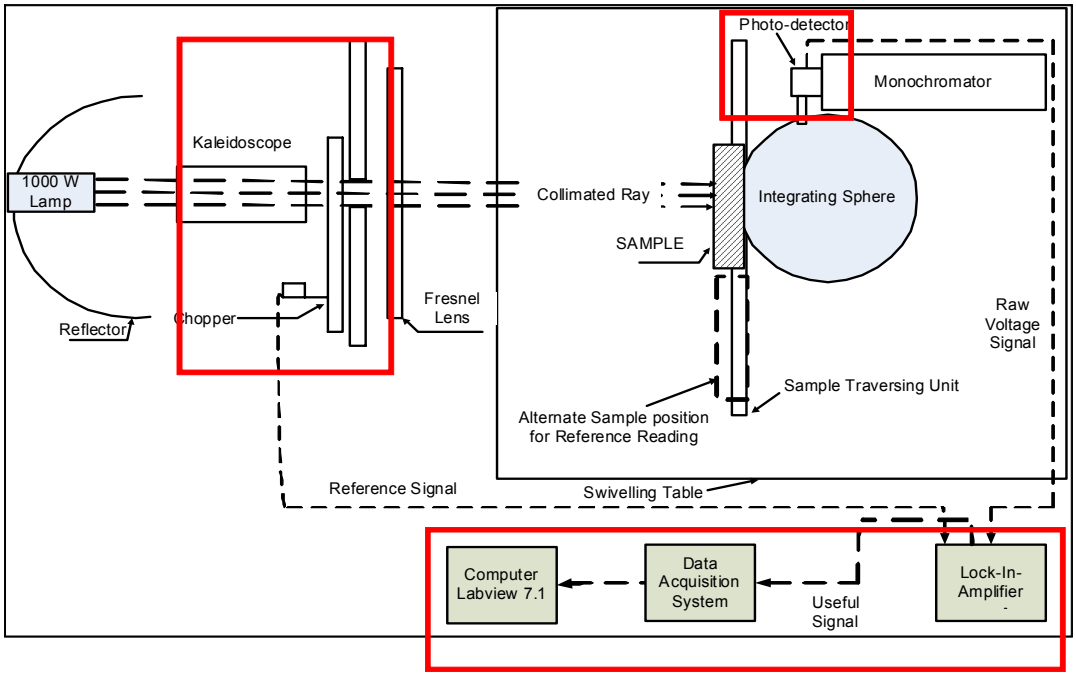

Figure 3.9: Schematic Layout of the BAI-IS

supply for photo-detector (5) Keithley DAQ card 7706 (6) Keithley multimeter 2700 (7) Labview 7.1 interface software and (8) Three stepper motor drives

The locally fabricated components are: (i) Chopper disc (ii) Kaleidoscope (iii) Power supply cabinet for stepper motor drivers (iv) Power supply cabinet for lamp feedback mechanism (v) Lamp holder and (vi) Optical switch for chopper disc.

The photographs of individual components are displayed in Appendix H and their brief descriptions are given in the following sections:

The Radiant Source

The integrating sphere uses artificial light to simulate natural sunlight. With artificial light one can get repeatable readings due to the stable intensity of the light source. Moreover, the artificial light can be used in a laboratory facility where the variable weather conditions cannot affect the experimental results.

The radiant source produces quasi-collimated irradiation of nearly uniform intensity over a broad area at the inlet port of the integrating sphere. The intensity level of the incoming radiation is strong enough that a useful signal can be retrieved. To simulate the sun, a 1000Watt Quartz-Tungsten Halogen FEL Lamp (Ushio Inc. or GE) was used as the radiant source. Its output flux was stabilized by a photo feedback system which controls lamp voltage based on the output of a silicon photovoltaic detector. Radiation from the lamp was directed by a rhodium coated ellipsoidal reflective concentrator (Melles Griot). The concentrated radiation was then focussed on a kaleidoscope section which is simply a square tube with smooth, specularly reflecting mirrored-walls. This section is important to ensure spatial uniformity of the incident radiation. The kaleidoscope output aperture is 3.5 cm x 3.5 cm and the maximum area of illumination at the sample plane is approximately 40cm x 40cm. A Fresnel lens was placed 18 cm away from the kaleidoscope. The fresnel lens is made of PTFE plastic, having high temperature resistance and very low absorptance over the entire solar spectral range. To achieve good light collection efficiency it is desirable to have low f-number of the lens so the diameter of the lens was chosen as 20 cm. The f-number of an optical system expresses the effectiveness of the aperture in relation to the brightness of an image and is quantified

as the ratio of the focal length to the aperture. Smaller the f-number the brighter the image and therefore the shorter the exposure required (Merriam-Webster Inc. 2005). Since such a large lens is not conventional and feasible for a glass lens, a plastic fresnel lens was used. In between the kaleidoscope and the fresnel lens a rotating chopper blocks the incident radiation at the rate of 50 Hz. The chopper is used to switch the light beam on and off repetitively which enables the related instruments to differentiate between useful signal and ambient light.

The Sample Mount

For transmittance measurement the sample needs to be mounted outside the sphere, but in front of and close to its inlet port. The sample mount moves the sample in front of the inlet port of the sphere to measure the sample reading and then moves the sample away from the inlet port to measure the reference signal. The sample mount was traversed horizontally by a lead-screw and stepper motor drive mechanism. This traversing mechanism can position the sample with an accuracy of 1mm.

Moreover, the integrating sphere, monochromator, sample mount, and photo-detector are mounted on a work table that can be swivelled about an axis that passes through the centre line of the inlet port of the integrating sphere. In this way the angle of incidence can be set to any value ranging from 0 deg to 60 deg with an accuracy of 1 deg.

Integrating Sphere

The integrating sphere is a 50 cm diameter hollow sphere coated with barium-sulphate, which provides a surface with very high diffuse reflectance ($\rho \simeq 0.9$) in the UV and visible spectra ($0.25\ \mu m < \lambda < 1.4 \mu m$) but lower reflectance at $\lambda > 1.9$ μm ($\rho = 0.83$) and still lower reflectance as the wavelength increases toward the NIR range ($\rho \simeq 0.77$ at λ =2.5 μm). The spectral reflectivity of the coating is shown in Figure 3.10. Moreover, aging, dust accumulation and natural surface contamination or physical damage can also cause reduction in ρ. In section 3.2

we have seen that ρ strongly influences the response of the integrating sphere. All these effects combined with a weaker signal from the lamp result in a poor signal-to-noise ratio for the photo-conductor to detect useful signals, which causes error in measurements at longer wavelength. Fortunately, most of the energy associated with solar radiation is found at shorter wavelength.

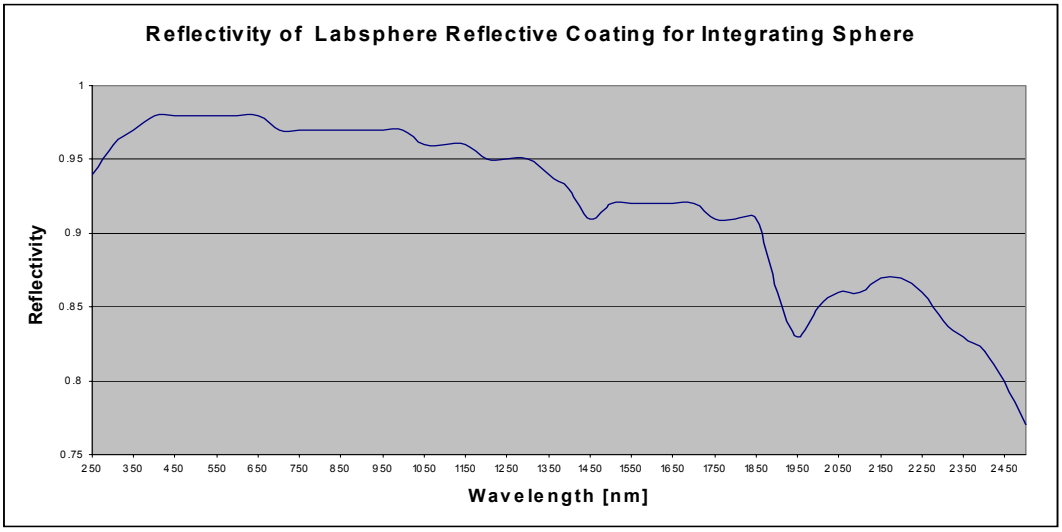

Figure 3.10: Typical Reflectivity of Integrating Sphere Coating (Labsphere Inc. 2005)

A baffle is used in the integrating sphere to prevent the direct viewing of the inlet port by the measurement port. Thus the detector receives only diffuse and hemispherically-integrated light after the second reflection from the sphere wall. The disadvantages of the baffle are additional signal loss due to its absorptance and its non-ideal performance since the sphere can no longer be considered as a perfect sphere. In order to minimize these effects, baffles should be as small as possible and diffuse in nature, coated with the same reflective coating as that of the sphere wall. It is also desirable to minimize the number of baffles in the integrating sphere (Hanssen et al. 2003).

Monochromator

The monochromator is an optical device that splits light into spectral components as shown in Figure 1.12. From the exit slit of the monochromator, light of a narrow spectral band strikes a photo-detector. In the BAI-IS the monochromator is a mirror-collimated littrow-style, thirty-degree quartz prism, taken from a Beckman DU spectrophotometer. Similar devices may use a quartz prism or a diffraction grating as a dispersing medium in the monochromator. A grating is less expensive and provides higher dispersion. The main disadvantage of a grating is that it scatters light more than a prism which creates unwanted reflections and introduces spectral impurity (Cary and Beckman 1941). Moreover, with a single diffraction grating it is not possible to cover the entire solar spectrum without incorporating order-sorting filters (Milburn 1994). The prism can cover the total solar spectrum and its angle can be changed with the help of mechanical linkages. The monochromator can disperse light between wavelength 0.2 μm and 2.0 μm.

The stepper motor positions were calibrated to set the wavelength scale. The wavelength is expressed as the function of prism angle and refractive index. The relationship between the wavelength and the stepper motor position is described by the spline curve fit is shown in Chapter 5. Exit slit width is controlled by another stepper motor to achieve the appropriate resolution and signal strength. The monochromator output is collected via a pair of plano-convex lens to focus the radiation on the active area of the detector.

The slit width affects the amount of light as well as the range of wavelengths or resolution detected by the photo-sensor. A wider slit opening enables more light to pass and results in a stronger signal. Resolution is an indicator to quantify the spectral purity of radiation that leaves the monochromator. Resolution is the ability of the monochromator to distinguish between two closely spaced wavelengths. As slit width increases, the resolution and the purity of optical measurement decreases which is shown in Figure 3.11. In Figure 3.11, the slitless condition represents a very wide slit opening.

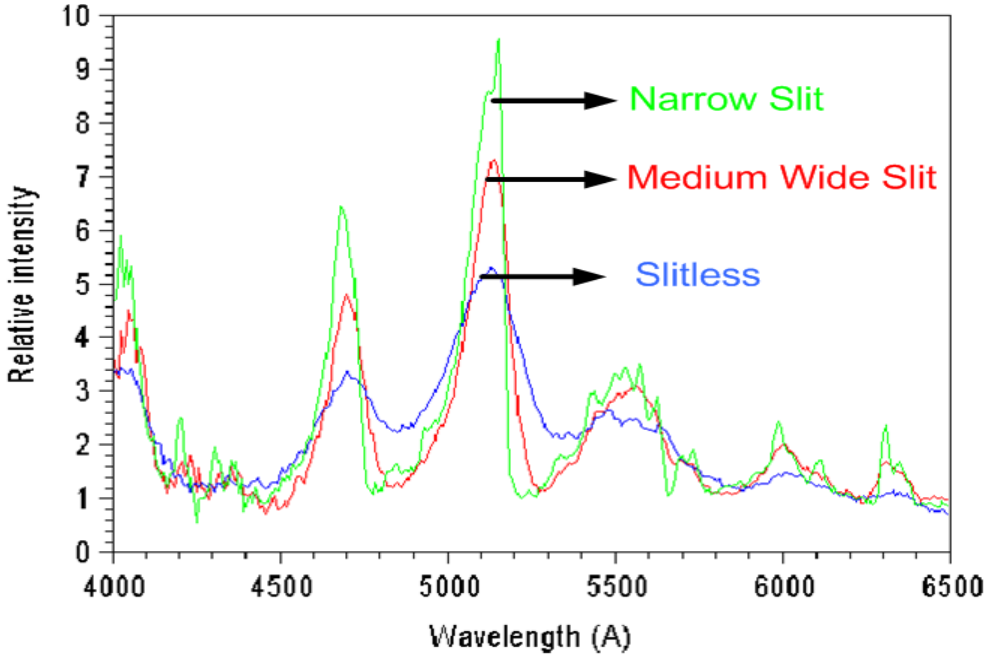

Figure 3.11: Resolution vs Slit Width (AstroSurf 2001)

Dispersion: When light strikes a prism it spreads light into its component wavelengths due to change in index of refraction at the prism surface. This optical phenomenon is known as dispersion. The emerging light from the monochromator does not comprise a single wavelength but represents the component wavelengths of the incident beam. The linear dispersion, d_λ, defines the width of the band of wavelength per unit of slit width. It describes, spatially "how far apart two wavelengths are." The linear dispersion, d_λ is also known as the "half-intensity band-width" and carries units of $\left(\frac{\mu m}{mm \text{ of slit width}}\right)$. Figure 3.12 shows d_λ can be tabulated for specific wavelengths (Beckman Instruments 1950). The "half-intensity band width" refers to the span of wavelength leaving the monochromator which contributes at least half as much energy as does the wavelength with the greatest energy. A smaller value of this bandwidth corresponds to narrow peaks and good energy resolution. This factor is constant for a grating but varies with wavelength for a prism (Jacobs and Kreis 1964). This is why, in general, the slit width needs to be adjusted at different wavelengths.

Resolution: It is very important to evaluate the limiting bandwidth of the monochromator at different nominal wavelengths. This limiting bandwidth is known as the spectral resolution, $\Delta\lambda_{\text{min}}$. This can be evaluated from d_λ. The Beckman DU monochromator has a limiting slit width of 0.1 mm below which if the slit is further narrowed, the spherical aberration and low energy of incident radiation will preclude signal measurement. By definition, at a certain nominal wavelength, if the half intensity band-width is multiplied by the limiting slit-width, it will provide the limiting bandwidth or the resolution ($\Delta\lambda_{\text{min}}$), specification of the monochromator (Pini 2003). Therefore,

$$\Delta\lambda_{\text{min}} = d_\lambda \times W_{slit-\text{minimum}}$$

It is obvious that in general $\tau(\lambda)$ will depend on slit width, because the detector would respond to the group of wavelengths, $\Delta\lambda$, transmitted through the slit opening. However, for a material that is not spectrally selective $\tau(\lambda)$ will not be a function of the slit width. In that case, to have a strong signal output, it is recommended to use the widest slit possible for all wavelengths.

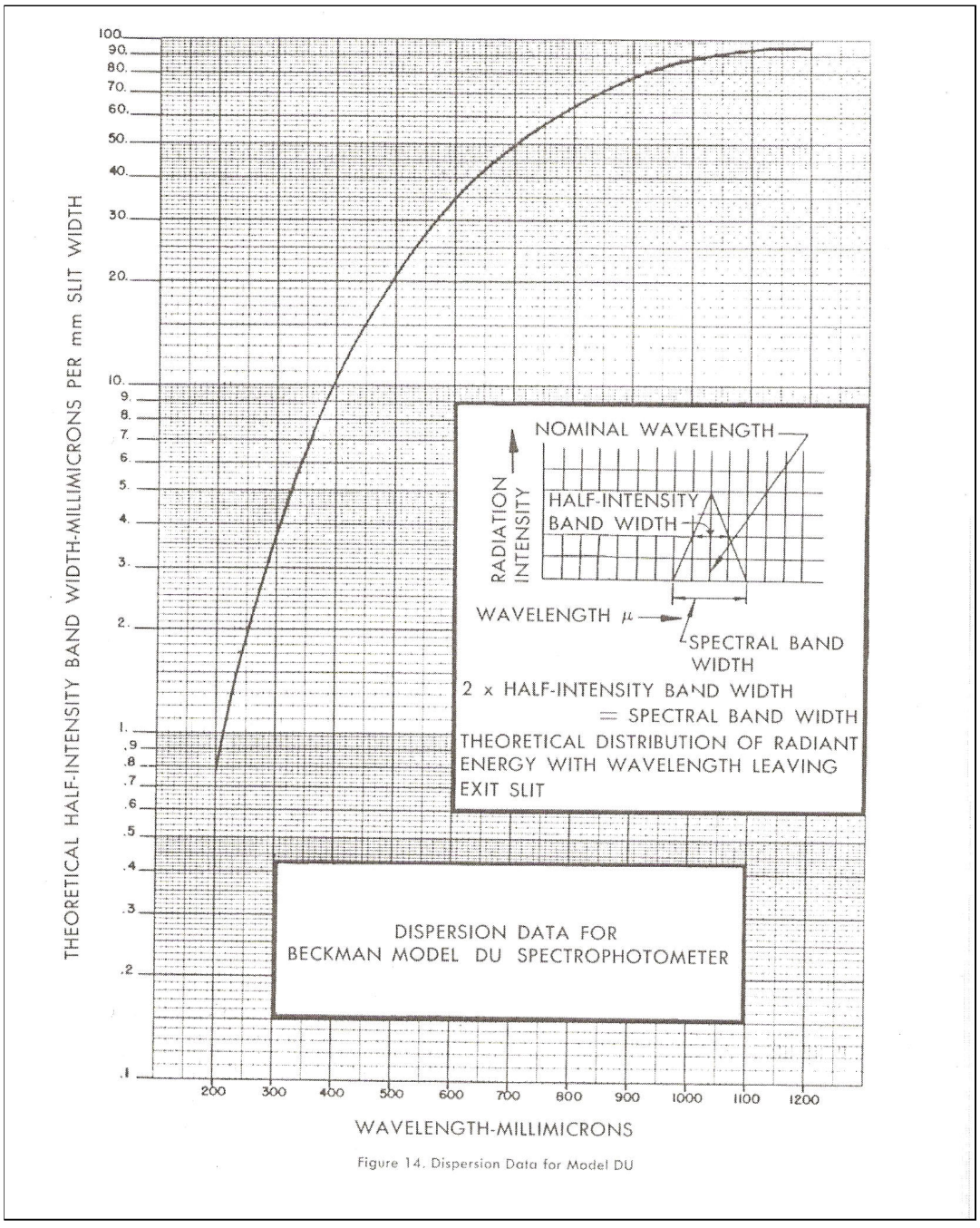

Figure 14. Dispersion Data for Model DU

Figure 3.12: d_λ versus λ for the Beckman DU Spectrophotometer (Beckman Instruments 1950)

At the fixed slit width of 2 mm, the spectral resolution at λ =400 nm can be calculated as follows:

d_λ=0.010 $\frac{\mu m}{mm}$ [From dispersion chart of DU spectrophotometer]

$\Delta\lambda_{\min} = 0.010 \left[\frac{\mu m}{mm}\right] \text{x } 2\ [mm] = 0.2\ \mu\text{m}$

Detector System

The radiation detector system comprises photo-detector, optical chopper and lock-in amplifier.

Photo-Detector: The desirable attributes of photo detectors are: fast and linear response; high signal-to-noise ratio; and low noise-equivalent-power. The model UVS/PBS-025/020-H (from Electro-Optical Systems Inc., USA) is a combination of photo-detector/receiver which has both a photo-diode and a photo-conductor sandwiched together. The Silicon (Si) photo-diode responds to the UV and VIS wavelength range (0.2 μm to 1.0 μm) and the Lead Sulphide (PbS) photo-conductor to the NIR wavelength range (1.0 μm to 2.6 μm). This module operates at 15 Volt-DC power supply consuming approximately 50 mA. The output signal from the detectors is delivered by two BNC terminated shielded signal cables. Each output is connected to an input location of the lock-in-amplifier.

The Si photo-diode is a P-N junction-semiconductor which is commonly used in radiometry, photometry and calorimetry. It has two junctions of dissimilar materials, which generates positive and negative charge carriers if incident radiation strikes the junctions. This causes photocurrent to flow through the external circuit that is proportional to the amount of light falling on the photodiode (Budde 1983).

The photoconductors are semiconductors made of nonmetallic solids whose conductivity increases when exposed to electromagnetic radiation. They have certain amounts of conduction electrons available at room temperature. With incident irradiation the energy of the absorbed photons releases additional charge carriers within the material by moving electrons from tightly bound valence state to conduction state, which lowers its resistance and increases conduction (Budde 1983).

Optical Chopper: The rotating-disc optical chopper (Model: Scitec 300CD) is used to convert the detector output signal into an AC signal. It consists of chopper control unit, chopping head, reference opto-pick-up unit and chopper disc. The chopper blade is a 13-inch diameter disc made of a thin metal sheet with 4 slots. The chopping frequency is set manually. The output from the reference pick-up is a pulsed voltage at chopping frequency which is used as a reference input by the lock-in-amplifier.

Lock-in-Amplifier (Scitec: Model 410): This amplifier processes signals which are buried in a relatively high level of noise and interference. The experiment was carried out in a room where ambient light is present. The lock-in-amplifier is used to remove the electronic noise and the interference of ambient light. This instrument along with the optical chopper separates the useful signal in response to the light emitted by the radiant source only.

The chopper blade has alternate open and blind plates which rotate in front of the kaleidoscope. Whenever the blind plate closes the opening only the ambient light enters the sphere as shown in Figure 3.13. Both the ambient light and the collimated light from the radiant source enter the sphere when the blade clears the kaleidoscope opening as shown in Figure 3.14. The Lock-in-amplifier measures the difference between these two signals to provide the useful reading (Figure 3.15). The lock-in-amplifier is also equipped with low pass filters to filter out electronic noise.

The key component of a lock-in-amplifier is the phase sensitive detector (PSD), supported by pre-amplifiers, post-detection amplifiers and a complete reference processing section. The basic concept is to retrieve a weak signal of known frequency from many strong noisy signals of different frequencies.

The PSD or demodulator multiplies the pre-amplified input signal and the reference signal, which either add or subtract the frequencies. If the input signal and the reference signal are of the same frequency then the difference in frequency becomes zero and a DC output signal is generated and this output signal is proportional to the amplitude of the input signal and the cosine of the phase difference between the signals. The noise signals will still be present at the output of the demodulator

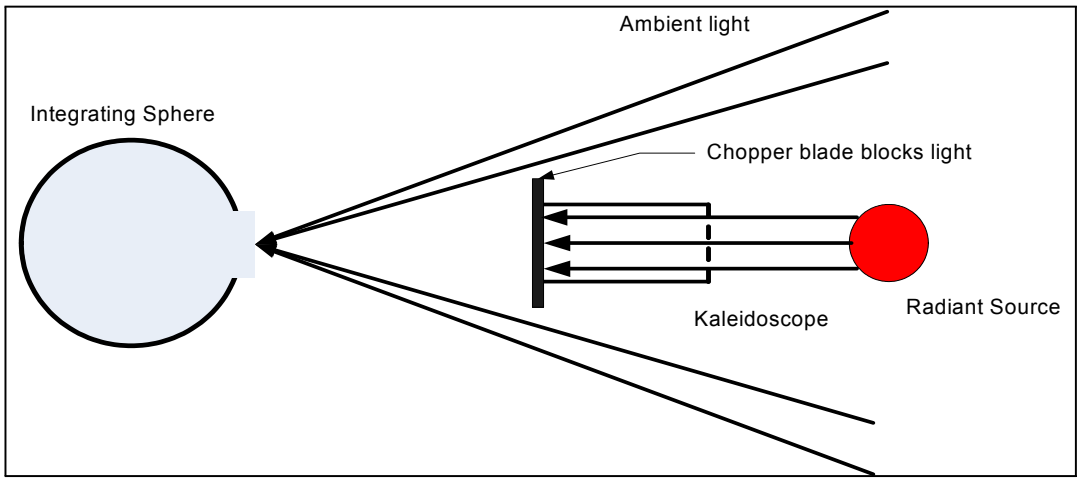

Figure 3.13: Chopper in Blocked Position

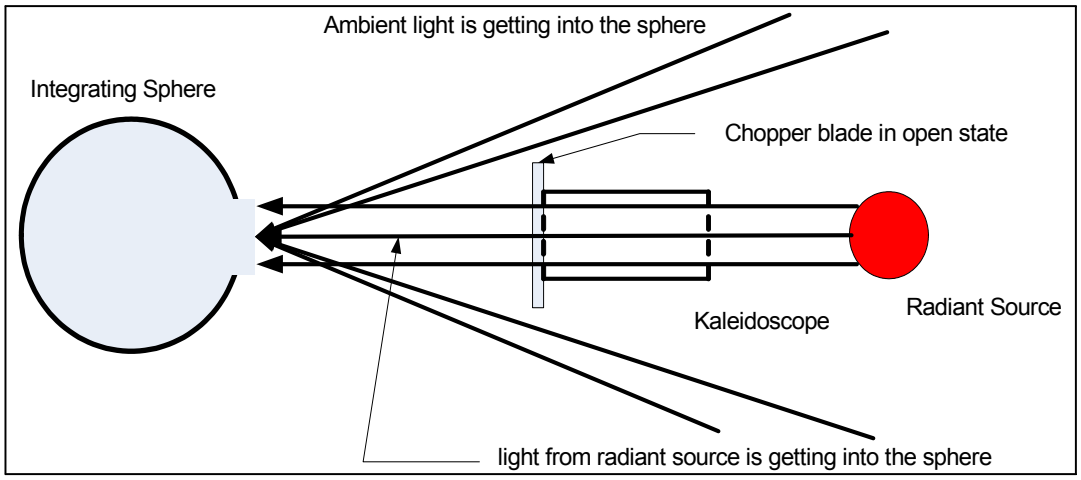

Figure 3.14: Chopper in Open Position

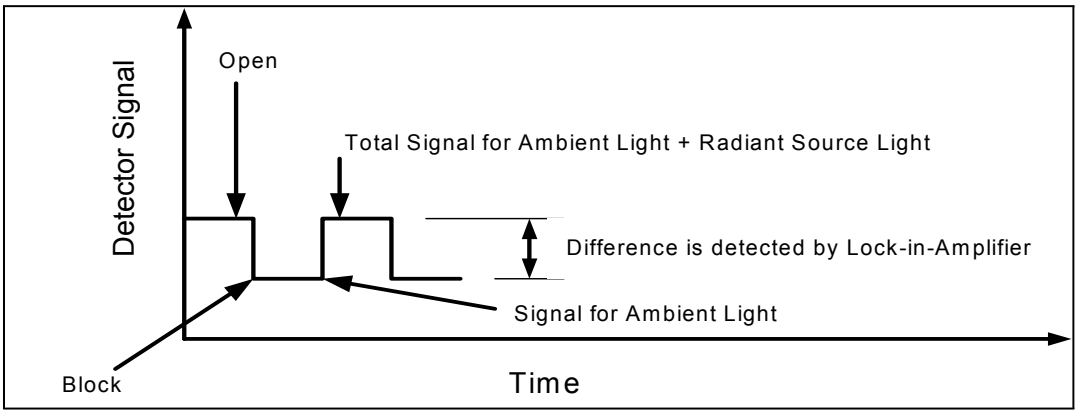

Figure 3.15: Basic Function of Lock-in-Amplifier

and may have amplitudes 1000 times larger than the DC offset but of different frequencies.

Low Pass Filter: As the various noise components on the input signal are at different frequencies to the reference signal their resultant frequency will be non-zero and will not contribute to the DC level of the output signal. This DC level (which is proportional to the input signal) can now be recovered by passing it from the demodulator through a low pass filter. The time-constant on the lock-in-amplifier sets the cut-off frequency for the low-pass filter (Boston Electronics Corporation 2006).

The Control System

The apparatus uses Labview 7.1, a graphical program, and a desktop personal computer as its primary control units. The two sets of output from the lock-in-amplifier for both sample and reference readings are recorded and stored using a data acquisition system. The Labview software is used as an interface to store the results in data files which are later used to calculate the corresponding spectral transmittance. Labview programmes are also used to control the stepper motors. These stepper motors are used to adjust prism angle for wavelength setting, to set exit slit width and to operate the sample traversing mechanism. Currently, the

detector amplifier gain is controlled manually. The lock-in-amplifier is also tuned manually to attain sufficient input signal gain and the appropriate phase shift and time-constant for retrieving useful signals.

3.3.3 Solar Optical Properties

Spectral readings are preferred for any sample to determine whether optical properties vary with wavelength. If the surface of interest is not spectrally selective then it is not necessary to take spectral readings. For design purposes, the weighted average value of a measured property are calculated. In order to cover the total relevant spectrum, spectral measurements were recorded at suitable wavelengths and then the spectrally averaged quantity was calculated. For example, for calculating solar heat gain, transmittance of a material can be averaged over the solar spectrum ranging from 0.3 μm to 3 μm. For daylighting calculations, the photometric range (0.38 μm to 0.76 μm) of the solar spectrum is considered (ASTM E 972-96 – Re-approved 2002).

The experiments were conducted with artificial light that only approximates the wavelength distribution of solar radiation. Since $\tau(\lambda)$ or $\rho(\lambda)$ is not a function of source spectrum the same optical property of a material can be measured with different apparatus having different radiant sources. Therefore, the most important benefit of taking spectral readings is to ensure that the spectrally-averaged optical properties are independent of the quality of the radiant sources.

Each optical property changes with the direction of incident radiation. A directional-directional property specifies a quantity for single incidence angle having only a single direction of transmitted or reflected radiation. But in reality radiation incident on a shading layer at a certain angle transmits or reflects in numerous directions. However, directional-directional quantities require numerous measurements over the hemispheres of all reflected or transmitted directions. The scope of this research was limited to the measurement of the directional-hemispherical quantity.

3.4 Cary-5000 Spectrophotometer

Figure 3.16: UV-VIS-NIR Spectrophotometer Cary 5000 (Varian Inc. 2004)

The Cary 5000 is a dual-beam spectrophotometer with a small integrating sphere (sphere diameter =110 mm). The Cary 5000 is a commercially available apparatus used to measure optical properties of thin, planar, and spatially uniform samples.

In this study the Cary 5000 apparatus was used to measure the component properties (e.g. the sheer fabric and blind slat of the sheer blind). The component properties are required to calculate the "effective" properties of the shading device assembly by using analytical models. The BAI-IS was used to measure the "effective" optical properties of the shading device assembly.

The Cary 5000 can measure spectral total and diffuse reflectance ($\rho_{t,\lambda}$ and $\rho_{d,\lambda}$) and spectral total and diffuse transmittance ($\tau_{t,\lambda}$ and $\tau_{d,\lambda}$). On the other hand, the BAI-IS is used to measure total spectral transmittance ($\tau_{t,\lambda}$) of a thick, non-uniform, scattering sample assembly (i.e., sheer blind assembly).

The Cary 5000 was used to measure the spectral properties of a holmium oxide reference sample, blind slat and sheer fabric material. It is capable of covering a

wavelength range from ultraviolet (0.2 μm) to the near infrared (2.5 μm) at normal and off-normal incidence. The optical design of the Cary 5000 is shown in Figure 3.17 (Varian Inc., 2002). The Cary 5000 uses two photo detectors, a photomultiplier

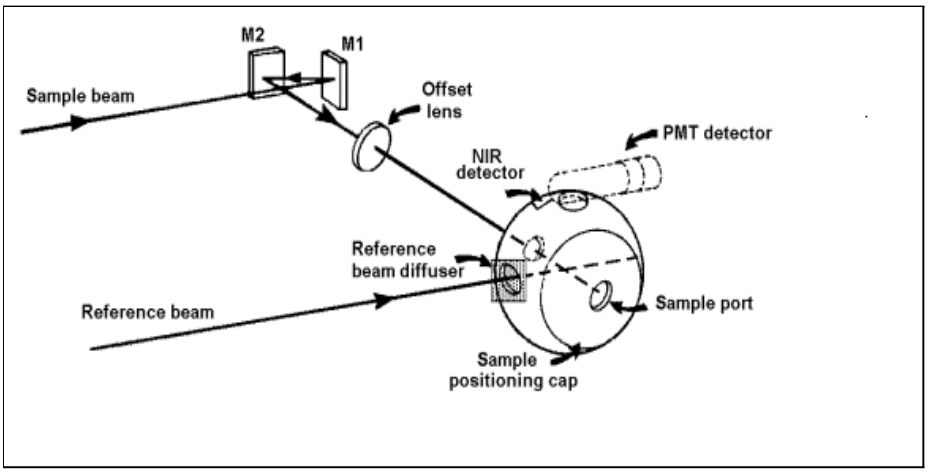

Figure 3.17: Dual Beam Design of Cary 5000 Spectrophotometer (Varian Inc., 2002)

tube (PMT) and photoconductive sensor (PbS). The PMT shows a liner response over a wavelength range of 0.2 μm to 0.8 μm and the PbS sensor shows a linear response over wavelength range of 0.8 μm to 3.2 μm. These detectors are alternately illuminated by sample and reference beams and are switched automatically according to the correct wavelength response.

The ANSI/ASHRAE 74-1988 standard suggests that measuring spectral transmittance or reflectance by using integrating sphere requires taking account for measurement correction for 100% and zero line errors. Cary 5000 uses 0% and 100% baseline calibration procedures which ensure equipment accuracy of $\pm$0.1 %. It is noted in the standard that, "the non-ideal 100% line occurs due to variations in signal from the two normal beams which are wavelength dependent. Similarly, the beam cross talk, light scattering or leaks and detector noise lead to a non-ideal zero line". The spectral optical property can be calculated as:

$$\rho_\lambda \text{ or } \tau_\lambda = \frac{M_\lambda - Z_\lambda}{100_\lambda - Z_\lambda}$$

where,

ρ_λ or τ_λ= Measured spectral reflectance or transmittance.

M_λ = signal recorded with the sample over the inlet port.

100_λ = 100 % baseline reading.

Z_λ = Zero baseline reading.

The detailed operating procedure for both transmittance and reflectance measurement is available in the operation manual from Varian Inc., 2002.

3.5 Calibration of the BAI-IS

Calibration of the BAI-IS involves checking the performance accuracy of the individual components. The radiation intensity and stability of the radiant source are important to obtain stable signal and sufficient signal-to-noise ratio. The accuracy of the wavelength scale and the adjustment of correct slit width for a specific wavelength provide the optimum performance of the monochromator.

At first the lamp needs to be placed at the focal point of the ellipsoidal concentrator. The lamp holder needs to be aligned properly in the lateral and longitudinal directions so that the maximum flux is obtained at the inlet port of the integrating sphere.

The mechanical alignment of optical path between radiant source, kaleidoscope and sphere inlet port is critical to get proper directional response at different profile angles. The optical path was aligned by using a laser diode and a specular reflecting mirror following the detailed procedure described by Jiang (2005).

The lock-in-amplifier is also calibrated with a standard signal generator to confirm its proper functionality as described in Appendix A.

Another important alignment is to focus the output radiation from the exit slit of the monochromator on the photo-detector active area. This is done with the

help of a pair of plano-convex lens which are placed between monochromator and the photodetector as shown in Figure 3.18. The first lens focuses the out-going radiation such that the image will look like a thin vertical line. The second lens focuses this line onto a small squared area which is incident on the active area of the photo detector. A small piece of white paper is temporarily placed on the detector active area and the centre of its sensing element is drawn on the paper with a pencil. With the light from the lamp the detector is placed in front of the monochromator in such a way that the beam of light through the sphere, monochromator and two pair lenses is focussed on the mark drawn on the paper.

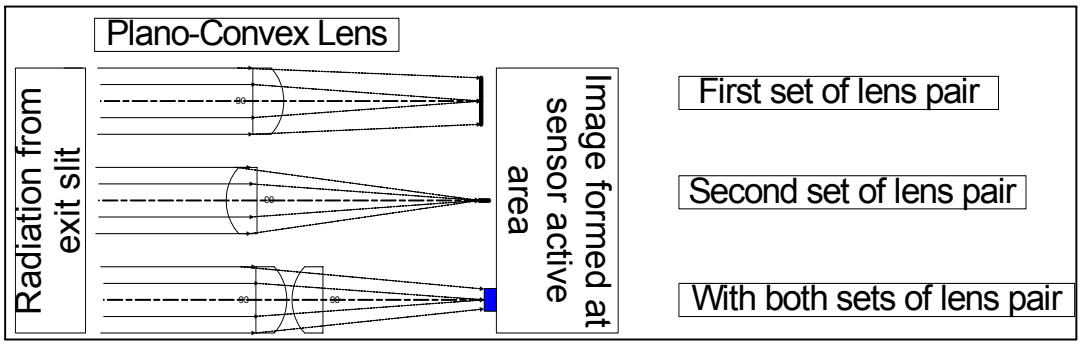

Figure 3.18: Lens Configuration at the Exit Slit of Monochromator

3.5.1 Radiant Source Calibration

The temporal and spatial stability of incoming radiation are critical for precision and accuracy (Platzer 1992). Temporal drift was measured by recording the photo detector reading over an hour at a certain wavelength (say, at $\lambda = 0.8$ μm).

For verifying spatial uniformity of the radiant source, a calibrated pyranometer (Eppley Black and White Pyranometer, Model: 8-48) was used to measure the radiant flux at the sample mount plane. The readings were taken at several points in the X-Y direction (keeping the origin at the center of the inlet port of the sphere). Two sets of such readings were taken - with and without the kaleidoscope to prove the effectiveness of the kaleidoscope. The kaleidoscope improves the spatial

uniformity of incident flux to within 10% variation over most of the illumination area (Milburn 1994).

The radiant flux level at the sample-mount was measured by using the same pyranometer. To achieve spatial and directional uniformity of irradiance the sample mount was positioned approximately 4 m away from the lamp. At 115V DC input to the lamp the average irradiance is approximately 95 W/m^2 at 50% duty cycle of the rotating chopper wheel. This level of radiant flux is available at the plane of inlet port over an area of 50cm x 50cm, which is sufficient to achieve satisfactory detector signal-to-noise ratio.

The radiant flux distribution of the 1000 Watt FEL lamp is presented in Figure 3.19. Note that the radiant source does not have high energy content for longer wavelengths, especially at $\lambda > 1.8$ μm and only 20% of the total energy from this radiant source is found at $1.1 < \lambda < 2.2$ μm (LOT-Oriel Group 2007). Ideally, the radiant source should include all of the solar wavelengths but need not reproduce any specific solar spectrum because properties are being measured at many wavelengths and can be recombined according to any desired solar spectrum or spectral analysis. The comparison of solar spectrum and 1000 Watt FEL lamp spectrum is shown in Figure 3.20.

3.5.2 Monochromator Calibration

The next step is to verify whether the correct wavelength is attained as the stepper motor changes the corresponding angular position of the prism inside the monochromator. This is verified by taking spectral readings of a holmium-oxide calibration glass with the Cary-5000 and comparing them with the corresponding BAI-IS readings. The holmium oxide was used as a reference material for wavelength calibration because the material has well defined and documented absorptions peaks. The glass sample is smooth, thin and homogeneous: length 51.3 mm x width 50.7 mm x thickness 2.0 mm.

Spectral transmittance of the holmium oxide glass was measured by the BAI-IS and by the Cary 5000 spectrophotometer over wavelengths $0.4 < \lambda < 2.0$ μm at

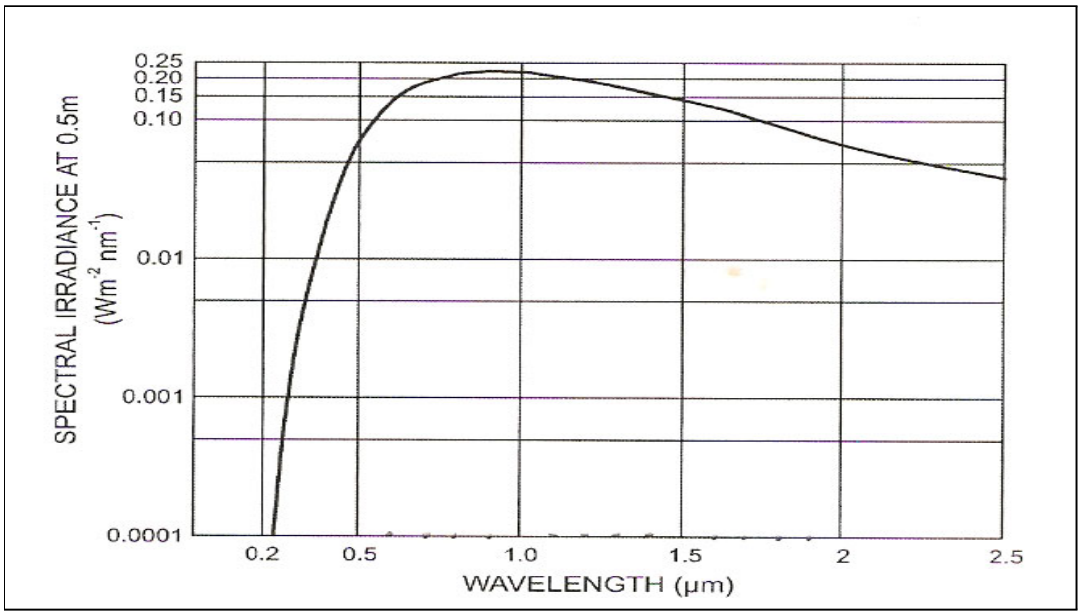

Figure 3.19: Quartz Tungsten Lamp (LOT-Oriel Group 2007)

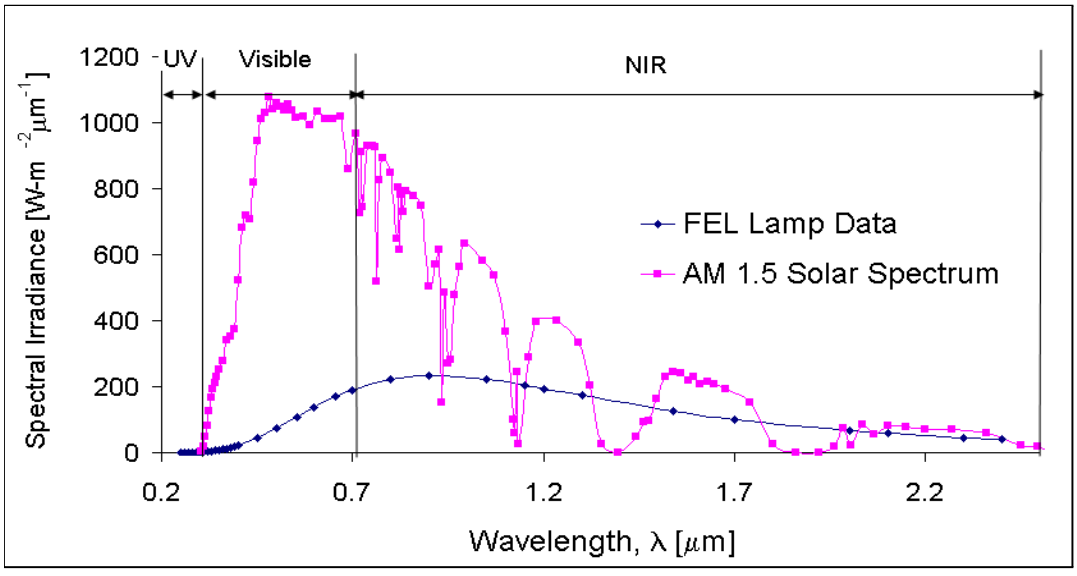

Figure 3.20: Comparison of Solar Spectrum at AM 1.5 Vs Spectral Irradiance of FEL Lamp (ASTM E 891 1982 and Schneider et al. 1998)

normal incidence. The measured values are plotted in Figure 3.21. The measurement data from the BAI-IS are excellent match with the results recorded by the Cary 5000. The weighted average solar transmittance of the glass is found to be $\tau_{Solar} = 0.854$ from Cary 5000 and $\tau_{Solar} = 0.868$ from the BAI-IS. The slit width was set at 2 mm. It is noted that the spectral resolution ($\Delta\lambda_{\min}$) of Cary 5000 is 1×10^{-5} μm and that of BAI-IS is 0.2 μm (Varian Inc. 2005)

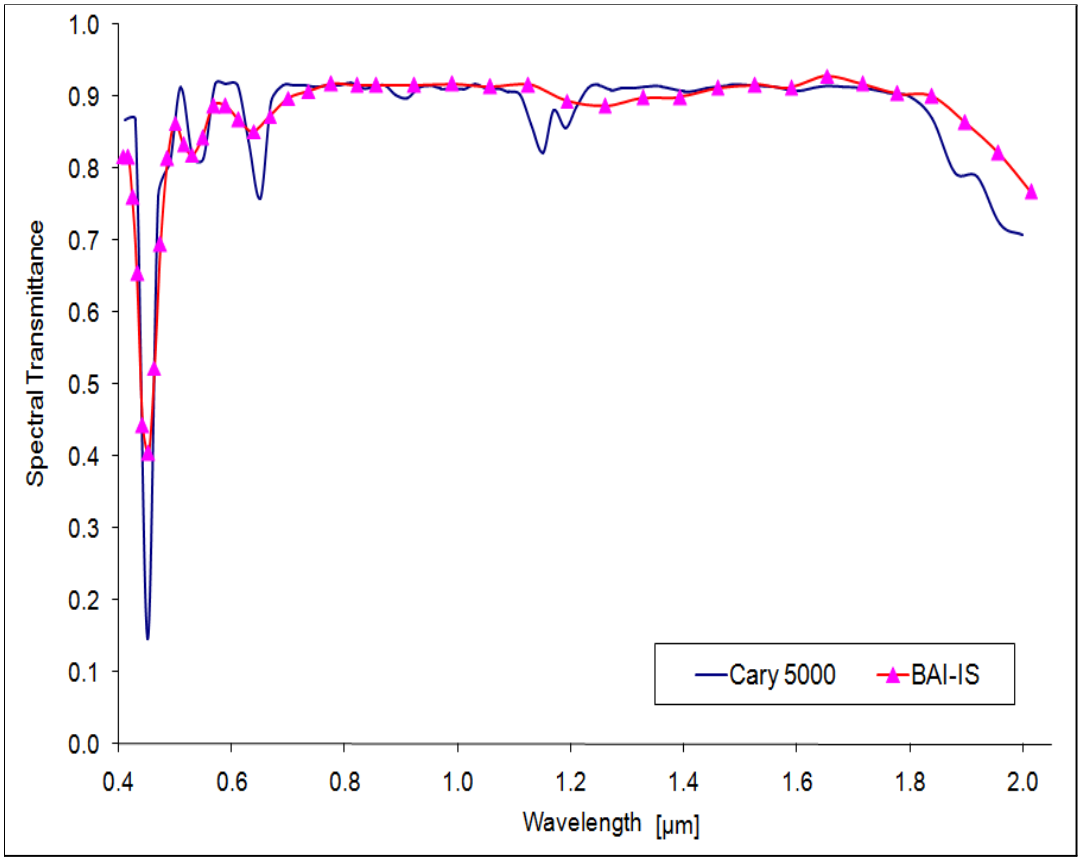

Figure 3.21: Spectral transmittance at normal incidence for Holmium Oxide glass filter using Cary 5000 and BAI-IS apparatus.

Chapter 4

Results and Discussions

4.1 Introduction

The experimental results are divided into two major parts:

(1) Results that compare solar transmittance of a venetian blind measured on the BAI-IS and based on those calculated from a relevant venetian blind model,

(2) Solar transmittance of a sheer blind using the BAI-IS and comparing to results obtained from multi-layer glazing/shading array model.

4.2 Sample Description

In this experiment, solar transmittance was measured for two types of louvered shading devices: (a) a venetian blind and (b) a sheer blind. To formulate the analytical model for these types of shading devices, the required inputs can be divided into four major categories:

1. Geometric parameters;
2. Optical properties of slat material;
3. Angular specification of incoming and outgoing radiation; and
4. Calculation parameters and formulation of model.

Geometric Parameters and Angular Specification of Radiation

The geometric parameters and angular specifications of incoming and outgoing radiation are summarized in Section 1.3 and shown in Figure 1.4 and Table 1.1.

The quality of the louvered blind test sample is important. The slat spacing, slat angle, slat width and slat thickness need to be uniform and accurate. The test specimen was fabricated as carefully as possible.

The specimen holders were made of rigid rectangular frames. For a venetian blind the frames were constructed from acrylic blocks and for the sheer blind the frames were built from wood. The frame sizes were selected to ensure that, during off-normal measurements, the frame did not cast a shadow on the inlet port of the integrating sphere. The sample holders are shown in the Figures 4.1 and 4.2.

Figure 4.1: Sheer Blind Sample

For venetian blind sample the Aluminium slats were installed without any slat deformation in accurately machined slots along the interior wall of the frame. The slots have dimensions of 2.54 mm (depth) x 1.2 mm (width) x 15 mm (length).

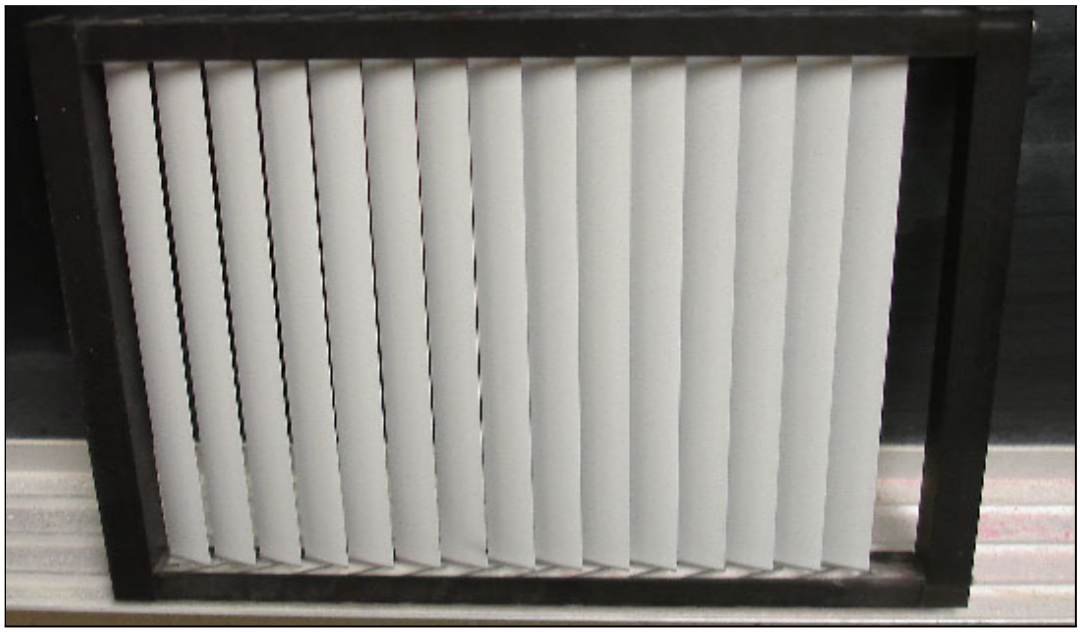

Figure 4.2: Venetian Blind Sample

For the sheer blind sample, the same fit was not possible because fabric slats and sheer facings are flexible. That is why the slots were not machined but at a certain slat angle the fabric slats were fixed on the wooden frame by using thumbtacks at two ends. In this way the fabric slat is kept tight. Since the thumbtacks were driven manually the slat spacing and slat angles were not as accurate as those in the venetian blind samples.

Another important simplification needs to be discussed about the test sample for the sheer blind. The sheer blind which is commercially available, has polyester fabric slats with slat width and spacing ranging from 50 mm to 100 mm. Also the fabric slats assume a wavy shape at different slat angles as shown in Figure 4.3.

At the same time the specimen thickness or depth must be limited to ensure that a sufficient number of slats are illuminated by the radiant source and the transmitted radiation is representative of the overall product. The BAI-IS was successfully used to test a 15 mm slat width with the venetian blind and a 16.7 mm slat width was used for the fabric slat test sample. At this slat width it is

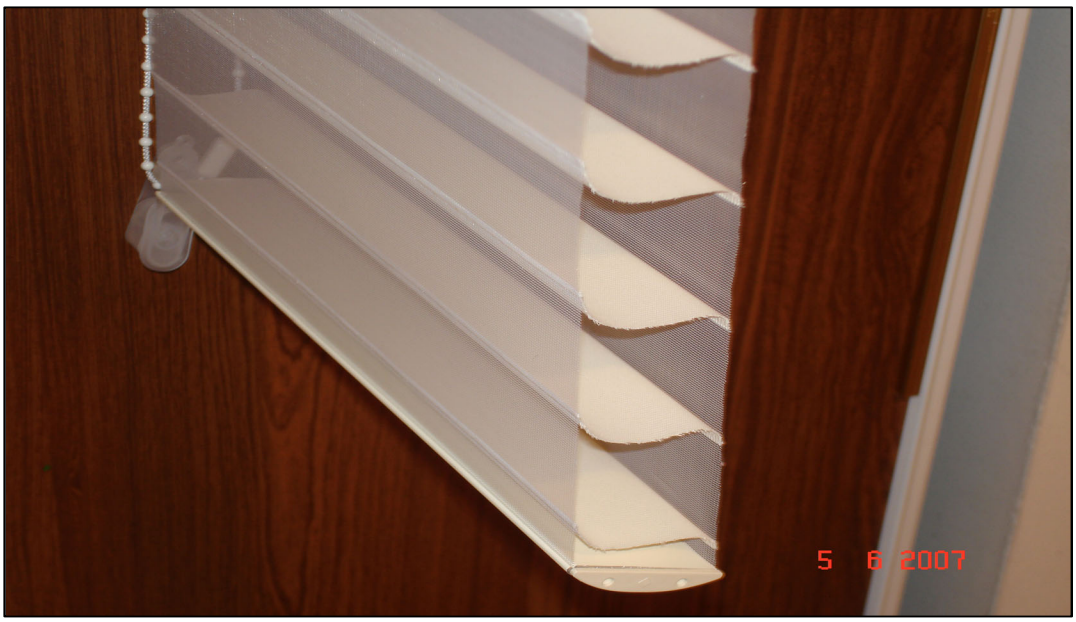

Figure 4.3: Wavy Contour of Fabric Slat on a Sheer Blind

not possible to reproduce the wavy cross section of the fabric slat for the custom-made sheer blind specimen. This is why, the fabric slats were modelled as flat slats. Since fabric thickness is considerably higher with respect to slat spacing a thickness correction was considered for the fabric slat model.

Optical Properties

The effective optical properties of the shading device assembly were measured by using the BAI-IS.

The optical properties of individual components are the primary inputs to calculate the effective optical properties of the shading / glazing assembly. These component properties were obtained by using the Cary-5000.

4.3 Measurement Using the BAI-IS

The measurement procedure for using the BAI-IS is discussed in Appendix J.

The BAI-IS measurement provides an effective optical property for one side of a louvered blind assembly. The sample blind was mounted parallel to the inlet port of the integrating sphere as shown in Figure 4.4.

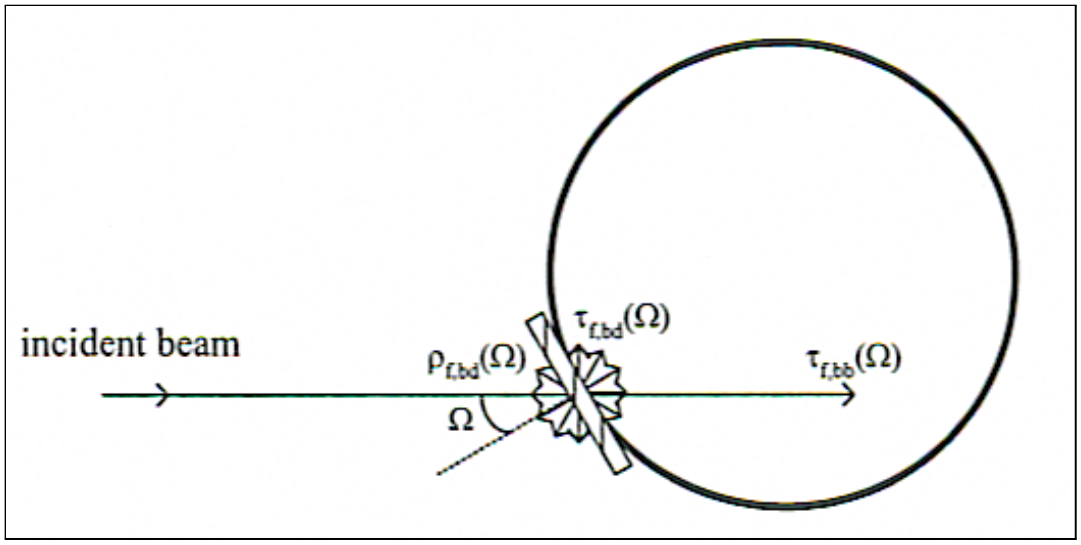

Figure 4.4: Total Transmittance Measurement Using the BAI-IS

With this configuration the total transmittance, $\tau_{f,t}(\Omega)$, of the sample can be measured (Youngberg 2000, Kotey 2005). The total transmittance is the sum of beam and diffuse components passing through the sample.

$$\tau_{f,t}(\Omega) = \tau_{f,bb}(\Omega) + \tau_{f,bd}(\Omega)$$

4.4 Solar Optical Properties of Glazing and Shading Layers

Solar optical properties of all the components of a window system are measured to estimate solar gain through the window. To locate and quantify optical properties for shading devices, analytical equations are formulated with certain simplifying approximations for ease of modelling, computational ability and data availability. It can be assumed that the incident radiation is unpolarized and only comprises beam radiation. The solar optical properties have specular and diffuse components. Shading layers are treated as two-dimensional layers parallel to the glazing layer(s) that have close thermo-optical contact with each other.

Incident Beam Radiation

The incident beam radiation on a plane, specular glazing layer leaves the layer as specularly reflected or transmitted radiation. This is why only three solar optical properties are required to describe a glazing layer:

(1) beam-to-beam reflectance from the front surface, $\rho_{f,bb}$

(2) beam-to-beam reflectance from the back surface, $\rho_{b,bb}$ and

(3) beam-to-beam transmittance. τ_{bb}.

It is known that beam-beam transmittance for front and back side of the glazing layer must be equal (Wright 1998). These three optical properties vary with wavelength, incidence angle and polarization.

In contrast, the incident beam that strikes any of the shading layers, has two parts when it leaves the layer:

(a) specularly transmitted and reflected portion and

(b) diffusely transmitted and reflected portion

As a result four additional beam-to-diffuse optical properties are necessary to characterize the shading device layer. Another exception for the shading layer is that, for beam-to-beam transmittance from the front and back side of the layer do

not necessarily have same value ($\tau_{f,bb} \neq \tau_{b,bb}$) (Wright and Kotey 2006). Therefore, a shading layer is characterized by the following eight properties in response to incident beam radiation as shown in Figure 4.6:

(1) beam-to-beam reflectance from the front surface, $\rho_{f,bb}$

(2) beam-to-beam reflectance from the back surface, $\rho_{b,bb}$

(3) beam-to-beam transmittance from the front surface, $\tau_{f,bb}$

(4) beam-to-beam transmittance from the back surface, $\tau_{b,bb}$

(5) beam-to-diffuse reflectance from the front surface, $\rho_{f,bd}$

(6) beam-to-diffuse reflectance from the back surface, $\rho_{b,bd}$

(7) beam-to-diffuse transmittance from the front surface, $\tau_{f,bd}$

(8) beam-to-diffuse transmittance from the back surface, $\tau_{b,bd}$

Incident Diffuse Radiation

For diffuse incident radiation on both the glazing and shading layers, the relevant optical properties are diffuse-diffuse reflected radiation on front and back side of the layer ($\rho_{f,dd}$ and $\rho_{b,dd}$) and diffuse-diffuse transmitted radiation (τ_{dd}). Diffuse-diffuse transmittance for front and back side of the layers must be equal. The relevant optical properties of glazing and shading layers are shown graphically in Figure 4.5 and 4.6 respectively.

In summary, a glazing layer is characterized by only six properties but a shading layer needs eleven solar optical properties.

Venetian Blind Model

In the venetian blind model (Kotey et al. 2007) each slat is divided into two sections with respect to beam radiation: illuminated and shaded portions. The fluxes of diffuse radiation are accounted for by using a net radiation technique to derive the beam-diffuse optical properties. In addition a correction is applied to account for slat thickness. Knowing the geometric parameters and the slat properties the effective optical properties of the blind layer can be calculated.

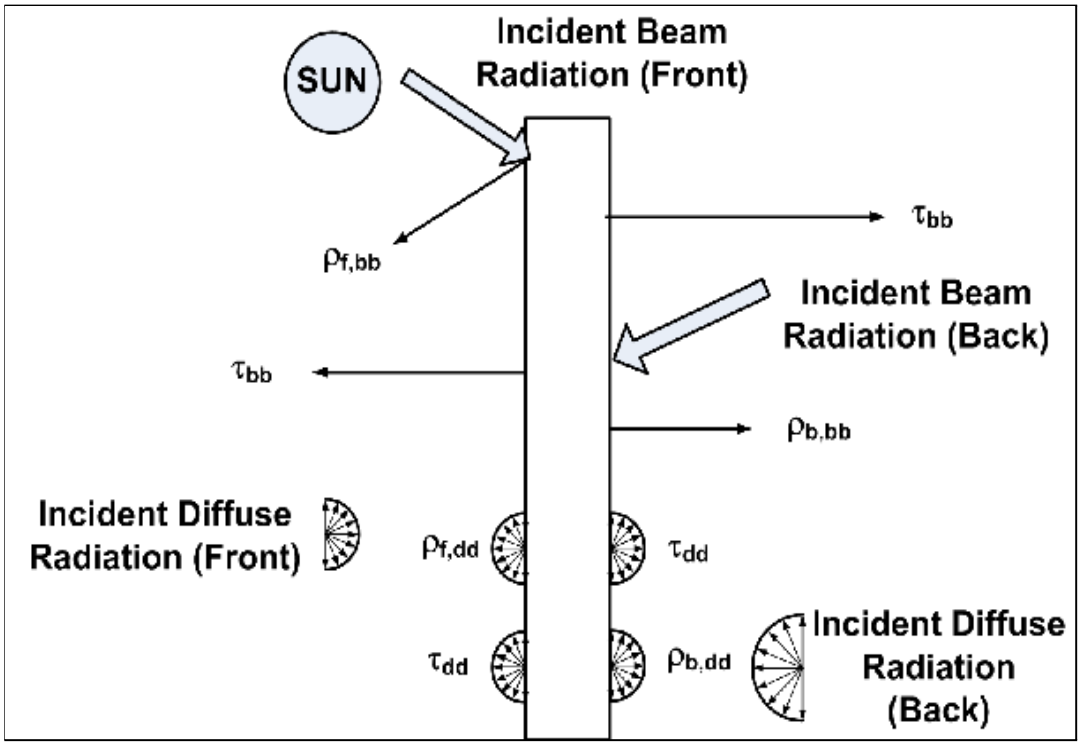

Figure 4.5: Optical Properties of a Glazing Layer

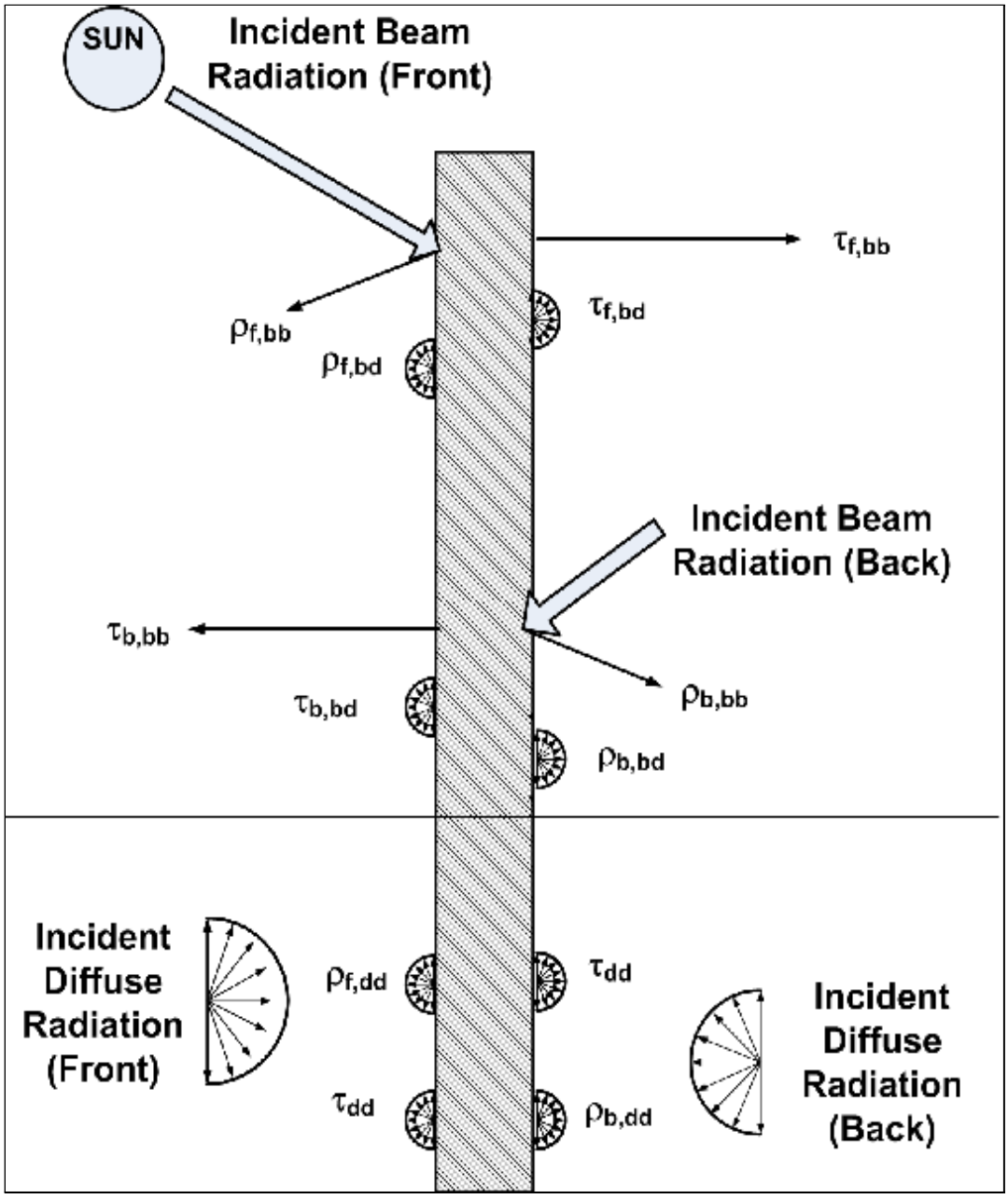

Figure 4.6: Optical Properties of a Shading Layer

4.5 Comparison of Experimental Results with Analytical Models

Experiments were conducted using the BAI-IS for venetian blinds, a shading device similar to a venetian blind but with fabric slats and a sheer blind. In all three cases the experimental results were compared with results calculated from available analytical models. The BAI-IS measurements are listed in Appendix C, Appendix D and Appendix E.

4.5.1 Venetian Blind

Previously, the solar transmittance of venetian blinds was measured using the BAI-IS (Jiang 2005) to compare the results with corresponding model (Wright and Yohoda 2005). To verify the operability of the refurbished BAI-IS apparatus, a venetian blind with white aluminium slats was tested. These results were compared with the results obtained from a model for venetian blind with curvature correction (Wright and Kotey 2007). The geometric parameters were :

Slat thickness, T=0.33 mm,

Slat width, w =14.85 mm,

Slat separation, s=12.375 mm.

$\frac{w}{r} = 2.2$

Slat reflectance, $\rho = 0.683$

The slats were opaque. It was also assumed that the solar optical properties do not vary with incidence angle. The slat angle was set at ϕ =30^0, 45^0 and 60^0. The data were collected at normal incidence: $\theta = \Omega = 0^0$.

For the model, the input parameters are the slat curvature, slat spacing, slat width and slat reflectance. The spectral reflectance of slat material is measured with Cary 5000 spectrophotometer for normal incidence. From the spectral quantities, the weighted average reflectance is calculated using the 50-points ordinate method over wavelength range between 0.4 μm to 2.0 μm. For a venetian blind,

the solar transmittance measured by using the BAI-IS agreed well with previous measurements and with the calculated results which are listed in Table 4.1.

Table 4.1: Comparison of Solar Transmittance of a Venetian Blind

Slat Angle	τ_{BAI-IS}	$\tau_{\text{Previous Measurement}}$	τ_{Model}
30^o	0.516	0.533	0.513
45^o	0.293	0.295	0.282
60^o	0.098	0.114	0.114

4.5.2 Fabric Blind (Without Sheer Layer Facings)

Next the aluminium slats were replaced with fabric slats and the experimental results were compared with the equivalent shading device model with thickness correction (FramePlus 2007). In this case it was assumed that the fabric slats were homogeneous, perfectly flat and transmit and/or reflect incident radiation diffusely because the slat fabric has a very tight weave. Since the optical properties of fabric material vary with incidence angle the direct-normal and off-normal solar optical properties of the slat fabric were measured using the Cary-5000 spectrophotometer. Kotey et al. (2008) had developed the off-normal measurement procedure by adopting cylindrical collars to hold fabric samples at 0^0, 15^0, 30^0, 45^0 and 60^0 incidence angles as shown in Figure 4.7.

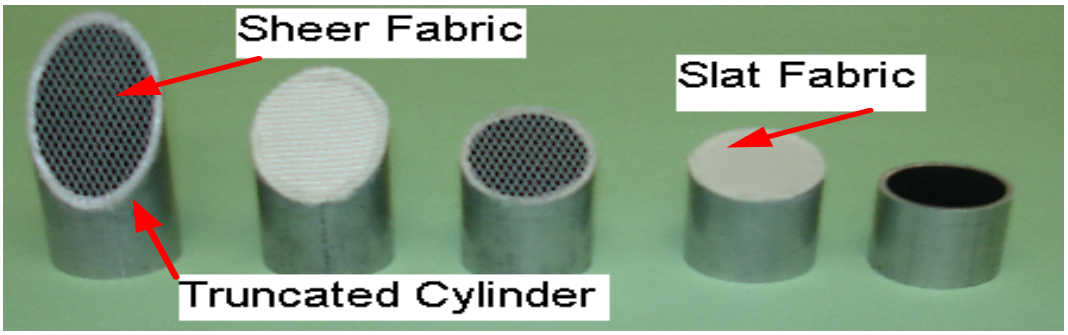

Figure 4.7: Cylindrical Aluminium Collar for Directional Measurement of Optical Properties by Cary 5000

It was observed that the slat fabric creates no specular reflection and allows no direct beam transmission at any angle of incidence.

$$\begin{aligned} \rho_{f,bb}^{Slat} &= 0 \\ \rho_{b,bb}^{Slat} &= 0 \\ \tau_{b,bb}^{Slat} &= 0 \end{aligned}$$

Moreover, the fabric was symmetrical so,

$$\begin{aligned} \rho_{f,bd}^{Slat} &= \rho_{b,bd}^{Slat} = \rho_{f,t}^{Slat} = \rho_{b,t}^{Slat} \\ \rho_{f,dd}^{Slat} &= \rho_{b,dd}^{Slat} \\ \tau_{f,t}^{Slat} &= \tau_{b,t}^{Slat} = \tau_{t}^{Slat} = \tau_{f,bd}^{Slat} = \tau_{b,bd}^{Slat} \end{aligned}$$

Optical Properties of Slat Fabric Using the Cary 5000

For fabric slats the incidence angle is dependent on profile angle and slat angle, assuming wall-azimuth angle is zero as shown in Figure 4.8. The slat properties were

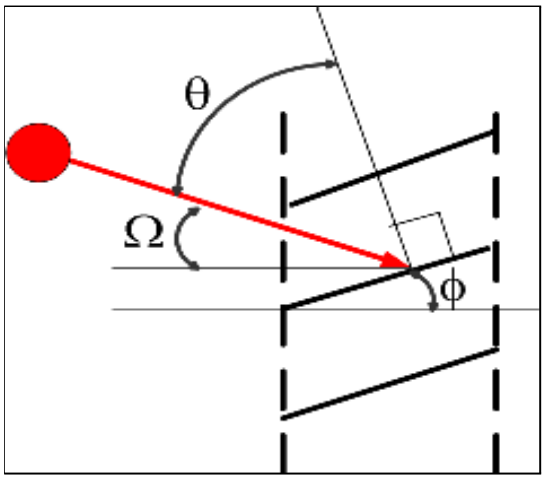

Figure 4.8: Relationship between Slat Angle, Profile Angle and Incidence Angle for Slat Fabric

measured using the Cary 5000 as listed in Table 4.2, which also includes curvefits shown in Figures 4.9 and 4.10.

In addition it was assumed that at $\theta = 90^0$

$$\begin{aligned} \rho(90) &= 0.5[1 + \rho(0)] \\ \tau(90) &= 0.5\tau(0) \end{aligned}$$

Table 4.2: Optical Properties of Slat Fabric.

θ [Deg]	$\rho^{Slat}_{f,bd}(\theta) = \rho^{Slat}_{b,bd}(\theta)$	$\tau^{Slat}_{f,bd}(\theta) = \tau^{Slat}_{b,bd}(\theta)$
0	0.644	0.328
15	0.659	0.333
30	0.666	0.323
45	0.674	0.301
60	0.695	0.266
75	0.741	0.220
90	0.822	0.164

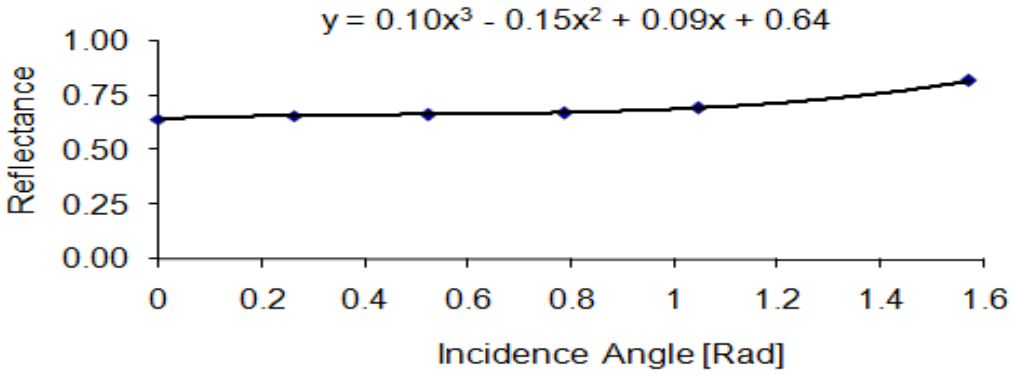

Figure 4.9: Beam-Diffuse Reflectance of a Slat Fabric

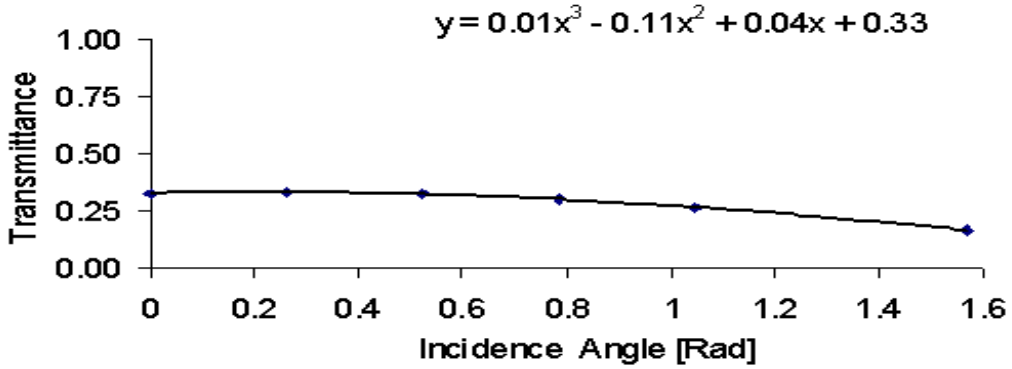

Figure 4.10: Beam-Diffuse Transmittance of a Slat Fabric

Effective Transmittance of Fabric Blind
(Without Sheer Facings)

To calculate the effective optical properties of the shading device, the inputs are total slat reflectance of front side of the slat ($\rho_{f,t}$), total slat reflectance of back side of the slat ($\rho_{b,t}$), total slat transmittance(τ_t), profile angle (Ω), incidence angle (ϕ), slat width (w), w/s ratio and slat thickness (T).

The slat width was set at w=16.68 mm and the thickness of the fabric was T=0.45 mm. The thickness of fabric slat was not negligible with respect to the slat separation, but curvature was neglected.

The output values are the eight effective beam optical properties for the entire blind layer, which include four beam-to-beam and four beam-to-diffuse properties. Among these effective beam properties, at any slat angle, the sum of beam-to-beam transmittance from front side of slat and the beam-to-diffuse transmittance from front side of slat is the total effective transmittance of the blind layer.

$$\tau_{f,t}(\phi) = \tau_{f,bb}(\phi) + \tau_{f,bd}(\phi)$$

This effective transmittance value obtained analytically for the blind layer at a certain slat angle was compared with the total transmittance value measured using

the BAI-IS. This experiment is carried out at slat angles and incidence angles listed in Table 4.3.

Table 4.3: Geometric parameter of fabric blind

Slat angle	Profile angle	Thickness	$\frac{\text{Slat width}}{\text{Slat separation}}$
$\phi[Deg]$	$\Omega[Deg]$	T [mm]	$\left[\frac{w}{s}\right]$
60	0	0.45	1.43
45	+30, 0, -30	0.45	1.28
30	0	0.45	1.3
0	+30, 0	0.45	1.4

Results are shown in Table 4.4. The experimental result and prediction agree well for the fabric blind. The largest discrepancy in solar transmittance was observed (approximately 0.03) at $\phi = 30^0$, $\Omega = 0^0$.

Table 4.4: Solar Transmittance of a Fabric Blind Without Sheer Facings

Slat angle, $\phi[Deg]$	Profile angle, $\Omega[Deg]$	τ_{BAI-IS}	τ_{Model}
60	0	0.34	0.34
45	0	0.47	0.45
30	0	0.61	0.58
0	0	0.97	0.96
0	30	0.54	0.53
45	30	0.33	0.35
45	-30	0.72	0.72

4.5.3 Sheer Blind:

Finally solar transmittance of the sheer blind was measured using the BAI-IS. The experimental results from the BAI-IS were compared with the results obtained from a multi-layer model for shading/glazing array (Wright and Kotey 2006).

The geometric parameters are same as those listed in Table 4.5.

Table 4.5: Geometric Properties of a Sheer Blind.

Slat angle ϕ $[Deg]$	Slat separation s [mm]	$\frac{\text{Slat width}}{\text{Slat separation}}$ $\frac{w}{s}$
60	11.7	1.4
45	13.1	1.3
30	12.5	1.3
0	11.8	1.4

The slat width remained at w=16.68 mm and again slat fabric thickness was $T = 0.45$ mm. For each slat angle the profile angles were set to $\Omega = 0^0$, $\pm 30^0$, $\pm 45^0$, and $\pm 60^0$. For slat angle $\phi = 0^0$ and $\phi = 45^0$ the wavelength range was set between 0.4 μm and 2.0 μm. It was observed that the sheer blind was not spectrally selective hence for slat angle $\phi = 30^0$ and $\phi = 60^0$ the wavelength range was reduced to $0.4 < \lambda < 1.0\ \mu m$. This saved time because measurement at $\lambda > 1.0\ \mu m$ is much more time consuming. At higher wavelengths ($\lambda \geq 1.0\ \mu m$), the radiant flux of the lamp and the reflectance of integrating sphere coating are low resulting in reduced S/N ratio of the photo-detector. To get more accurate results the scan time and number of readings were increased.

To calculate the effective solar transmittance of a sheer blind using the multi-layer shading/glazing array the effective properties of two sheer layers and the slat layer were evaluated. For these analytical calculations off-normal optical properties were measured for both the slat and sheer fabric by using the Cary 5000 (Kotey et al. 2008).

It was observed that the slat fabric creates no specular reflection and allows no direct beam transmission at any angle of incidence. Similarly, the sheer fabric does not create specular reflection.

$$\rho_{f,bb}^{sheer} = \rho_{b,bb}^{sheer} = 0$$

Due to its open weave the sheer fabric allows beam and diffuse transmittance.

Moreover, the fabric was symmetrical so:

$$\begin{aligned} \rho_{f,t}^{sheer} &= \rho_{b,t}^{sheer} = \rho_{f,bd}^{sheer} = \rho_{b,bd}^{sheer} = \rho_{bd}^{sheer} \\ \tau_{f,t}^{Sheer} &= \tau_{b,t}^{Sheer} = \tau_{t}^{Sheer} = \tau_{f,bd}^{Sheer} = \tau_{b,bd}^{Sheer} \end{aligned}$$

Effective Optical Properties of the Sheer Blind Layer

To calculate the effective optical properties of the shading device, the inputs are total slat reflectance of front side of the slat ($\rho_{f,t}$), total slat reflectance of back side of the slat ($\rho_{b,t}$), total slat transmittance(τ_t), profile angle (Ω), incidence angle (ϕ), slat width (w), w/s ratio and slat thickness (T).

The outputs are the eight effective beam optical properties for the entire blind layer, which include four beam-to-beam and four beam-to-diffuse properties. Similarly, the outputs were three effective diffuse optical properties for the entire blind layer including diffuse-diffuse transmittance and reflectance (Kotey and Wright 2007). The effective properties of the blind layer are listed in Tables 4.6, 4.7, 4.8 and 4.9.

Table 4.6: Calculated Effective Solar Optical Properties of a Sheer Blind Layer

At $\phi = 0^0$							
Blind	Incidence Angle, θ [Deg] on Slat						
Layer	30	45	60	90	120	135	150
Optical	Profile Angle, Ω [Deg] = θ on Sheer Blind						
Properties	60	45	30	0	-30	-45	-60
$\rho_{f,bb}$	0	0	0	0	0	0	0
$\rho_{b,bb}$	0	0	0	0	0	0	0
$\tau_{f,bb}$	0	0	0.177	0.963	0.177	0	0
$\tau_{b,bb}$	0	0	0.177	0.963	0.177	0	0
$\rho_{f,bd}$	0.618	0.551	0.386	0.030	0.407	0.551	0.588
$\rho_{b,bd}$	0.618	0.551	0.386	0.030	0.407	0.551	0.588
$\tau_{f,bd}$	0.345	0.395	0.360	0	0.383	0.395	0.322
$\tau_{b,bd}$	0.345	0.395	0.360	0	0.383	0.395	0.322
$\rho_{f,dd}$	0.356	0.352	0.341	0.367	0.356	0.352	0.341
$\rho_{b,dd}$	0.356	0.352	0.341	0.367	0.356	0.352	0.341
τ_{dd}	0.602	0.597	0.584	0.602	0.602	0.597	0.584

Table 4.7: Calculated Effective Solar Opticl Properties of a Sheer Blind Layer

At $\phi = 30^0$							
Blind	Incidence Angle, θ [Deg] on Slat						
Layer	0	15	30	60	90	105	120
Optical	Profile Angle, Ω [Deg] = θ on Sheer Blind						
Properties	60	45	30	0	-30	-45	-60
$\rho_{f,bb}$	0	0	0	0	0	0	0
$\rho_{b,bb}$	0	0	0	0	0	0	0
$\tau_{f,bb}$	0	0	0	0.323	0.960	0.487	0
$\tau_{b,bb}$	0	0.487	0.960	0.323	0	0	0
$\rho_{f,bd}$	0.654	0.639	0.591	0.354	0.033	0.237	0.503
$\rho_{b,bd}$	0.490	0.2237	0.026	0.354	0.635	0.639	0.674
$\tau_{f,bd}$	0.288	0.332	0.370	0.261	0	0.247	0.445
$\tau_{b,bd}$	0.429	0.247	0	0.261	0.339	0.332	0.295
$\rho_{f,dd}$	0.372	0.386	0.384	0.373	0.409	0.386	0.384
$\rho_{b,dd}$	0.372	0.386	0.384	0.373	0.409	0.386	0.384
τ_{dd}	0.565	0.576	0.573	0.553	0.564	0.576	0.573

Table 4.8: Calculated Effective Solar Opticl Properties of a Sheer Blind Layer

At $\phi = 45^0$							
Blind	Incidence Angle, θ [Deg] on Slat						
Layer	-15	0	15	45	75	90	105
Optical	Profile Angle, Ω [Deg] = $\theta onSheerBlind$						
Properties	60	45	30	0	-30	-45	-60
$\rho_{f,bb}$	0	0	0	0	0	0	0
$\rho_{b,bb}$	0	0	0	0	0	0	0
$\tau_{f,bb}$	0	0	0	0.097	0.597	0.954	0.319
$\tau_{b,bb}$	0.319	0.954	0.597	0.097	0	0	0
$\rho_{f,bd}$	0.702	0.654	0.634	0.506	0.231	0.038	0.303
$\rho_{b,bd}$	0.303	0.030	0.230	0.506	0.633	0.733	0.702
$\tau_{f,bd}$	0.278	0.312	0.349	0.359	0.125	0	0.347
$\tau_{b,bd}$	0.347	0	0.155	0.359	0.265	0.246	0.278
$\rho_{f,dd}$	0.431	0.421	0.431	0.428	0.424	0.466	0.431
$\rho_{b,dd}$	0.431	0.421	0.431	0.428	0.424	0.466	0.431
τ_{dd}	0.542	0.537	0.542	0.532	0.487	0.509	0.542

Table 4.9: Calculated Effective Solar Optical Properties of a Sheer Blind Layer

At $\phi = 60^0$							
Blind	Incidence Angle, θ [Deg] on Slat						
Layer	-30	-15	0	30	60	75	90
Optical	Profile Angle, Ω [Deg] = θ on Sheer Blind						
Properties	60	45	30	0	-30	-45	-60
$\rho_{f,bb}$	0	0	0	0	0	0	0
$\rho_{b,bb}$	0	0	0	0	0	0	0
$\tau_{f,bb}$	0	0	0	0	0.171	0.455	0.929
$\tau_{b,bb}$	0.929	0.455	0.171	0	0	0	0
$\rho_{f,bd}$	0.734	0.708	0.661	0.624	0.475	0.322	0.059
$\rho_{b,bd}$	0.047	0.316	0.461	0.624	0.684	0.726	0.826
$\tau_{f,bd}$	0.228	0.266	0.288	0.343	0.285	0.158	0
$\tau_{b,bd}$	0	0.202	0.313	0.343	0.247	0.175	0.15
$\rho_{f,dd}$	0.5	0.5	0.484	0.5	0.497	0.503	0.556
$\rho_{b,dd}$	0.5	0.5	0.484	0.5	0.497	0.503	0.556
τ_{dd}	0.464	0.468	0.458	0.464	0.43	0.397	0.419

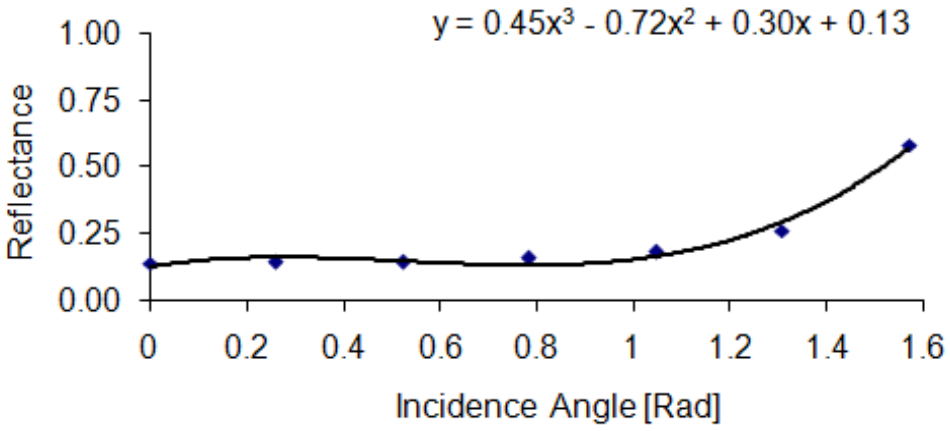

Figure 4.11: Beam-Diffuse Reflectance of a Sheer Fabric

Optical Properties of Sheer Fabric

The optical properties of the sheer fabric were measured the same way as described in Section 4.5.2. For the sheer fabric (i.e., the facing material) $\theta = \Omega$ assuming wall-azimuth angle zero. The beam optical properties of sheer fabric are listed in Table 4.10 and shown in Figures 4.11, 4.12 and 4.13.

Table 4.10: Optical Properties of Sheer Fabric

θ	$\rho_{f,bd}^{Sheer}(\theta) = \rho_{b,bd}^{Sheer}(\theta)$	$\tau_{f,bb}^{Sheer}(\theta) = \tau_{b,bb}^{Sheer}(\theta)$	$\tau_{f,bd}^{Sheer}(\theta) = \tau_{b,bd}^{Sheer}(\theta)$
0	0.133	0.708	0.161
15	0.152	0.702	0.154
30	0.143	0.697	0.165
45	0.142	0.677	0.178
60	0.187	0.624	0.178
90	0.567	0.354	0.800

To derive the diffuse-to-diffuse reflectance and transmittance of the sheer fabric it is necessary to integrate the directional property over a hemisphere. Let the total

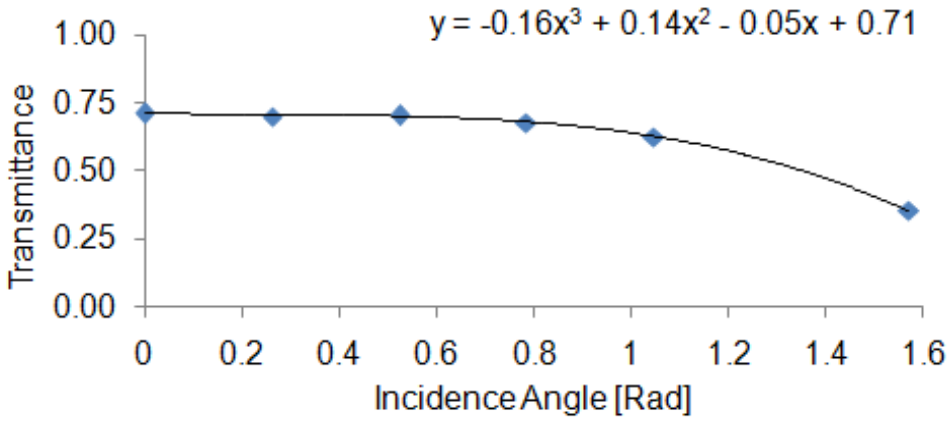

Figure 4.12: Beam-Beam Transmittance of a Sheer Fabric

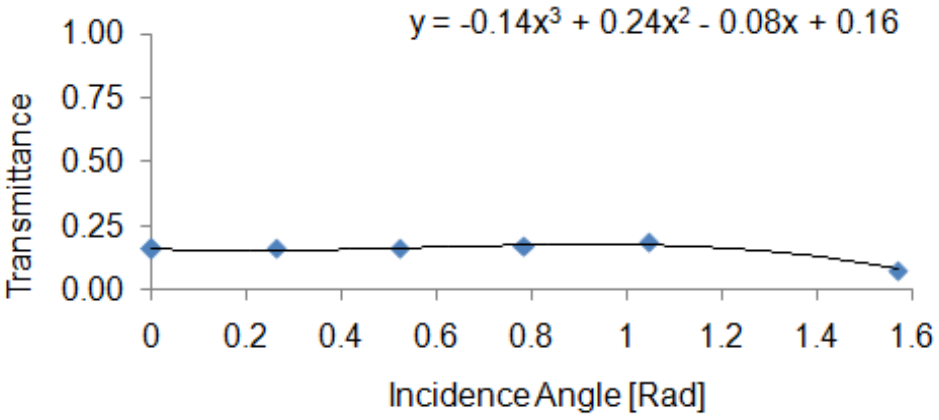

Figure 4.13: Beam-Diffuse Transmittance of a Sheer Fabric

transmittance or reflectance at certain incidence angle θ and surface azimuth angle γ be $\tau_t(\theta, \gamma)$ and $\rho_t(\theta, \gamma)$.

Let us assume that along γ the optical properties remain constant and it varies only with incidence angle θ, such that:

$$\begin{aligned} \tau_t(\theta, \gamma) &= \tau_t(\theta) \\ \rho_t(\theta, \gamma) &= \rho_t(\theta) \end{aligned}$$

Integrating the total directional properties over the hemisphere as shown in Figure

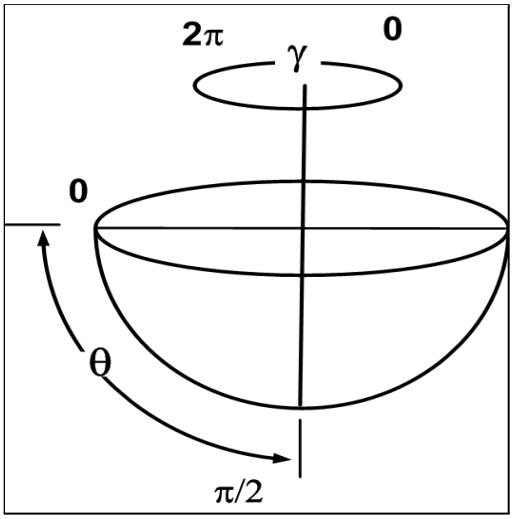

Figure 4.14: Hemispherical Properties by Integration

4.14, the diffuse-diffuse properties of the sheer fabric can be obtained as follows:

$$\tau_{dd} = \frac{\int_0^{\frac{\pi}{2}} \tau_t(\theta) \cos\theta d\theta}{\int_0^{\frac{\pi}{2}} \cos\theta d\theta} \tag{4.1}$$

$$\rho_{dd} = \frac{\int_0^{\frac{\pi}{2}} \rho_t(\theta) \cos\theta d\theta}{\int_0^{\frac{\pi}{2}} \cos\theta d\theta} \tag{4.2}$$

Here

$$\begin{aligned} \tau_t^{Sheer}(\theta) &= \tau_{bb}^{Sheer}(\theta) + \tau_{bd}^{Sheer}(\theta) \\ \rho_t^{Sheer}(\theta) &= \rho_{bd}^{Sheer}(\theta) \end{aligned}$$

From the measured optical properties of the sheer fabric the directional property functions were developed as shown in Figures 4.15 and 4.16.

The transmittance function and reflectance function were integrated according to Equations 4.1 and 4.2 to derive the diffuse-diffuse properties of the sheer layer. The diffuse-diffuse properties of the sheer fabric are listed in Table 4.11.

Table 4.11: Diffuse-Diffuse Properties of a Sheer Blind

Wavelength Range, λ $[\mu m]$	$\boldsymbol{\tau}_{dd}^{Sheer}$	$\boldsymbol{\rho}_{f,dd}^{Sheer} = \boldsymbol{\rho}_{b,dd}^{Sheer}$
0.4 to 1.0	0.837	0.165
0.4 to 2.0	0.838	0.165

$$\tau_t^{Sheer}(\theta) = -0.37\theta^3 + 0.53\theta^2 - 0.21\theta + 0.87$$

$$\rho_t^{Sheer}(\theta) = 0.35\theta^3 - 0.48\theta^2 + 0.18\theta + 0.13$$

The optical properties of the sheer fabric in the wavelength range $\lambda = 0.4\mu m$ to $\lambda = 1.0\mu m$ are listed in Appendix G.

Multi-Layer Shading/Glazing Array

A sheer blind has one layer of sheer facing on the outdoor side (layer 3), a shading layer with fabric slats (layer 2) in between the two sheer facings and another layer of sheer facing on the indoor side (layer 1). All the layers are arranged as shown in Figure 4.17 and 4.18.

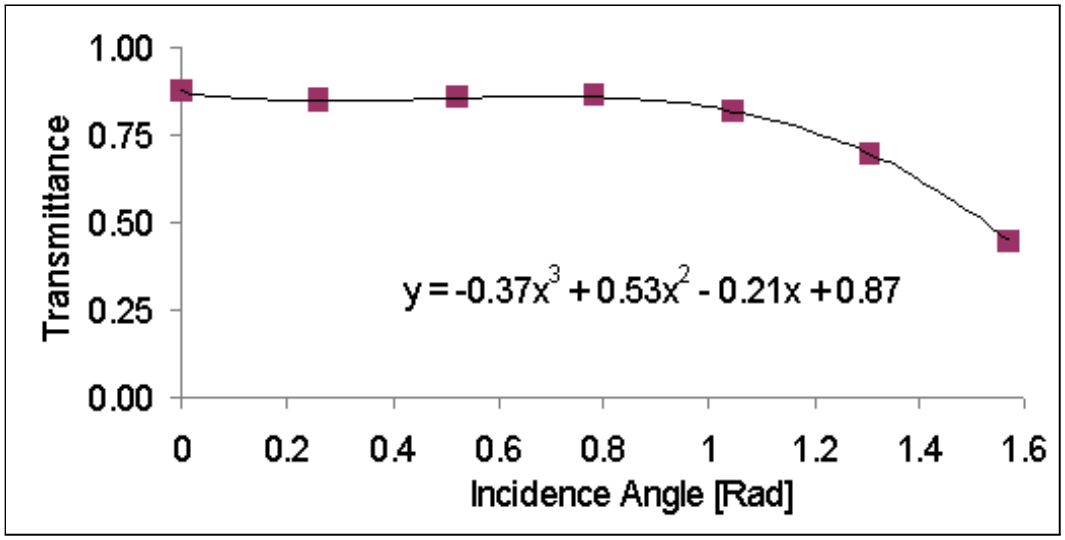

Figure 4.15: Total Transmittance of a Sheer Fabric (0.4 to 2.0 micron)

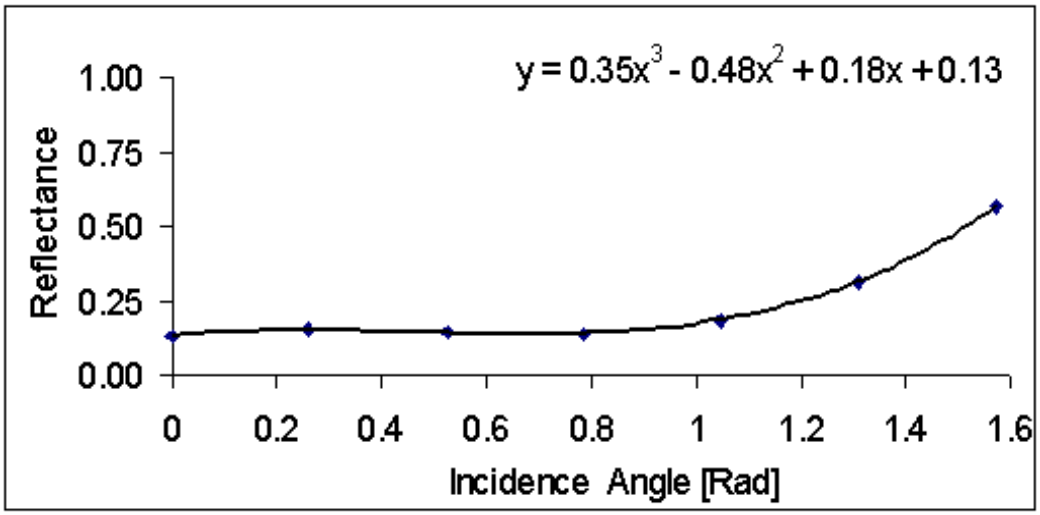

Figure 4.16: Total Reflectance of a Sheer Fabric (0.4 to 2.0 micron)

$$I_{beam} = B_4^- = 95$$
$$I_{diff} = D_4^- = 0$$

The effective optical properties of the sheer and slat layers are shown in Table 4.12. This Table is a representative example valid for $\phi = 0^0$, $\Omega = 0^0$.

Table 4.12: Calculation Parameters for Three Component Layers of a Sheer Blind

Properties	Sheer Fabric-3	Blind Layer-2	Sheer Fabric-1
$\rho_{f,bb}$	0	0	0
$\rho_{b,bb}$	0	0	0
$\tau_{f,bb}$	0.708	0.963	0.708
$\tau_{b,bb}$	0.708	0.963	0.708
$\rho_{f,bd}$	0.133	0.030	0.133
$\rho_{b,bd}$	0.133	0.030	0.133
$\tau_{f,bd}$	0.161	0	0.161
$\tau_{b,bd}$	0.161	0	0.161
$\rho_{f,dd}$	0.165	0.367	0.165
$\rho_{b,dd}$	0.165	0.367	0.165
τ_{dd}	0.837	0.602	0.837

The 14x14 matrix was solved to account for the fluxes at different layers as shown in Figure 4.18. For each slat angles the radiation fluxes are listed in Tables 4.13, 4.14, 4.15 and 4.16.

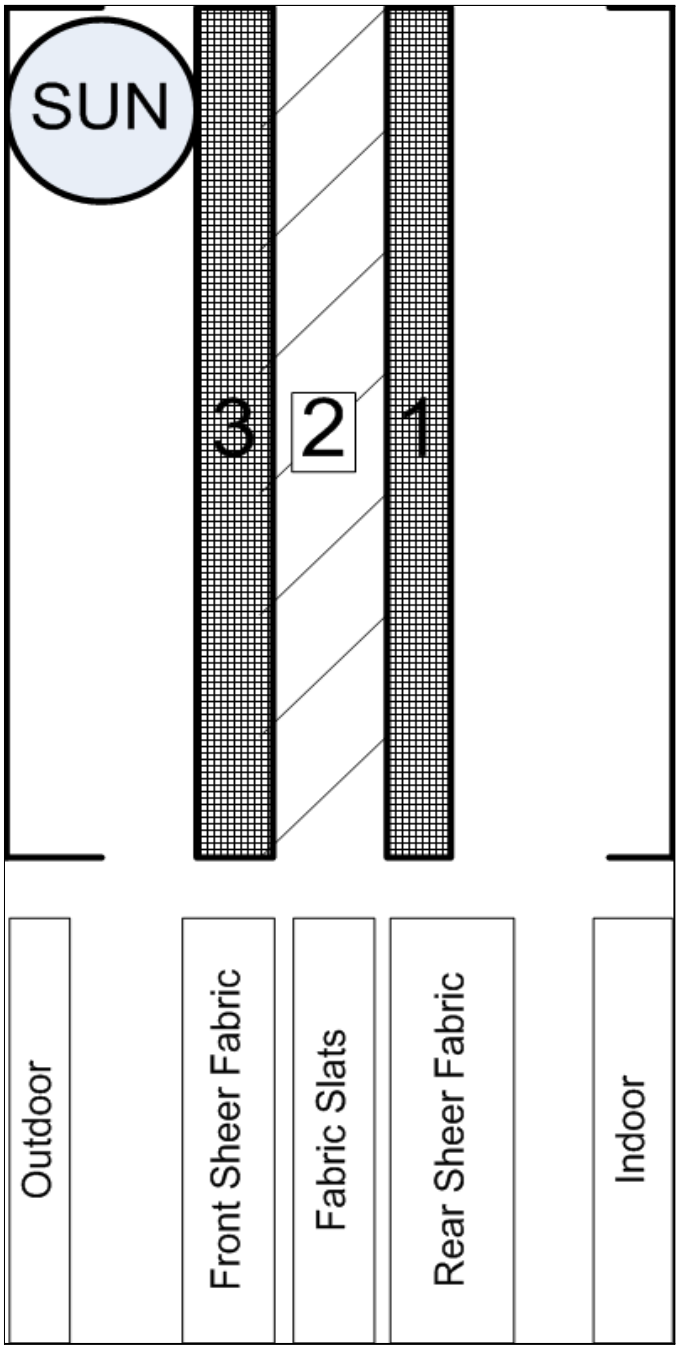

Figure 4.17: Sheer Blind Multi-Layer Model

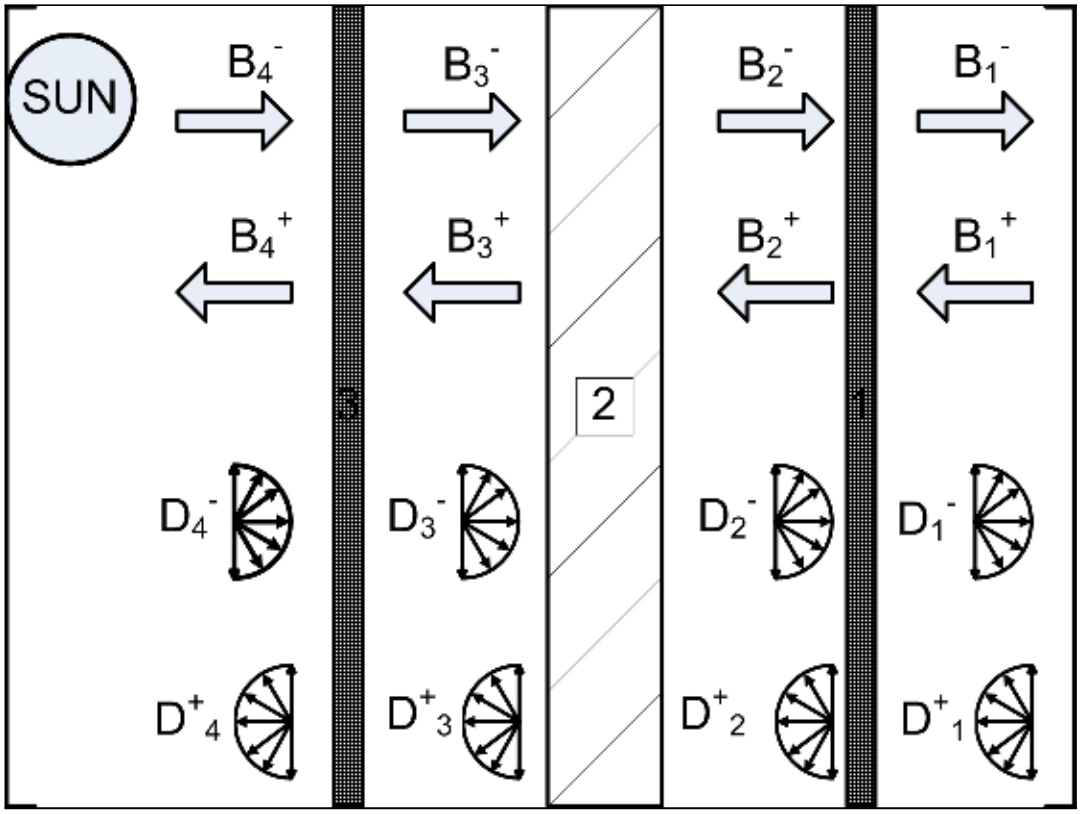

Figure 4.18: Beam and Diffuse Flux Components in a Sheer Blind Layer Array

Table 4.13: Radiation Flux in a Sheer Blind at 0 Deg. Slat Angle

Radiation Flux	**Profile angle,** Ω [Deg]						
$\left[\frac{Watt}{m^2}\right]$	60	45	30	0	-30	-45	-60
B_1^-	0	0	8	46	8	0	0
B_1^+	0	0	0	0	0	0	0
D_1^-	32	35	35	23	37	35	30
D_1^+	0	0	0	0	0	0	0
B_2^-	0	0	12	65	12	0	0
B_2^+	0	0	0	0	0	0	0
D_2^-	38	42	39	15	42	42	36
D_2^+	6	7	8	11	8	7	6
B_3^-	59	64	67	67	67	64	59
B_3^+	0	0	0	0	0	0	0
D_3^-	25	24	21	17	22	24	25
D_3^+	49	48	38	15	40	48	47
B_4^-	95	95	95	95	95	95	95
B_4^+	0	0	0	0	0	0	0
D_4^-	0	0	0	0	0	0	0
D_4^+	58	55	45	26	47	55	56

Table 4.14: Radiation Flux in a Sheer Blind at 30 Deg. Slat Angle

Radiation Flux	**Profile angle,** Ω [Deg]						
$\left[\frac{Watt}{m^2}\right]$	60	45	30	0	-30	-45	-60
B_1^-	0	0	0	15	45	21	0
B_1^+	0	0	0	0	0	0	0
D_1^-	28	32	34	30	22	31	36
D_1^+	0	0	0	0	0	0	0
B_2^-	0	0	0	22	64	31	0
B_2^+	0	0	0	0	0	0	0
D_2^-	34	38	41	32	15	32	43
D_2^+	5	6	7	8	12	10	7
B_3^-	59	64	67	67	66	64	59
B_3^+	0	0	0	0	0	0	0
D_3^-	26	25	23	21	18	21	25
D_3^+	51	54	52	36	16	29	43
B_4^-	95	95	95	95	95	95	95
B_4^+	0	0	0	0	0	0	0
D_4^-	0	0	0	0	0	0	0
D_4^+	60	60	57	43	27	39	53

Table 4.15: Radiation Flux in a Sheer Blind at 45 Deg. Slat Angle

Radiation Flux	**Profile angle,** Ω [Deg]						
$\left[\frac{Watt}{m^2}\right]$	60	45	30	0	-30	-45	-60
B_1^-	0	0	0	5	28	41	12
B_1^+	0	0	0	0	0	0	0
D_1^-	28	30	33	34	25	23	34
D_1^+	0	0	0	0	0	0	0
B_2^-	0	0	0	7	40	61	19
B_2^+	0	0	0	0	0	0	0
D_2^-	33	36	39	39	22	15	37
D_2^+	5	6	6	7	9	12	9
B_3^-	59	64	67	67	67	64	59
B_3^+	0	0	0	0	0	0	0
D_3^-	26	25	24	23	20	19	23
D_3^+	56	56	56	48	28	17	33
B_4^-	95	95	95	95	95	95	95
B_4^+	0	0	0	0	0	0	0
D_4^-	0	0	0	0	0	0	0
D_4^+	64	62	61	53	37	29	45

Table 4.16: Radiation Flux in a Sheer Blind at 60 Deg. Slat Angle

Radiation Flux	**Profile angle,** Ω [Deg]						
$\left[\frac{Watt}{m^2}\right]$	60	45	30	0	-30	-45	-60
B_1^-	0	0	0	0	8	20	34
B_1^+	0	0	0	0	0	0	0
D_1^-	24	27	28	31	29	24	23
D_1^+	0	0	0	0	0	0	0
B_2^-	0	0	0	0	11	29	55
B_2^+	0	0	0	0	0	0	0
D_2^-	28	32	33	37	32	23	16
D_2^+	5	5	5	6	7	8	12
B_3^-	59	64	66	67	66	64	59
B_3^+	0	0	0	0	0	0	0
D_3^-	27	26	24	24	22	22	21
D_3^+	59	61	58	57	46	35	20
B_4^-	95	95	95	95	95	95	95
B_4^+	0	0	0	0	0	0	0
D_4^-	0	0	0	0	0	0	0
D_4^+	66	66	62	61	52	44	34

From Figure 4.18 and 4.19 the solar transmittance of a sheer blind can be evaluated as:

$$\tau = \frac{B_1^- + D_1^-}{B_4^-}$$

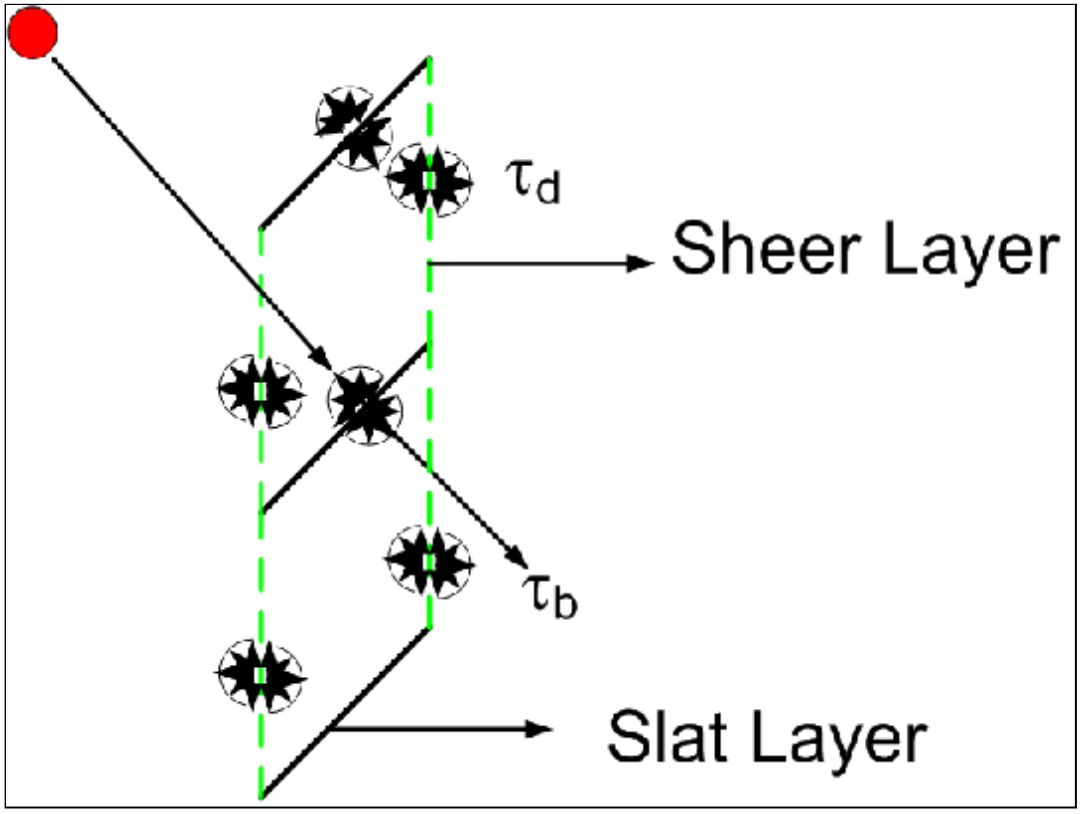

Figure 4.19: Transmitted Radiation through a Sheer Blind

Effective Solar Transmittance of a Sheer Blind

The effective solar transmittance of a sheer blind is summarized in Table 4.17.

The effective solar transmittance of a sheer blind are graphically displayed in Table 4.18. The experimental results from BAI-IS and the calculated result from multi-layer shading/glazing array were compared for four different slat angles at

different profile angles. The differences are reasonable and both sets of results are in good agreement with each other. For most cases the differences in solar transmittance were within 0.04. The maximum differences can be observed (approximately 0.1) on the left side of the bottom two figures where the incident ray was parallel to, or nearly parallel, to the slats. The reason for this discrepancy is explained in Sections 4.6 and 4.7.

This demonstration concludes that the relevant shading device models are valid, experimental results are reliable and BAI-IS provides authentic estimation of optical properties for calculating solar gain of different types of louvered shading devices.

Table 4.17: Solar Transmittance of a Sheer Blind

Slat angle, $\phi[Deg]$	Profile angle, $\Omega[Deg]$	τ_{BAI-IS}	τ_{Model}
0	60	0.33	0.34
0	45	0.37	0.37
0	30	0.52	0.45
0	0	0.73	0.72
0	-30	0.49	0.47
0	-45	0.36	0.37
0	-60	0.31	0.31
30	60	0.27	0.30
30	45	0.30	0.33
30	30	0.35	0.36
30	0	0.49	0.48
30	-30	0.69	0.71
30	-45	0.56	0.56
30	-60	0.34	0.38
45	60	0.26	0.29
45	45	0.30	0.32
45	30	0.32	0.35
45	0	0.42	0.41
45	-30	0.63	0.55
45	-45	0.73	0.68
45	-60	0.56	0.49
60	60	0.21	0.25
60	45	0.27	0.28
60	30	0.29	0.29
60	0	0.31	0.33
60	-30	0.47	0.39
60	-45	0.56	0.46
60	-60	0.63	0.60

Table 4.18: Solar Transmittance of a Sheer Blind

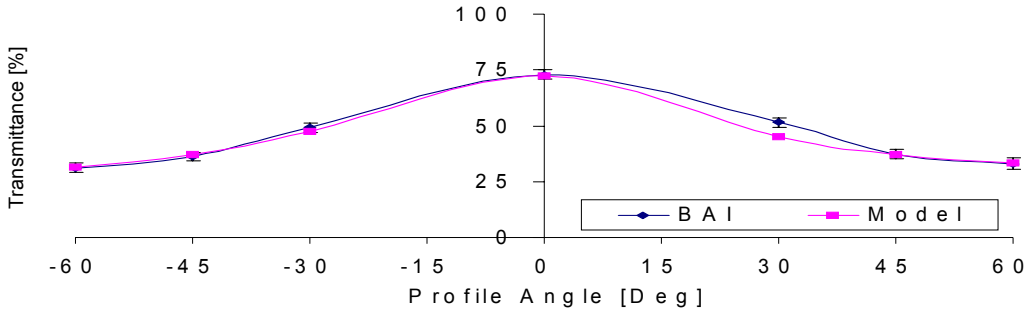

Solar Transmittance of a Sheer Blind at 0 Deg Slat Angle

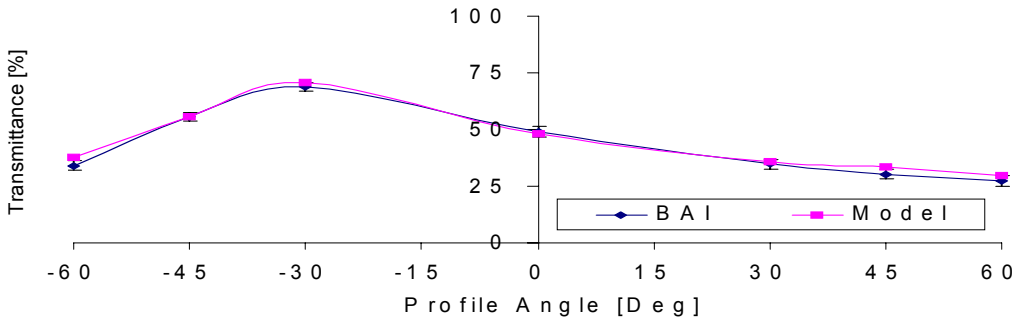

Solar Transmittance of a Sheer Blind at 30 Deg Slat Angle

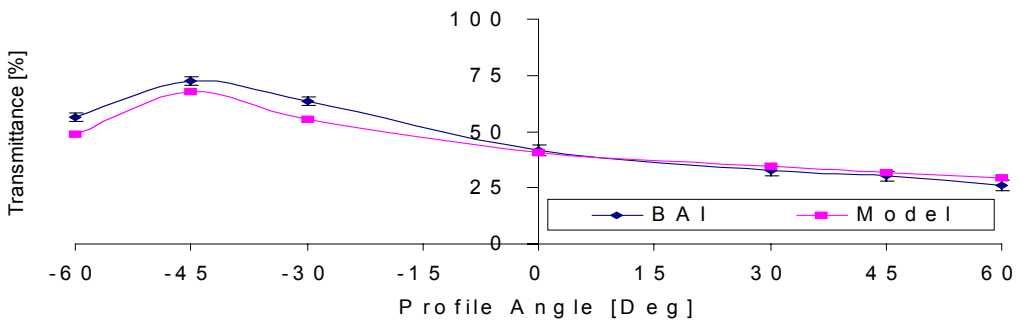

Solar Transmittance of a Sheer Blind at 45 Deg Slat Angle

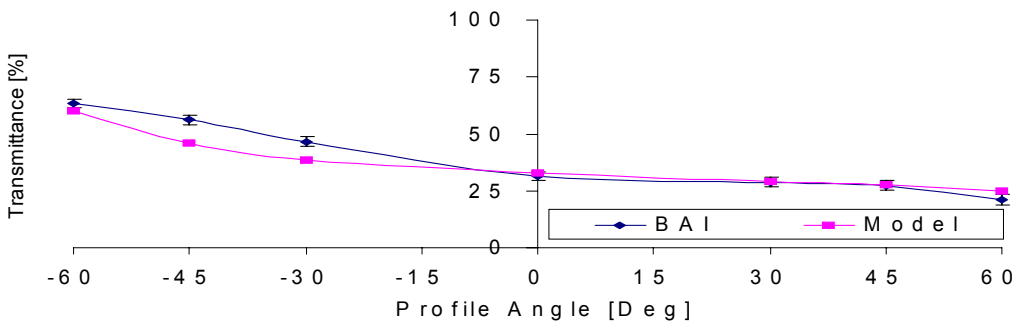

Solar Transmittance of a Sheer Blind at 60 Deg Slat Angle

4.6 Observations and Discussions

4.6.1 Measuring Solar Transmittance of a Venetian Blind and Sheer Blind

Slat properties are different for a venetian blind and a sheer blind. Venetian blind has metallic slats which are slightly curved, very thin and opaque. In contrast the fabric slats are flat, thicker with respect to slat spacing and translucent in nature. Both are spectrally non-selective. The slat properties of a venetian blind were assumed to be independent of incidence angle. Since the solar transmittance measured using the BAI-IS and that from the model calculations were in good agreement for a venetian blind, the assumption of considering constant slat properties was deemed to be reasonable. However, for fabric slat and sheer fabric properties a detailed study was undertaken to measure the optical properties at different incidence angles. With these angle-dependent optical properties of the fabric the relevant shading device models showed good match between BAI-IS result and model output for the effective solar transmittance value.

It was also observed that at higher slat angles, deeper profile angles and especially with maximum transmission cases when $\phi + \Omega \approx 0$, the difference between experimental results and model are comparatively larger. For sheer blind this is prominent because of non-uniformity of slat spacing, inaccuracy in sample positioning and error in setting the true slat tilt angle. Due to the difference in the area of exposed surface to incoming radiation and view factor, the slat orientation at deeper profile angle, higher slat angle and specially in case of negative profile angle the transmittance value is more sensitive to accuracy in geometric parameters as shown in Figure 4.20.

Another important factor is also relevant here. While measuring directional properties with additional collars inside the integrating sphere the assumption of having a perfectly spherical shape and Lambertian reflecting surfaces is violated. So, for calculating model output the input optical properties from the Cary 5000 may not be free of additional uncertainties.

The effective solar transmittance was compared for a venetian blind, a fabric

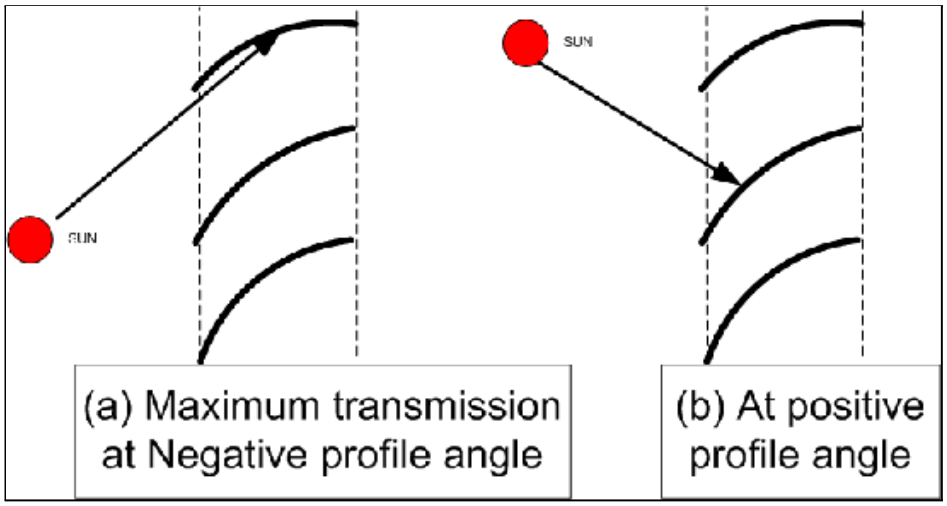

Figure 4.20: Sensitivity of Optical Properties on Slat Orientation

blind and a sheer blind for the same slat and profile angles which are listed in Table 4.19. This comparison indicates that without the sheer fabric the blind with fabric slat shows better transmittance than the sheer blind because the two shear facings reflect and absorb some radiation.

Table 4.19: Solar transmittance of a Venetian Blind, a Fabric Blind Without Sheer Facings and a Sheer Blind

Slat Angle	Profile Angle	Venetian Blind	Fabric Blind	Sheer Blind
ϕ, [Deg]	Ω, [Deg]	$\tau_{f,t}$	$\tau_{f,t}$	$\tau_{f,t}$
0	0	0.93	0.97	0.73
30	0	0.52	0.61	0.50
45	0	0.29	0.47	0.42
60	0	0.10	0.34	0.32

As soon as two sheer facings are added, the sheer blind exhibits lower transmittance than the fabric blind but still shows higher transmittance than venetian blind at higher slat angles (at ϕ =45 Deg. and ϕ =60 Deg). On the other hand, for lower slat angles a sheer blind has lower transmittance than venetian blind (at

ϕ =0 Deg and ϕ =30 Deg). At low slat angles a venetian blind and a sheer blind both have almost the same opening for direct beam transmission. Due to the presence of sheer facings some beam transmissions are blocked and some are converted into diffuse transmission. So the solar transmittance is lower in a sheer blind with respect to a venetian blind. At high slat angles both the venetian blind and sheer blind allow mostly diffuse transmission. A venetian blind has only slat surfaces to offer diffuse transmission but a sheer blind has slats as well as the sheer facings to offer diffuse transmission. Due to this higher view factor for a sheer blind the solar transmittance is higher as compared to a venetian blind at higher slat angles.

However, it is to be noted that these comparisons must be done with louvered blinds having similar geometry and the same optical properties of the components. In the experiment the optical properties of venetian blind slat, sheer facing and fabric slat are not equal and the geometric parameters (w/s, T, w) are also different. Therefore the comparison of transmittance may not reflect accurate conclusions.

Since the sheer blind offers more solar transmittance than a venetian blind it is better suited to daylighting than a venetian blind. The presence of sheer fabric and fabric slat control the light in a diffused manner which makes it possible to provide softer illumination.

The BAI-IS apparatus has its limitations for measurement. The major issues are speed, getting higher chopper speed and ensuring an accurate light feedback mechanism.

The measurements were not instantaneous. First, the BAI-IS uses a single beam technique, so for each spectral transmittance measurement the sample needs to be moved in front of the integrating sphere and away again. Due to the limitations of the hardware the speed of the sample traversing mechanism was very time consuming: 3 to 5 minutes per measurement. Second, whenever the wavelength was adjusted, the photo-detector required about 30 seconds to reach a stable steady state for recording the measured voltage. Third, multiple readings were taken to minimize the measurement uncertainties.

The temporal stability of lamp radiation is essential for accurate transmittance measurement. Increased lamp input voltage increases S/N ratio for the photo-

detector. With the existing custom made circuitry for the lamp feedback mechanism both stability and lamp voltage were less than ideal. Better stability and S/N ratio would improve measurement accuracy and reduce total measurement time by reducing scan time, wait-time and number of scans per measurement.

The optical chopper mechanism uses a locally fabricated 13-inch diameter chopper wheel attached to a commercial motor and control unit. This unit was designed to rotate a 4-inch diameter chopper wheel up to 20 kHz. The current motor and the control unit can not turn the 13-inch diameter disc faster than 70 Hz (i.e., 1050 rev/min). Higher chopper speed enables better noise filtration capability and signal stability of the system which can improve measurement speed.

4.7 Dimensional Integrity of Sample

For true optical measurement, it is very important to have accurate dimensional parameters of sample blind. In this section the effect of change in the geometric parameters of the sample on the overall transmittance measurement are discussed.

4.7.1 Slat Spacing, s

The slat spacings were measured for each sample. The standard deviation of all these measurement provides the extent of non-uniformity of slat spacing.

$$\sigma_{slat-spacing} = \pm\sqrt{\frac{1}{n-1}\sum_{i=1}^{n}(s_i - \overline{s})^2}$$

Where,

s_i= slat spacing of the i-th slat opening.

$\overline{s}$= Average slat spacing of all openings

The standard deviation of slat spacings for different sheer blind samples are listed in Table 4.20

Table 4.20: Standard deviation of slat spacings

ϕ [Deg.]	Slat spacing, s [mm]	% Deviation
0	11.8	8
30	12.5	7
40	13.1	5
60	11.7	9

Table 4.21: Uncertainity due to Error in Slat Spacing

ϕ [Deg.]	Slat spacing, s [mm]	Ω [Deg.]	Transmittance
60	**11.7**	60	0.**218**
60	**10.5**	60	0.**207**
60	**11.7**	-60	0.**596**
60	**10.5**	-60	0.**591**

After investigating the analytical model it was observed that at higher slat and profile angles the impact of slat spacing variation is comparatively high. For $\phi = 60^0$ and $\Omega = 60^0$ a 10% change in slat spacing changes the transmittance by 0.01. However, the change in transmittance is not prominent in the case of maximum transmission position i.e, when $\phi + \Omega = 0$ as listed in Table 4.21. The change in transmittance is more sensitive to situations at higher slat angles and deeper profile angles at minimum transmission cases (when $\phi + \Omega > 0$) but less important for peak transmission cases when $\phi + \Omega = 0$.

Keeping the slat width constant the increased slat spacing enables more light energy to transmit directly or with fewer reflections through the louvered blind surface. If the slat spacing exceeds the slat width it ensures no overlapping of adjacent slats. In this situation there will be more additional direct transmission of beam-beam radiation and hence increase transmittance through blind layer. Due to inaccuracy in slat spacing for a sheer blind sample, at some instances the adjacent slats do not overlap and this is not accounted for in the calculation. This is why there may be error in transmittance measurement.

Table 4.22: Uncertainity due to Error in Slat Angle

Slat angle [Deg.]	**Profile angle**	**Transmittance**
60	60	0.**22**
63	60	0.**21**
60	-60	0.**60**
63	-60	**0.55**

4.7.2 Slat Angle, ϕ

The slat angle was not set with precision. For this experiment the error in slat angle setting was estimated to be approximately $\pm 5^0$. Let us consider a sheer blind with $\phi = 60^0$. It was observed that for $\Omega = 60^0$, a 3^0 change in slat angle changed solar transmittance by 0.10 and for $\Omega = -60^0$, a 3^0 change in slat angle changed solar transmittance by 0.05 as listed in Table 4.22.

4.7.3 Slat Thickness, T

Slat thickness also influences transmittance of the sheer blind. For $\phi = 60^0$ and $\Omega = 0^0$ a change in 0.1 mm thickness of fabric slat changes the transmittance by 0.002 . At $\Omega = -60^0$ when the peak transmission occurs the change in transmittance is 0.01 for the same 0.1 mm thickness change. The thickness in slat fabric represents blockage of incident radiation.

It was observed that the sensitivity of $\tau_{f,t}$ with respect to T increases as Ω decreases from 0^0 to -60^0. As the profile angle decreases the slat area occupies a larger portion of the total area perpendicular to incident radiation. This means at profile angle Ω=0^0 the sample port area that receives the incoming radiation takes the shape of a circle. As the profile angle reduces the illuminated projected area of the entrance port reduces to ellipse as shown in Figure 4.21. However, the area blocked by the slats remains constant within this projected area exposed to sample port. Therefore the ratio of unblocked area to the projected area decreases and the errors in transmittance measurement increases.

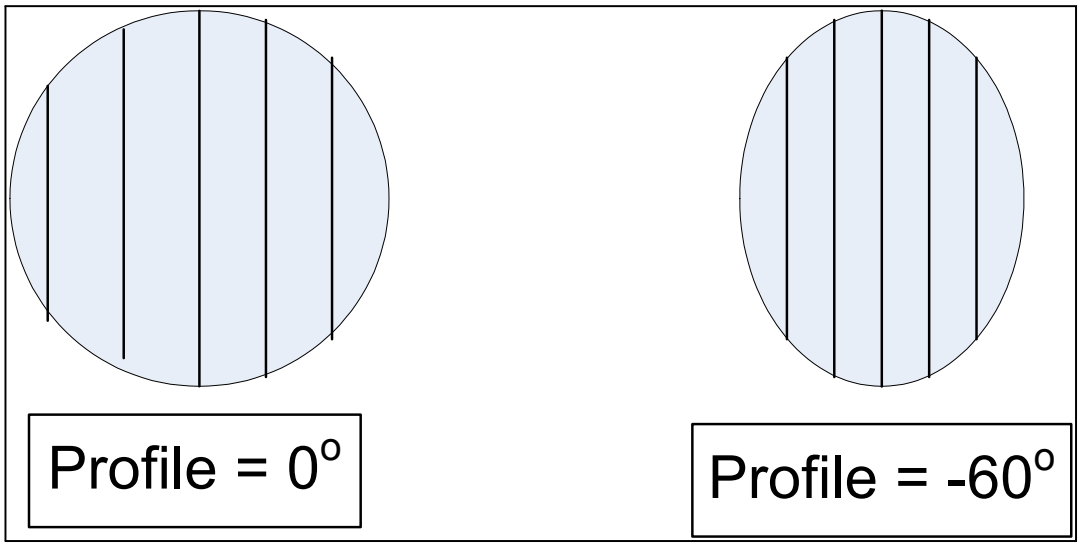

Figure 4.21: Projected area of inlet port for different profile angles (Jiang 2005)

The non-uniform sample design may cause an additional change in transmittance by 0.05 to 0.06 especially at higher slat and deeper profile angles. This is the likely cause of larger discrepancies in results between model and experiments at maximum transmission cases when the incident radiation is more closely aligned with the slats.

4.8 Conclusion

As far as the refurbishment and experimental results were concerned, both were done successfully. The experimental data had an excellent agreement with modelled results for the sheer blind. The solar transmittance obtained from the BAI-IS correlates well in terms of trend and magnitude with the analytical results obtained from shading device model. Due to inaccuracies with the dimensional attributes of the sample the following comments are offered:

A 10% change in slat spacing for sheer blind sample changes the transmittance by ± 0.01 for high slat angle ($\phi = 60^0$) and at high profile angle ($\Omega = 60^0$).

A 10% change in slat angle for sheer blind sample changes the transmittance by a maximum ± 0.05 for high slat angle ($\phi = 60^0$) and at the maximum transmission configuration when ($\phi + \Omega \approx 0^0$).

A small change (δT =0.1mm) in slat thickness changes the transmittance by ± 0.01 for high slat angle ($\phi = 60^0$) and at maximum transmission configuration when ($\phi + \Omega \approx 0^0$).

Despite the limitations of the existing lamp feedback mechanism, the chopper and slow sample traversing speed the transmittance measurement uncertainty was low ($\delta \tau_{Solar} < 0.01$) due to the strict control of the measurement process by adopting multiple measurements and allowing more scan time and wait-time for voltage readings to reach steady state.

Chapter 5

Uncertainty Analysis

The uncertainty in solar transmittance measurement was in general:

$$\frac{\delta\tau_{Solar}}{\tau_{Solar}} < \pm 1.0\%$$

The uncertainty in wavelength setting was estimated to be:

$$\delta\lambda = \pm 0.02\ \mu m$$

Although $\delta\lambda$ represents some uncertainty in λ_i, the wavelength(s) at which $\tau(\lambda_i)$ were measured, it was assumed that $\delta\lambda$ has little or no influence on $\delta\tau_{Solar}$. This is especially clear for the measurements of samples that are not spectrally selective such as the sheer blind considered in this study.

The detailed calculations of uncertainty analysis are shown in Appendix I.

Chapter 6

Conclusions and Recommendations

6.1 Conclusions

The custom-made broad area illuminating spectrophotometer was successfully re-furbished at the solar thermal research laboratory, University of Waterloo, by replacing old, non-standard equipment and control devices. All components were calibrated and tested. It is well established that this larger integrating sphere is capable of measuring directional hemispherical spectral transmittance of different louvered type shading devices using an artificial source. Spectral quantities can be recorded for wavelengths from 0.4 μm to 2.0 μm, which covers approximately 95% of the total solar spectrum energy.

The solar transmittance of a sheer blind was measured. Directional-hemispherical solar transmittance measurements were compared with analytical results. This comparison showed that the experiment and prediction agree well in most cases. The largest discrepancies in transmission (approximately 0.10) were observed when the incident ray was parallel to, or nearly parallel to the slats. The discrepancies were analyzed and the apparent causes were examined showing that non-uniform slat spacing, slat thickness and slat angle are key factors regarding the solar transmittance of a sheer blind.

6.2 Recommendations

1. Lamp feedback mechanism : It was found that the existing lamp feedback mechanism does not keep the lamp voltage sufficiently steady. It was also noted that increased voltage enables more radiative energy to pass through the integrating sphere and monochromator providing better signal-to-noise ratio. However, it is not possible to increase the lamp voltage to 120 V DC with the existing power supply because the control circuitry cannot withstand this excess input. In order to increase the power input as well as to have stable incident radiation, it is recommended to replace the existing sub-system with a commercial lamp feedback mechanism.

2. To increase the chopper frequency, it is recommended that the chopper motor be upgraded. Increased chopper speed will reduce noise leading to reduced scan times and more samples per reading. The faster sampling rate can reduce the single reading scan time by 2 to 3 minutes, which can reduce total sample processing time by an estimated 1 to 2 hours.

3. The measurement process is laborious and time consuming. It was observed that for a set of readings in the short wavelength range, with the Si photo-diode sensor, one reading at a single wavelength takes 5 to 9 minutes to sufficiently reduce uncertainty. For higher profile angles, the sample needs to be moved further aside to be clear of the inlet port. For the long wavelength range the total time for each measurement is 8 to 12 minutes to accommodate more sample readings. The traversing mechanism is slow so it takes about 60% of total time to move the sample. For a complete set of readings, it takes 14 to15 hours including setup time. By upgrading the traversing mechanism the total scan time can be reduced to 8 or 9 hours.

4. For future experiments better sheer blind samples need to be fabricated to ensure that the slat spacing, slat angles and slat thickness are uniform.

5. In this research the fabricated sheer blind sample did not represent the actual product. Since the BAI-IS cannot measure optical properties of very thick scattering samples, the sheer blind sample was fabricated with reduced slat

width and slat separation. The sample slats were flat. However, the actual product has a more complex geometry (Figure 4.3). Therefore, a proper analytical model needs to be formulated to represent the actual product.

6. The integrating sphere and the monochromator are the primary components of the BAI-IS. The sphere coating should be investigated for re-coating to improve the wall reflectance and hence the signal-to-noise ratio, particularly at wavelengths above 1.0 μm.

7. Due to time constraints, only one shade of fabric was used to fabricate the sample sheer blind. A sheer blind with darker shade should also be tested to check if the analytical model works well for a wide variety of products.

8. The width of the slat fabric can be extended beyond 16.68 mm to detect the apparatus limitation for sample thickness at which the outscattering loss will not be compensated. For experiments with sheer blinds having a realistic 2 or 3-inch slat width, a much larger sphere with larger sample port would be needed. With the existing sphere, a larger port diameter will enable measurement over larger area of the blind sample. Even though a larger inlet port will increase the incoming radiant flux but this increased port diameter will also increase the back-reflection of the sample. This increase in port fraction, f, will increase internal sample reflectance error and reduce sphere response as discussed in Section 2.4.1 and 2.4.2.

Solar optical property measurement for shading devices and other advanced glazing materials will become more popular and demanding since the energy sector is in the midst of tremendous pressure for conservation to save natural resources and protect the environment. The BAI-IS apparatus has been refurbished to continue research to standardize the measurement process, analyze errors and study optical properties of different types of materials.

Appendix

Appendix A

Lock-in Amplifier Check Guide

A.1 Introduction

This guide is aimed at users of 410 lock-in amplifiers to aid as a check of the boards. It is also useful as a basic introduction into how the board works (Smith, J.W. 2005)

A.2 Basic Test Set-up

A.2.1 Switch and Dial Positions

Switch and dial positions on the front panel of the lock-in-amplifier are shown in Table A.1.

A.2.2 Signal Inputs

The input signal should be connected to a 1V peak amplitude sinewave at 30Hz and the reference should be connected to a TTL or CMOS level square wave at the same frequency. Most signal generators will have suitable outputs for these signals.

Table A.1: Switch Positions in The Lock-in-Amplifier

Output Time Constant	100μs
Offset Control	Off
Reference Coarse Phase Shift	0°
Reference Fine Phase Shift	0°
Reference 1F / 2F	1F
Input Sensitivity	1V

A.2.3 Major Signal Waveforms

The input and reference signal inputs should appear as shown in Figure A.1:

With these inputs, the output should look similar to the top graph of the following waveforms. By adjusting the course phase adjustment, it should be possible to produce the other waveforms as shown in Figure A.2:

A.2.4 Time Constant

By increasing the value of the time constant. It should be possible to slowly flatten the output waveform so that it gets closer and closer to a DC level as is shown in Figure A.3.

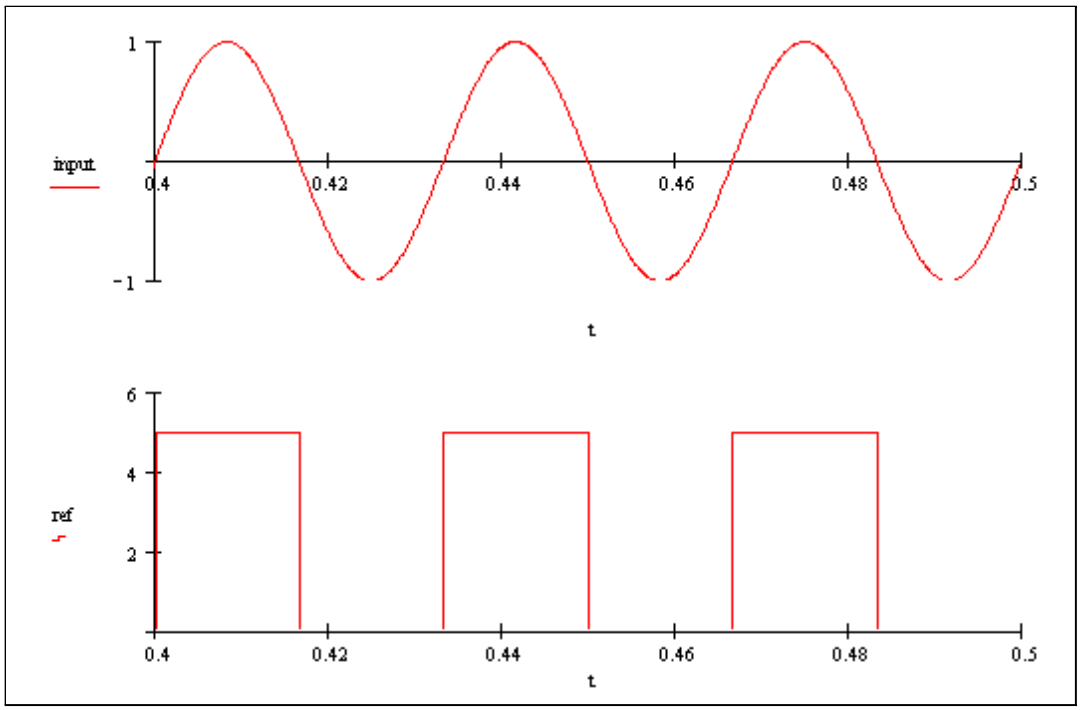

Figure A.1: Typical Input and Reference Signal of a Lock-in-Amplifier

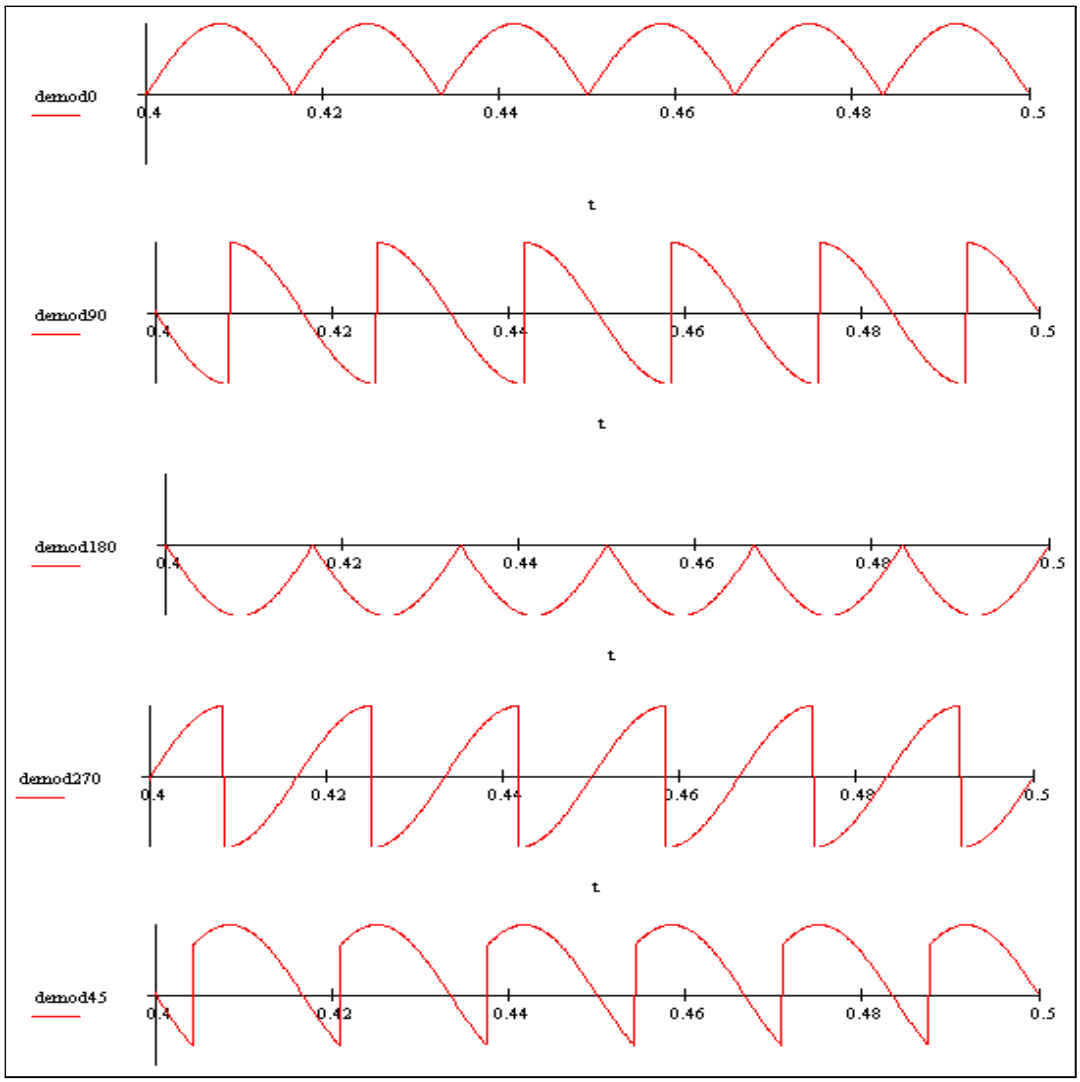

Figure A.2: Output Waveform of Lock-in-Amplifier

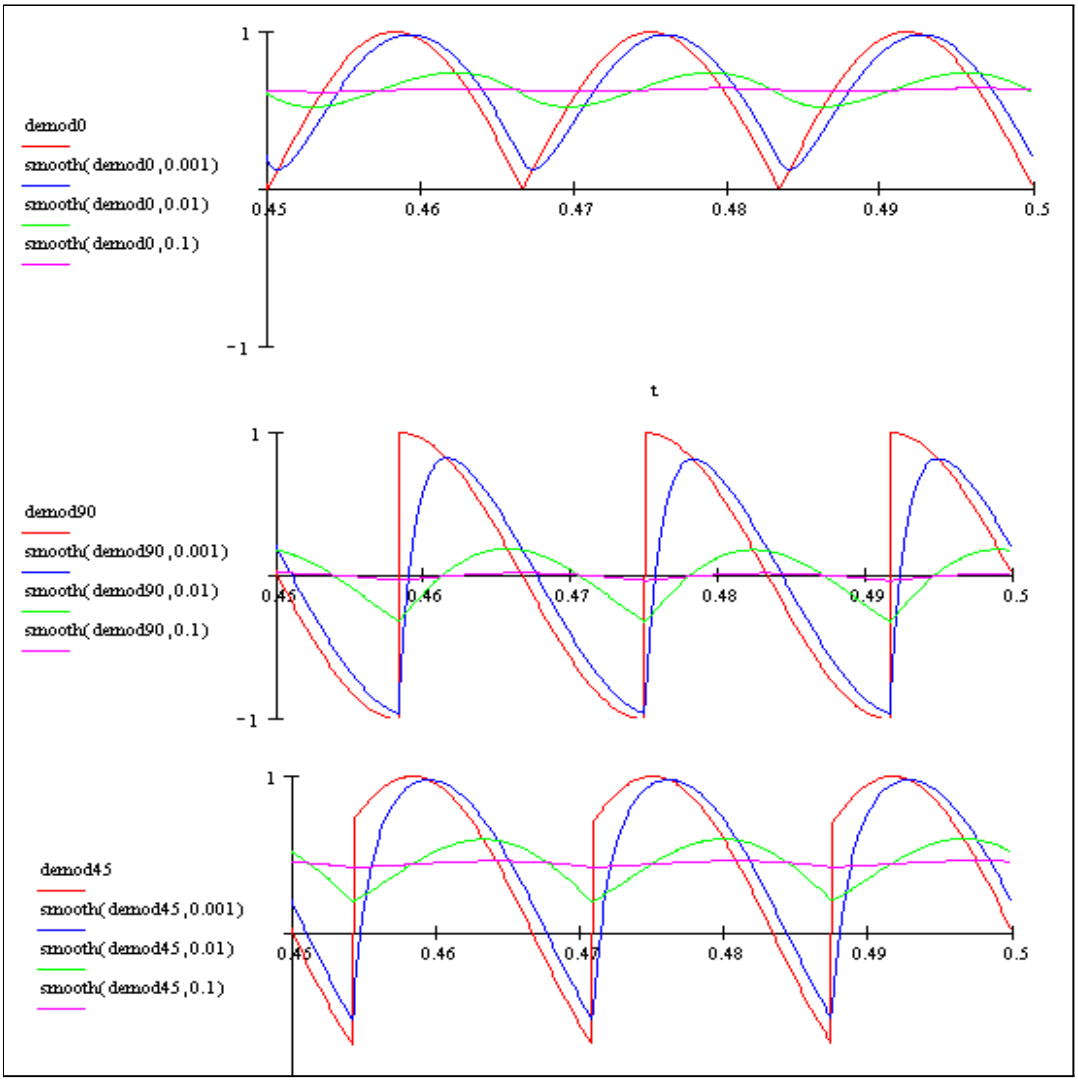

Figure A.3: The Effect of Time Constant in a Lock-in-Amplifier

Appendix B

Typical Reflectance Data of Integrating Sphere Coating(Labsphere Inc. 2007)

Table B.1: Reflectance Data of Labsphere Reflective Coating for Integrating Sphere

Wavelength [μm]	Reflectance	Wavelength [μm]	Reflectance
0.25	0.94	1.40	0.93
0.30	0.96	1.45	0.91
0.35	0.97	1.50	0.92
0.40	0.98	1.55	0.92
0.45	0.98	1.60	0.92
0.50	0.98	1.65	0.92
0.55	0.98	1.70	0.92
0.60	0.98	1.75	0.91
0.65	0.98	1.80	0.91
0.70	0.97	1.85	0.91
0.75	0.97	1.90	0.86
0.80	0.97	1.95	0.83
0.85	0.97	2.00	0.85
0.90	0.97	2.05	0.86
0.95	0.97	2.10	0.86
1.00	0.97	2.15	0.87
1.05	0.96	2.20	0.87
1.10	0.96	2.25	0.86
1.15	0.96	2.30	0.84
1.20	0.95	2.35	0.83
1.25	0.95	2.40	0.82
1.30	0.95	2.45	0.8
1.35	0.94	2.50	0.77

Appendix C

Spectral Transmittance Measurement of a Sheer Blind Using the BAI-IS

Table C.1: Transmittance of a Sheer Blind at Slat Angle 0 Deg and Profile Angle 0 Deg

Wavelength	Transmittance	Wavelength	Transmittance	Wavelength	Transmittance
λ, [μm]	$\tau(\lambda)$	λ, [μm]	$\tau(\lambda)$	λ, [μm]	$\tau(\lambda)$
0.40	0.79	0.70	0.73	1.28	0.74
0.41	0.75	0.71	0.73	1.31	0.74
0.42	0.77	0.72	0.73	1.34	0.73
0.43	0.75	0.74	0.73	1.36	0.73
0.44	0.74	0.75	0.73	1.39	0.73
0.45	0.72	0.76	0.73	1.42	0.75
0.47	0.71	0.77	0.73	1.45	0.74
0.48	0.70	0.79	0.73	1.48	0.75
0.50	0.69	0.80	0.73	1.51	0.74
0.52	0.70	0.82	0.73	1.54	0.74
0.53	0.70	0.83	0.73	1.57	0.74
0.54	0.70	0.85	0.73	1.59	0.74
0.55	0.70	0.86	0.73	1.62	0.76
0.56	0.70	0.86	0.73	1.65	0.75
0.57	0.70	0.88	0.73	1.68	0.75
0.58	0.70	0.91	0.73	1.70	0.74
0.59	0.70	0.93	0.73	1.73	0.76
0.60	0.70	0.95	0.73	1.76	0.76
0.60	0.70	0.97	0.73	1.79	0.76
0.61	0.70	0.99	0.73	1.81	0.69
0.62	0.71	1.01	0.73	1.84	0.69
0.63	0.71	1.04	0.81	1.86	0.69
0.64	0.73	1.07	0.77	1.89	0.71
0.64	0.73	1.10	0.77	1.92	0.68
0.65	0.73	1.13	0.75	1.94	0.73
0.66	0.73	1.16	0.74	1.97	0.72
0.67	0.72	1.19	0.73	1.99	0.72
0.68	0.73	1.22	0.74		
0.69	0.73	1.25	0.74		

Table C.2: Transmittance of a Sheer Blind at Slat Angle 0 Deg and Profile Angle 30 Deg

Wavelength	Transmittance	Wavelength	Transmittance	Wavelength	Transmittance
λ, [μm]	$\tau(\lambda)$	λ, [μm]	$\tau(\lambda)$	λ, [μm]	$\tau(\lambda)$
0.40	0.51	0.70	0.51	1.28	0.57
0.41	0.50	0.71	0.51	1.31	0.56
0.42	0.47	0.72	0.51	1.34	0.58
0.43	0.45	0.74	0.51	1.36	0.58
0.44	0.42	0.75	0.51	1.39	0.59
0.45	0.42	0.76	0.51	1.42	0.59
0.47	0.43	0.77	0.51	1.45	0.58
0.48	0.44	0.79	0.51	1.48	0.59
0.50	0.45	0.80	0.51	1.51	0.60
0.52	0.46	0.82	0.51	1.54	0.59
0.53	0.48	0.83	0.51	1.57	0.60
0.54	0.49	0.85	0.51	1.59	0.61
0.55	0.50	0.86	0.51	1.62	0.63
0.56	0.57	0.86	0.51	1.65	0.65
0.57	0.50	0.88	0.51	1.68	0.65
0.58	0.49	0.91	0.51	1.70	0.67
0.59	0.49	0.93	0.51	1.73	0.69
0.60	0.49	0.95	0.51	1.76	0.69
0.60	0.49	0.97	0.51	1.79	0.71
0.61	0.49	0.99	0.51	1.81	0.74
0.62	0.50	1.01	0.51	1.84	0.75
0.63	0.50	1.04	0.55	1.86	0.76
0.64	0.50	1.07	0.54	1.89	0.77
0.64	0.50	1.10	0.54	1.92	0.77
0.65	0.50	1.13	0.54	1.94	0.77
0.66	0.51	1.16	0.54	1.97	0.80
0.67	0.51	1.19	0.54	1.99	0.77
0.68	0.51	1.22	0.54		
0.69	0.51	1.25	0.55		

Table C.3: Transmittance of a Sheer Blind at Slat Angle 0 Deg and Profile Angle 45 Deg

Wavelength	Transmittance	Wavelength	Transmittance	Wavelength	Transmittance
λ, [μm]	$\tau(\lambda)$	λ, [μm]	$\tau(\lambda)$	λ, [μm]	$\tau(\lambda)$
0.40	0.31	0.70	0.40	1.28	0.38
0.41	0.32	0.71	0.39	1.31	0.38
0.42	0.32	0.72	0.40	1.34	0.38
0.43	0.31	0.74	0.39	1.36	0.40
0.44	0.30	0.75	0.40	1.39	0.39
0.45	0.30	0.76	0.40	1.42	0.39
0.47	0.32	0.77	0.39	1.45	0.38
0.48	0.33	0.79	0.39	1.48	0.38
0.50	0.35	0.80	0.39	1.51	0.36
0.52	0.35	0.82	0.39	1.54	0.36
0.53	0.35	0.83	0.39	1.57	0.36
0.54	0.36	0.85	0.39	1.59	0.35
0.55	0.36	0.86	0.39	1.62	0.34
0.56	0.37	0.86	0.39	1.65	0.35
0.57	0.37	0.88	0.39	1.68	0.36
0.58	0.38	0.91	0.39	1.70	0.38
0.59	0.38	0.93	0.39	1.73	0.38
0.60	0.38	0.95	0.39	1.76	0.41
0.60	0.39	0.97	0.39	1.79	0.43
0.61	0.38	0.99	0.40	1.81	0.44
0.62	0.38	1.01	0.39	1.84	0.44
0.63	0.39	1.04	0.37	1.86	0.47
0.64	0.39	1.07	0.37	1.89	0.42
0.64	0.39	1.10	0.38	1.92	0.50
0.65	0.40	1.13	0.38	1.94	0.47
0.66	0.39	1.16	0.38	1.97	0.48
0.67	0.39	1.19	0.38	1.99	0.49
0.68	0.39	1.22	0.38		
0.69	0.40	1.25	0.38		

Table C.4: Transmittance of a Sheer Blind at Slat Angle 0 Deg and Profile Angle 60 Deg

Wavelength	Transmittance	Wavelength	Transmittance	Wavelength	Transmittance
λ, [μm]	$\tau(\lambda)$	λ, [μm]	$\tau(\lambda)$	λ, [μm]	$\tau(\lambda)$
0.40	0.05	0.70	0.33	1.28	0.35
0.41	0.18	0.71	0.34	1.31	0.35
0.42	0.21	0.72	0.34	1.34	0.35
0.43	0.22	0.74	0.34	1.36	0.35
0.44	0.22	0.75	0.34	1.39	0.35
0.45	0.23	0.76	0.34	1.42	0.35
0.47	0.25	0.77	0.35	1.45	0.36
0.48	0.27	0.79	0.35	1.48	0.35
0.50	0.29	0.80	0.35	1.51	0.35
0.52	0.30	0.82	0.35	1.54	0.34
0.53	0.30	0.83	0.35	1.57	0.35
0.54	0.32	0.85	0.35	1.59	0.37
0.55	0.32	0.86	0.35	1.62	0.36
0.56	0.33	0.86	0.35	1.65	0.38
0.57	0.32	0.88	0.35	1.68	0.37
0.58	0.33	0.91	0.35	1.70	0.38
0.59	0.33	0.93	0.35	1.73	0.41
0.60	0.32	0.95	0.35	1.76	0.43
0.60	0.33	0.97	0.36	1.79	0.46
0.61	0.33	0.99	0.36	1.81	0.47
0.62	0.33	1.01	0.37	1.84	0.50
0.63	0.33	1.04	0.33	1.86	0.48
0.64	0.33	1.07	0.33	1.89	0.48
0.64	0.33	1.10	0.33	1.92	0.51
0.65	0.33	1.13	0.34	1.94	0.52
0.66	0.33	1.16	0.34	1.97	0.58
0.67	0.33	1.19	0.35	1.99	0.54
0.68	0.34	1.22	0.35		
0.69	0.34	1.25	0.35		

Table C.5: Transmittance of a Sheer Blind at Slat Angle 0 Deg and Profile Angle -30 Deg

Wavelength	Transmittance	Wavelength	Transmittance	Wavelength	Transmittance
λ, [μm]	τ(λ)	λ, [μm]	τ(λ)	λ, [μm]	τ(λ)
0.40	0.40	0.60	0.49	0.76	0.52
0.41	0.44	0.60	0.50	0.77	0.51
0.42	0.44	0.61	0.50	0.79	0.52
0.43	0.43	0.62	0.50	0.80	0.52
0.44	0.42	0.63	0.50	0.82	0.52
0.45	0.42	0.64	0.51	0.83	0.52
0.47	0.44	0.64	0.51	0.85	0.52
0.48	0.45	0.65	0.51	0.86	0.52
0.50	0.47	0.66	0.51	0.86	0.52
0.52	0.47	0.67	0.51	0.88	0.52
0.53	0.45	0.68	0.51	0.91	0.52
0.54	0.46	0.69	0.51	0.93	0.52
0.55	0.48	0.70	0.51	0.95	0.52
0.56	0.48	0.71	0.51	0.97	0.52
0.57	0.49	0.72	0.51	0.99	0.52
0.58	0.49	0.74	0.52	1.01	0.52
0.59	0.50	0.75	0.52		

Table C.6: Transmittance of a Sheer Blind at Slat Angle 0 Deg and Profile Angle -45 Deg

Wavelength	Transmittance	Wavelength	Transmittance	Wavelength	Transmittance
λ, [μm]	τ(λ)	λ, [μm]	τ(λ)	λ, [μm]	τ(λ)
0.40	0.22	0.60	0.37	0.76	0.39
0.41	0.27	0.60	0.37	0.77	0.39
0.42	0.28	0.61	0.37	0.79	0.39
0.43	0.28	0.62	0.38	0.80	0.39
0.44	0.27	0.63	0.38	0.82	0.39
0.45	0.28	0.64	0.38	0.83	0.39
0.47	0.30	0.64	0.38	0.85	0.38
0.48	0.32	0.65	0.38	0.86	0.38
0.50	0.34	0.66	0.38	0.86	0.38
0.52	0.34	0.67	0.38	0.88	0.38
0.53	0.35	0.68	0.38	0.91	0.38
0.54	0.36	0.69	0.39	0.93	0.38
0.55	0.37	0.70	0.39	0.95	0.38
0.56	0.36	0.71	0.39	0.97	0.38
0.57	0.36	0.72	0.39	0.99	0.38
0.58	0.37	0.74	0.39	1.01	0.38
0.59	0.37	0.75	0.39		

Table C.7: Transmittance of a Sheer Blind at Slat Angle 0 Deg and Profile Angle -60 Deg

Wavelength	Transmittance	Wavelength	Transmittance	Wavelength	Transmittance
λ, [μm]	τ(λ)	λ, [μm]	τ(λ)	λ, [μm]	τ(λ)
0.40	0.16	0.60	0.32	0.76	0.33
0.41	0.15	0.60	0.32	0.77	0.32
0.42	0.20	0.61	0.32	0.79	0.32
0.43	0.21	0.62	0.32	0.80	0.33
0.44	0.22	0.63	0.32	0.82	0.33
0.45	0.22	0.64	0.33	0.83	0.33
0.47	0.24	0.64	0.32	0.85	0.33
0.48	0.26	0.65	0.33	0.86	0.33
0.50	0.28	0.66	0.32	0.86	0.33
0.52	0.29	0.67	0.32	0.88	0.33
0.53	0.29	0.68	0.33	0.91	0.33
0.54	0.31	0.69	0.32	0.93	0.33
0.55	0.31	0.70	0.32	0.95	0.33
0.56	0.31	0.71	0.33	0.97	0.33
0.57	0.31	0.72	0.32	0.99	0.33
0.58	0.31	0.74	0.33	1	0.33
0.59	0.32	0.75	0.33		

Table C.8: Transmittance of a Sheer Blind at Slat Angle 30 Deg and Profile Angle 0 Deg

Wavelength	Transmittance	Wavelength	Transmittance	Wavelength	Transmittance
λ, [μm]	τ(λ)	λ, [μm]	τ(λ)	λ, [μm]	τ(λ)
0.40	0.38	0.60	0.50	0.76	0.51
0.41	0.39	0.60	0.50	0.77	0.52
0.42	0.40	0.61	0.50	0.79	0.52
0.43	0.40	0.62	0.50	0.80	0.53
0.44	0.41	0.63	0.50	0.82	0.53
0.45	0.43	0.64	0.50	0.83	0.53
0.47	0.45	0.64	0.50	0.85	0.53
0.48	0.46	0.65	0.50	0.86	0.54
0.50	0.47	0.66	0.50	0.86	0.54
0.52	0.48	0.67	0.50	0.88	0.54
0.53	0.48	0.68	0.50	0.91	0.54
0.54	0.48	0.69	0.50	0.93	0.54
0.55	0.48	0.70	0.50	0.95	0.55
0.56	0.48	0.71	0.50	0.97	0.56
0.57	0.49	0.72	0.50	0.99	0.57
0.58	0.49	0.74	0.50	1.01	0.57
0.59	0.49	0.75	0.51		

Table C.9: Transmittance of a Sheer Blind at Slat Angle 30 Deg and Profile Angle 30 Deg

Wavelength	Transmittance	Wavelength	Transmittance	Wavelength	Transmittance
λ, [μm]	τ(λ)	λ, [μm]	τ(λ)	λ, [μm]	τ(λ)
0.41	0.19	0.60	0.34	0.77	0.38
0.42	0.20	0.61	0.34	0.79	0.38
0.43	0.22	0.62	0.34	0.80	0.39
0.44	0.22	0.63	0.34	0.82	0.39
0.45	0.23	0.64	0.35	0.83	0.39
0.47	0.25	0.64	0.34	0.85	0.39
0.48	0.28	0.65	0.35	0.86	0.39
0.50	0.29	0.66	0.35	0.86	0.40
0.52	0.30	0.67	0.36	0.88	0.40
0.53	0.31	0.68	0.37	0.91	0.41
0.54	0.32	0.69	0.37	0.93	0.43
0.55	0.32	0.70	0.38	0.95	0.44
0.56	0.32	0.71	0.38	0.97	0.46
0.57	0.33	0.72	0.38	0.99	0.49
0.58	0.33	0.74	0.38	1.01	0.52
0.59	0.33	0.75	0.38		
0.60	0.33	0.76	0.38		

Table C.10: Transmittance of a Sheer Blind at Slat Angle 30 Deg and Profile Angle 45 Deg

Wavelength	Transmittance	Wavelength	Transmittance	Wavelength	Transmittance
λ, [μm]	τ(λ)	λ, [μm]	τ(λ)	λ, [μm]	τ(λ)
0.40	0.17	0.60	0.31	0.76	0.33
0.41	0.20	0.60	0.31	0.77	0.33
0.42	0.20	0.61	0.32	0.79	0.33
0.43	0.20	0.62	0.32	0.80	0.33
0.44	0.22	0.63	0.32	0.82	0.33
0.45	0.24	0.64	0.32	0.83	0.33
0.47	0.26	0.64	0.32	0.85	0.33
0.48	0.27	0.65	0.32	0.86	0.33
0.50	0.28	0.66	0.33	0.86	0.33
0.52	0.29	0.67	0.32	0.88	0.33
0.53	0.29	0.68	0.33	0.91	0.33
0.54	0.29	0.69	0.32	0.93	0.33
0.55	0.30	0.70	0.33	0.95	0.32
0.56	0.30	0.71	0.33	0.97	0.33
0.57	0.31	0.72	0.33	0.99	0.34
0.58	0.31	0.74	0.33	1.01	0.33
0.59	0.31	0.75	0.33		

Table C.11: Transmittance of a Sheer Blind at Slat Angle 30 Deg and Profile Angle 60 Deg

Wavelength	Transmittance	Wavelength	Transmittance	Wavelength	Transmittance
λ, [μm]	$\tau(\lambda)$	λ, [μm]	$\tau(\lambda)$	λ, [μm]	$\tau(\lambda)$
0.42	0.01	0.61	0.31	0.79	0.31
0.43	0.06	0.62	0.31	0.80	0.31
0.44	0.10	0.63	0.32	0.82	0.31
0.45	0.13	0.64	0.32	0.83	0.31
0.47	0.17	0.64	0.32	0.85	0.32
0.48	0.20	0.65	0.31	0.86	0.32
0.50	0.22	0.66	0.32	0.86	0.32
0.52	0.24	0.67	0.32	0.88	0.33
0.53	0.24	0.68	0.32	0.91	0.34
0.54	0.23	0.69	0.32	0.93	0.35
0.55	0.24	0.70	0.32	0.95	0.36
0.56	0.25	0.71	0.32	0.97	0.38
0.57	0.25	0.72	0.31	0.99	0.41
0.58	0.25	0.74	0.31	1.01	0.46
0.59	0.28	0.75	0.31		
0.60	0.29	0.76	0.31		
0.60	0.30	0.77	0.31		

Table C.12: Transmittance of a Sheer Blind at Slat Angle 30 Deg and Profile Angle -30 Deg

Wavelength	Transmittance	Wavelength	Transmittance	Wavelength	Transmittance
λ, [μm]	$\tau(\lambda)$	λ, [μm]	$\tau(\lambda)$	λ, [μm]	$\tau(\lambda)$
0.40	0.61	0.60	0.70	0.76	0.70
0.41	0.63	0.60	0.69	0.77	0.70
0.42	0.64	0.61	0.69	0.79	0.70
0.43	0.64	0.62	0.70	0.80	0.70
0.44	0.65	0.63	0.70	0.82	0.70
0.45	0.66	0.64	0.69	0.83	0.70
0.47	0.67	0.64	0.70	0.85	0.70
0.48	0.67	0.65	0.70	0.86	0.70
0.50	0.68	0.66	0.70	0.86	0.71
0.52	0.68	0.67	0.70	0.88	0.71
0.53	0.68	0.68	0.70	0.91	0.70
0.54	0.68	0.69	0.70	0.93	0.70
0.55	0.69	0.70	0.70	0.95	0.71
0.56	0.69	0.71	0.70	0.97	0.70
0.57	0.69	0.72	0.70	0.99	0.71
0.58	0.69	0.74	0.70	1	0.69
0.59	0.70	0.75	0.70		

Table C.13: Transmittance of a Sheer Blind at Slat Angle 30 Deg and Profile Angle -45 Deg

Wavelength	Transmittance	Wavelength	Transmittance	Wavelength	Transmittance
λ, [μm]	τ(λ)	λ, [μm]	τ(λ)	λ, [μm]	τ(λ)
0.40	0.36	0.60	0.57	0.76	0.61
0.41	0.42	0.60	0.57	0.77	0.58
0.42	0.44	0.61	0.57	0.79	0.58
0.43	0.46	0.62	0.58	0.80	0.57
0.44	0.48	0.63	0.58	0.82	0.58
0.45	0.50	0.64	0.58	0.83	0.58
0.47	0.52	0.64	0.58	0.85	0.58
0.48	0.53	0.65	0.58	0.86	0.58
0.50	0.54	0.66	0.58	0.86	0.58
0.52	0.54	0.67	0.58	0.88	0.58
0.53	0.54	0.68	0.59	0.91	0.58
0.54	0.54	0.69	0.59	0.93	0.58
0.55	0.56	0.70	0.59	0.95	0.58
0.56	0.56	0.71	0.59	0.97	0.58
0.57	0.57	0.72	0.59	0.99	0.58
0.58	0.57	0.74	0.60	1	0.57
0.59	0.57	0.75	0.60		

Table C.14: Transmittance of a Sheer Blind at Slat Angle 30 Deg and Profile Angle -60 Deg

Wavelength	Transmittance	Wavelength	Transmittance	Wavelength	Transmittance
λ, [μm]	τ(λ)	λ, [μm]	τ(λ)	λ, [μm]	τ(λ)
		0.60	0.34	0.76	0.38
0.41	0.08	0.60	0.34	0.77	0.38
0.42	0.13	0.61	0.34	0.79	0.38
0.43	0.17	0.62	0.34	0.80	0.38
0.44	0.20	0.63	0.35	0.82	0.38
0.45	0.24	0.64	0.35	0.83	0.38
0.47	0.27	0.64	0.37	0.85	0.38
0.48	0.29	0.65	0.37	0.86	0.38
0.50	0.30	0.66	0.37	0.86	0.39
0.52	0.31	0.67	0.37	0.88	0.39
0.53	0.30	0.68	0.38	0.91	0.40
0.54	0.32	0.69	0.38	0.93	0.41
0.55	0.32	0.70	0.38	0.95	0.42
0.56	0.33	0.71	0.38	0.97	0.44
0.57	0.33	0.72	0.38	0.99	0.47
0.58	0.33	0.74	0.38	1	0.51
0.59	0.34	0.75	0.38		

Table C.15: Transmittance of a Sheer Blind at Slat Angle 45 Deg and Profile Angle 0 Deg

Wavelength	Transmittance	Wavelength	Transmittance	Wavelength	Transmittance
λ, [μm]	$\tau(\lambda)$	λ, [μm]	$\tau(\lambda)$	λ, [μm]	$\tau(\lambda)$
0.41	0.17	0.70	0.45	1.25	0.41
0.42	0.23	0.71	0.45	1.28	0.40
0.43	0.27	0.72	0.45	1.31	0.40
0.44	0.29	0.74	0.45	1.34	0.40
0.45	0.32	0.75	0.45	1.36	0.40
0.47	0.35	0.76	0.45	1.39	0.39
0.48	0.37	0.77	0.45	1.42	0.38
0.50	0.39	0.79	0.46	1.45	0.38
0.52	0.40	0.80	0.46	1.48	0.36
0.53	0.41	0.82	0.46	1.51	0.34
0.54	0.42	0.83	0.46	1.54	0.34
0.55	0.42	0.85	0.46	1.57	0.31
0.56	0.42	0.86	0.47	1.59	0.28
0.57	0.43	0.86	0.46	1.62	0.37
0.58	0.43	0.88	0.47	1.65	0.38
0.59	0.43	0.91	0.47	1.68	0.41
0.60	0.43	0.93	0.47	1.70	0.40
0.60	0.43	0.95	0.48	1.73	0.42
0.61	0.43	0.97	0.49	1.76	0.45
0.62	0.44	0.99	0.49	1.79	0.18
0.63	0.44	1.01	0.51	1.81	0.19
0.64	0.44	1.04	0.42	1.84	0.19
0.64	0.44	1.07	0.42	1.86	0.13
0.65	0.44	1.10	0.42	1.89	0.05
0.66	0.44	1.13	0.42	1.92	0.07
0.67	0.44	1.16	0.42	1.94	0.05
0.68	0.45	1.19	0.41	1.97	0.14
0.69	0.45	1.22	0.42		

Table C.16: Transmittance of a Sheer Blind at Slat Angle 45 Deg and Profile Angle 30 Deg

Wavelength	Transmittance	Wavelength	Transmittance	Wavelength	Transmittance
λ, [μm]	τ(λ)	λ, [μm]	τ(λ)	λ, [μm]	τ(λ)
0.40	0.23	0.69	0.34	1.22	0.34
0.41	0.26	0.70	0.34	1.25	0.34
0.42	0.27	0.71	0.34	1.28	0.33
0.43	0.26	0.72	0.34	1.31	0.34
0.44	0.25	0.74	0.34	1.34	0.34
0.45	0.26	0.75	0.34	1.36	0.33
0.47	0.27	0.76	0.35	1.39	0.34
0.48	0.29	0.77	0.34	1.42	0.33
0.50	0.30	0.79	0.35	1.45	0.32
0.52	0.30	0.80	0.35	1.48	0.32
0.53	0.28	0.82	0.35	1.51	0.31
0.54	0.29	0.83	0.35	1.54	0.30
0.55	0.31	0.85	0.35	1.57	0.29
0.56	0.31	0.86	0.35	1.59	0.28
0.57	0.31	0.86	0.35	1.62	0.29
0.58	0.33	0.88	0.35	1.65	0.30
0.59	0.34	0.91	0.35	1.68	0.30
0.60	0.33	0.93	0.35	1.70	0.29
0.60	0.33	0.95	0.36	1.73	0.30
0.61	0.34	0.97	0.36	1.76	0.31
0.62	0.34	0.99	0.36	1.79	0.32
0.63	0.33	1.01	0.37	1.81	0.32
0.64	0.34	1.04	0.34	1.84	0.32
0.64	0.33	1.07	0.34	1.86	0.33
0.65	0.33	1.10	0.34	1.89	0.31
0.66	0.34	1.13	0.34	1.92	0.33
0.67	0.34	1.16	0.34	1.94	0.26
0.68	0.34	1.19	0.34		

Table C.17: Transmittance of a Sheer Blind at Slat Angle 45 Deg and Profile Angle 45 Deg

Wavelength	Transmittance	Wavelength	Transmittance	Wavelength	Transmittance
λ, [μm]	$\tau(\lambda)$	λ, [μm]	$\tau(\lambda)$	λ, [μm]	$\tau(\lambda)$
0.40	0.21	0.69	0.37	1.22	0.27
0.41	0.22	0.70	0.36	1.25	0.27
0.42	0.24	0.71	0.36	1.28	0.26
0.43	0.23	0.72	0.36	1.31	0.25
0.44	0.22	0.74	0.36	1.34	0.24
0.45	0.23	0.75	0.36	1.36	0.24
0.47	0.24	0.76	0.35	1.39	0.24
0.48	0.26	0.77	0.32	1.42	0.23
0.50	0.27	0.79	0.33	1.45	0.22
0.52	0.28	0.80	0.33	1.48	0.24
0.53	0.28	0.82	0.34	1.51	0.20
0.54	0.29	0.83	0.34	1.54	0.22
0.55	0.29	0.85	0.34	1.57	0.20
0.56	0.29	0.86	0.34	1.59	0.17
0.57	0.29	0.86	0.34		
0.58	0.30	0.88	0.35		
0.59	0.30	0.91	0.35		
0.60	0.30	0.93	0.35		
0.60	0.31	0.95	0.36		
0.61	0.31	0.97	0.37		
0.62	0.31	0.99	0.38		
0.63	0.31	1.01	0.39		
0.64	0.31	1.04	0.28		
0.64	0.31	1.07	0.25		
0.65	0.31	1.10	0.26		
0.66	0.37	1.13	0.27		
0.67	0.37	1.16	0.30		
0.68	0.37	1.19	0.27		

Table C.18: Transmittance of a Sheer Blind at Slat Angle 45 Deg and Profile Angle 60 Deg

Wavelength	Transmittance	Wavelength	Transmittance	Wavelength	Transmittance
λ, [μm]	τ(λ)	λ, [μm]	τ(λ)	λ, [μm]	τ(λ)
0.41	0.17	0.70	0.29	1.25	0.25
0.42	0.12	0.71	0.29	1.28	0.25
0.43	0.16	0.72	0.29	1.31	0.26
0.44	0.18	0.74	0.29	1.34	0.15
0.45	0.19	0.75	0.28	1.36	0.17
0.47	0.21	0.76	0.28	1.39	0.19
0.48	0.20	0.77	0.30	1.42	0.18
0.50	0.23	0.79	0.30	1.45	0.20
0.52	0.23	0.80	0.31	1.48	0.20
0.53	0.24	0.82	0.32	1.51	0.17
0.54	0.24	0.83	0.32	1.54	0.17
0.55	0.24	0.85	0.32	1.57	0.15
0.56	0.25	0.86	0.32	1.59	0.23
0.57	0.25	0.86	0.33	1.62	0.14
0.58	0.26	0.88	0.34	1.65	0.11
0.59	0.26	0.91	0.35	1.68	0.14
0.60	0.26	0.93	0.35	1.70	0.16
0.60	0.27	0.95	0.37	1.73	0.16
0.61	0.26	0.97	0.38	1.76	0.17
0.62	0.27	0.99	0.40	1.79	0.12
0.63	0.28	1.01	0.42	1.81	0.14
0.64	0.28	1.04	0.24	1.84	0.11
0.64	0.29	1.07	0.24	1.86	0.20
0.65	0.29	1.10	0.25	1.89	0.14
0.66	0.29	1.13	0.25	1.92	0.13
0.67	0.29	1.16	0.25	1.94	0.16
0.68	0.29	1.19	0.26		
0.69	0.29	1.22	0.26		

Table C.19: Transmittance of a Sheer Blind at Slat Angle 45 Deg and Profile Angle -30 Deg

Wavelength	Transmittance	Wavelength	Transmittance	Wavelength	Transmittance
λ, [μm]	$\tau(\lambda)$	λ, [μm]	$\tau(\lambda)$	λ, [μm]	$\tau(\lambda)$
0.40	0.57	0.70	0.63	1.28	0.65
0.41	0.60	0.71	0.63	1.31	0.66
0.42	0.60	0.72	0.63	1.34	0.66
0.43	0.59	0.74	0.64	1.36	0.67
0.44	0.58	0.75	0.63	1.39	0.66
0.45	0.58	0.76	0.63	1.42	0.67
0.47	0.59	0.77	0.64	1.45	0.65
0.48	0.59	0.79	0.63	1.48	0.66
0.50	0.60	0.80	0.63	1.51	0.63
0.52	0.60	0.82	0.63	1.54	0.66
0.53	0.65	0.83	0.64	1.57	0.68
0.54	0.64	0.85	0.63	1.59	0.67
0.55	0.67	0.86	0.64	1.62	0.69
0.56	0.65	0.86	0.64	1.65	0.70
0.57	0.65	0.88	0.64	1.68	0.71
0.58	0.63	0.91	0.64	1.70	0.71
0.59	0.62	0.93	0.65	1.73	0.72
0.60	0.62	0.95	0.65	1.76	0.71
0.60	0.63	0.97	0.65	1.79	0.76
0.61	0.63	0.99	0.65	1.81	0.76
0.62	0.63	1.01	0.66	1.84	0.76
0.63	0.63	1.04	0.65	1.86	0.75
0.64	0.63	1.07	0.65	1.89	0.78
0.64	0.63	1.10	0.66	1.92	0.75
0.65	0.63	1.13	0.59	1.94	0.79
0.66	0.63	1.16	0.62	1.97	0.79
0.67	0.63	1.19	0.62	2	0.81
0.68	0.63	1.22	0.61		
0.69	0.64	1.25	0.65		

Table C.20: Transmittance of a Sheer Blind at Slat Angle 45 Deg and Profile Angle -45 Deg

Wavelength	Transmittance	Wavelength	Transmittance	Wavelength	Transmittance
λ, [μm]	$\tau(\lambda)$	λ, [μm]	$\tau(\lambda)$	λ, [μm]	$\tau(\lambda)$
0.40	0.69	0.70	0.74	1.28	0.73
0.41	0.71	0.71	0.74	1.31	0.73
0.42	0.72	0.72	0.74	1.34	0.73
0.43	0.71	0.74	0.74	1.36	0.73
0.44	0.70	0.75	0.74	1.39	0.74
0.45	0.70	0.76	0.74	1.42	0.73
0.47	0.70	0.77	0.74	1.45	0.74
0.48	0.71	0.79	0.74	1.48	0.73
0.50	0.71	0.80	0.74	1.51	0.72
0.52	0.71	0.82	0.74	1.54	0.73
0.53	0.72	0.83	0.74	1.57	0.71
0.54	0.72	0.85	0.74	1.59	0.71
0.55	0.72	0.86	0.74	1.62	0.69
0.56	0.73	0.86	0.75	1.65	0.70
0.57	0.73	0.88	0.74	1.68	0.70
0.58	0.73	0.91	0.75	1.70	0.71
0.59	0.74	0.93	0.74	1.73	0.68
0.60	0.72	0.95	0.74	1.76	0.66
0.60	0.74	0.97	0.74	1.79	0.70
0.61	0.72	0.99	0.75	1.81	0.68
0.62	0.74	1.01	0.75	1.84	0.70
0.63	0.73	1.04	0.69	1.86	0.69
0.64	0.74	1.07	0.70	1.89	0.71
0.64	0.74	1.10	0.71	1.92	0.68
0.65	0.74	1.13	0.72	1.94	0.67
0.66	0.74	1.16	0.72	1.97	0.68
0.67	0.74	1.19	0.71	2	0.76
0.68	0.73	1.22	0.73		
0.69	0.74	1.25	0.73		

Table C.21: Transmittance of a Sheer Blind at Slat Angle 45 Deg and Profile Angle -60 Deg

Wavelength	Transmittance	Wavelength	Transmittance	Wavelength	Transmittance
λ, [μm]	$\tau(\lambda)$	λ, [μm]	$\tau(\lambda)$	λ, [μm]	$\tau(\lambda)$
0.40	0.35	0.70	0.57	1.28	0.59
0.41	0.43	0.71	0.58	1.31	0.59
0.42	0.45	0.72	0.59	1.34	0.64
0.43	0.45	0.74	0.60	1.36	0.59
0.44	0.47	0.75	0.60	1.39	0.59
0.45	0.47	0.76	0.60	1.42	0.59
0.47	0.50	0.77	0.60	1.45	0.56
0.48	0.52	0.79	0.60	1.48	0.57
0.50	0.53	0.80	0.60	1.51	0.57
0.52	0.54	0.82	0.60	1.54	0.57
0.53	0.53	0.83	0.60	1.57	0.53
0.54	0.54	0.85	0.60	1.59	0.58
0.55	0.54	0.86	0.61	1.62	0.59
0.56	0.55	0.86	0.61	1.65	0.60
0.57	0.55	0.88	0.61	1.68	0.59
0.58	0.55	0.91	0.61	1.70	0.53
0.59	0.55	0.93	0.62	1.73	0.55
0.60	0.55	0.95	0.62	1.76	0.65
0.60	0.56	0.97	0.63	1.79	0.60
0.61	0.56	0.99	0.64	1.81	0.69
0.62	0.56	1.01	0.64	1.84	0.67
0.63	0.56	1.04	0.55	1.86	0.68
0.64	0.56	1.07	0.55	1.89	0.72
0.64	0.57	1.10	0.54	1.92	0.69
0.65	0.57	1.13	0.57	1.94	0.65
0.66	0.57	1.16	0.57	1.97	0.67
0.67	0.57	1.19	0.57	2	0.72
0.68	0.57	1.22	0.57		
0.69	0.57	1.25	0.58		

Table C.22: Transmittance of a Sheer Blind at Slat Angle 60 Deg and Profile Angle 0 Deg

Wavelength	Transmittance	Wavelength	Transmittance	Wavelength	Transmittance
λ [µm]	τ(λ)	λ [µm]	τ(λ)	λ [µm]	τ(λ)
0.40	0.14	0.60	0.32	0.76	0.34
0.41	0.19	0.60	0.32	0.77	0.34
0.42	0.19	0.61	0.32	0.79	0.35
0.43	0.20	0.62	0.33	0.80	0.34
0.44	0.21	0.63	0.33	0.82	0.35
0.45	0.22	0.64	0.33	0.83	0.35
0.47	0.25	0.64	0.33	0.85	0.35
0.48	0.27	0.65	0.33	0.86	0.35
0.50	0.28	0.66	0.34	0.86	0.35
0.52	0.29	0.67	0.34	0.88	0.35
0.53	0.32	0.68	0.34	0.91	0.35
0.54	0.32	0.69	0.34	0.93	0.35
0.55	0.33	0.70	0.34	0.95	0.35
0.56	0.32	0.71	0.34	0.97	0.35
0.57	0.33	0.72	0.34	0.99	0.35
0.58	0.31	0.74	0.34	1	0.35
0.59	0.31	0.75	0.34		

Table C.23: Transmittance of a Sheer Blind at Slat Angle 60 Deg and Profile Angle 30 Deg

Wavelength	Transmittance	Wavelength	Transmittance	Wavelength	Transmittance
λ [µm]	τ(λ)	λ [µm]	τ(λ)	λ [µm]	τ(λ)
0.40	0.16	0.60	0.29	0.76	0.31
0.41	0.22	0.60	0.30	0.77	0.31
0.42	0.23	0.61	0.30	0.79	0.31
0.43	0.22	0.62	0.30	0.80	0.31
0.44	0.22	0.63	0.29	0.82	0.31
0.45	0.22	0.64	0.31	0.83	0.31
0.47	0.23	0.64	0.30	0.85	0.31
0.48	0.24	0.65	0.30	0.86	0.31
0.50	0.26	0.66	0.31	0.86	0.31
0.52	0.27	0.67	0.30	0.88	0.31
0.53	0.27	0.68	0.31	0.91	0.31
0.54	0.28	0.69	0.31	0.93	0.31
0.55	0.27	0.70	0.31	0.95	0.31
0.56	0.28	0.71	0.31	0.97	0.31
0.57	0.28	0.72	0.31	0.99	0.31
0.58	0.29	0.74	0.31	1	0.31
0.59	0.29	0.75	0.31		

Table C.24: Transmittance of a Sheer Blind at Slat Angle 60 Deg and Profile Angle 45 Deg

Wavelength	Transmittance	Wavelength	Transmittance	Wavelength	Transmittance
λ, [μm]	τ(λ)	λ, [μm]	τ(λ)	λ, [μm]	τ(λ)
0.40	0.09	0.60	0.28	0.76	0.30
0.41	0.16	0.60	0.28	0.77	0.30
0.42	0.19	0.61	0.28	0.79	0.30
0.43	0.19	0.62	0.29	0.80	0.30
0.44	0.19	0.63	0.29	0.82	0.30
0.45	0.20	0.64	0.29	0.83	0.30
0.47	0.23	0.64	0.29	0.85	0.30
0.48	0.24	0.65	0.29	0.86	0.30
0.50	0.25	0.66	0.29	0.86	0.30
0.52	0.25	0.67	0.30	0.88	0.30
0.53	0.26	0.68	0.30	0.91	0.30
0.54	0.27	0.69	0.30	0.93	0.31
0.55	0.28	0.70	0.30	0.95	0.31
0.56	0.27	0.71	0.30	0.97	0.31
0.57	0.28	0.72	0.30	0.99	0.31
0.58	0.27	0.74	0.30	1	0.32
0.59	0.28	0.75	0.30		

Table C.25: Transmittance of a Sheer Blind at Slat Angle 60 Deg and Profile Angle 60 Deg

Wavelength	Transmittance	Wavelength	Transmittance	Wavelength	Transmittance
λ, [μm]	τ(λ)	λ, [μm]	τ(λ)	λ, [μm]	τ(λ)
0.40	-2.95	0.60	0.23	0.76	0.25
0.41	-0.91	0.60	0.22	0.77	0.25
0.42	-0.38	0.61	0.23	0.79	0.25
0.43	-0.16	0.62	0.23	0.80	0.25
0.44	-0.03	0.63	0.24	0.82	0.25
0.45	0.04	0.64	0.24	0.83	0.25
0.47	0.10	0.64	0.24	0.85	0.25
0.48	0.15	0.65	0.24	0.86	0.25
0.50	0.18	0.66	0.24	0.86	0.25
0.52	0.20	0.67	0.24	0.88	0.25
0.53	0.20	0.68	0.25	0.91	0.25
0.54	0.21	0.69	0.25	0.93	0.25
0.55	0.22	0.70	0.24	0.95	0.25
0.56	0.22	0.71	0.25	0.97	0.25
0.57	0.23	0.72	0.25	0.99	0.25
0.58	0.23	0.74	0.25	1	0.24
0.59	0.23	0.75	0.25		

Table C.26: Transmittance of a Sheer Blind at Slat Angle 60 Deg and Profile Angle -30 Deg

Wavelength	Transmittance	Wavelength	Transmittance	Wavelength	Transmittance
λ [µm]	τ(λ)	λ [µm]	τ(λ)	λ [µm]	τ(λ)
0.40	-0.07	0.60	0.51	0.76	0.51
0.41	0.13	0.60	0.51	0.77	0.51
0.42	0.22	0.61	0.51	0.79	0.50
0.43	0.29	0.62	0.52	0.80	0.51
0.44	0.32	0.63	0.52	0.82	0.50
0.45	0.35	0.64	0.52	0.83	0.50
0.47	0.38	0.64	0.52	0.85	0.50
0.48	0.41	0.65	0.52	0.86	0.50
0.50	0.43	0.66	0.52	0.86	0.51
0.52	0.44	0.67	0.52	0.88	0.51
0.53	0.44	0.68	0.51	0.91	0.51
0.54	0.44	0.69	0.51	0.93	0.51
0.55	0.45	0.70	0.51	0.95	0.51
0.56	0.45	0.71	0.51	0.97	0.52
0.57	0.45	0.72	0.51	0.99	0.53
0.58	0.49	0.74	0.51	1	0.53
0.59	0.50	0.75	0.51		

Table C.27: Transmittance of a Sheer Blind at Slat Angle 60 Deg and Profile Angle -45 Deg

Wavelength	Transmittance	Wavelength	Transmittance	Wavelength	Transmittance
λ [µm]	τ(λ)	λ [µm]	τ(λ)	λ [µm]	τ(λ)
		0.60	0.57	0.76	0.59
0.41	0.36	0.60	0.57	0.77	0.59
0.42	0.43	0.61	0.57	0.79	0.59
0.43	0.44	0.62	0.57	0.80	0.59
0.44	0.47	0.63	0.58	0.82	0.59
0.45	0.49	0.64	0.59	0.83	0.59
0.47	0.51	0.64	0.58	0.85	0.59
0.48	0.52	0.65	0.59	0.86	0.59
0.50	0.54	0.66	0.59	0.86	0.59
0.52	0.54	0.67	0.59	0.88	0.59
0.53	0.55	0.68	0.59	0.91	0.59
0.54	0.55	0.69	0.59	0.93	0.60
0.55	0.55	0.70	0.59	0.95	0.60
0.56	0.55	0.71	0.59	0.97	0.60
0.57	0.56	0.72	0.59	0.99	0.61
0.58	0.57	0.74	0.59	1	0.62
0.59	0.57	0.75	0.59		

Table C.28: Transmittance of a Sheer Blind at Slat Angle 60 Deg and Profile Angle -60 Deg

Wavelength	Transmittance	Wavelength	Transmittance	Wavelength	Transmittance
λ [µm]	$\tau(\lambda)$	λ [µm]	$\tau(\lambda)$	λ [µm]	$\tau(\lambda)$
0.40	0.41	0.60	0.64	0.76	0.66
0.41	0.49	0.60	0.64	0.77	0.66
0.42	0.52	0.61	0.65	0.79	0.66
0.43	0.55	0.62	0.65	0.80	0.66
0.44	0.56	0.63	0.65	0.82	0.67
0.45	0.58	0.64	0.65	0.83	0.66
0.47	0.59	0.64	0.65	0.85	0.67
0.48	0.60	0.65	0.65	0.86	0.67
0.50	0.61	0.66	0.65	0.86	0.66
0.52	0.62	0.67	0.65	0.88	0.67
0.53	0.61	0.68	0.65	0.91	0.66
0.54	0.62	0.69	0.66	0.93	0.66
0.55	0.62	0.70	0.66	0.95	0.66
0.56	0.63	0.71	0.66	0.97	0.66
0.57	0.64	0.72	0.66	0.99	0.67
0.58	0.64	0.74	0.66	1	0.67
0.59	0.64	0.75	0.66		

Appendix D

Spectral Transmittance Measurement of a Fabric Blind (Without Sheer Facings) Using the BAI-IS

Table D.1: Transmittance of a Fabric Blind (Without any Sheer Facings) at Slat Angle 0 Deg and Profile Angle 0 Deg

Wavelength	Transmittance	Wavelength	Transmittance	Wavelength	Transmittance
λ, [μm]	τ(λ)	λ, [μm]	τ(λ)	λ, [μm]	τ(λ)
0.40	0.97	0.60	0.96	0.76	0.97
0.41	0.96	0.60	0.97	0.77	0.97
0.42	0.95	0.61	0.97	0.79	0.97
0.43	0.95	0.62	0.97	0.80	0.97
0.44	0.95	0.63	0.97	0.82	0.97
0.45	0.95	0.64	0.97	0.83	0.97
0.47	0.95	0.64	0.97	0.85	0.97
0.48	0.96	0.65	0.97	0.86	0.97
0.50	0.96	0.66	0.97	0.86	0.97
0.52	0.96	0.67	0.97	0.88	0.97
0.53	0.94	0.68	0.97	0.91	0.97
0.54	0.97	0.69	0.97	0.93	0.97
0.55	0.97	0.70	0.97	0.95	0.97
0.56	0.97	0.71	0.97	0.97	0.97
0.57	0.96	0.72	0.97	0.99	0.97
0.58	0.97	0.74	0.97	1	0.97
0.59	0.97	0.75	0.97		

Table D.2: Transmittance of a Fabric Blind (Without any Sheer Facings) at Slat Angle 30 Deg and Profile Angle 0 Deg

Wavelength	Transmittance	Wavelength	Transmittance	Wavelength	Transmittance
λ, [μm]	τ(λ)	λ, [μm]	τ(λ)	λ, [μm]	τ(λ)
0.40	0.48	0.60	0.61	0.76	0.63
0.41	0.50	0.60	0.62	0.77	0.63
0.42	0.50	0.61	0.62	0.79	0.63
0.43	0.50	0.62	0.62	0.80	0.63
0.44	0.51	0.63	0.62	0.82	0.63
0.45	0.53	0.64	0.62	0.83	0.63
0.47	0.55	0.64	0.62	0.85	0.63
0.48	0.57	0.65	0.62	0.86	0.63
0.50	0.58	0.66	0.63	0.86	0.63
0.52	0.59	0.67	0.63	0.88	0.63
0.53	0.61	0.68	0.63	0.91	0.63
0.54	0.62	0.69	0.63	0.93	0.63
0.55	0.62	0.70	0.63	0.95	0.63
0.56	0.63	0.71	0.63	0.97	0.63
0.57	0.62	0.72	0.63	0.99	0.64
0.58	0.61	0.74	0.63	1	0.64
0.59	0.61	0.75	0.63		

Table D.3: Transmittance of a Fabric Blind (Without any Sheer Facings) at Slat Angle 45 Deg and Profile Angle 0 Deg

Wavelength	Transmittance	Wavelength	Transmittance	Wavelength	Transmittance
λ [μm]	τ(λ)	λ [μm]	τ(λ)	λ [μm]	τ(λ)
0.40	0.18	0.60	0.48	0.76	0.50
0.41	0.26	0.60	0.49	0.77	0.50
0.42	0.30	0.61	0.49	0.79	0.50
0.43	0.33	0.62	0.49	0.80	0.50
0.44	0.36	0.63	0.49	0.82	0.50
0.45	0.39	0.64	0.49	0.83	0.50
0.47	0.42	0.64	0.49	0.85	0.50
0.48	0.44	0.65	0.49	0.86	0.50
0.50	0.45	0.66	0.49	0.86	0.50
0.52	0.46	0.67	0.50	0.88	0.50
0.53	0.46	0.68	0.50	0.91	0.50
0.54	0.48	0.69	0.50	0.93	0.50
0.55	0.48	0.70	0.49	0.95	0.50
0.56	0.48	0.71	0.50	0.97	0.51
0.57	0.48	0.72	0.50	0.99	0.52
0.58	0.48	0.74	0.50	1	0.52
0.59	0.48	0.75	0.50		

Table D.4: Transmittance of a Fabric Blind (Without any Sheer Facings) at Slat Angle 60 Deg and Profile Angle 0 Deg

Wavelength	Transmittance	Wavelength	Transmittance	Wavelength	Transmittance
λ [μm]	τ(λ)	λ [μm]	τ(λ)	λ [μm]	τ(λ)
0.40	0.26	0.60	0.34	0.76	0.36
0.41	0.27	0.60	0.35	0.77	0.36
0.42	0.23	0.61	0.35	0.79	0.36
0.43	0.23	0.62	0.35	0.80	0.36
0.44	0.23	0.63	0.35	0.82	0.36
0.45	0.24	0.64	0.35	0.83	0.36
0.47	0.26	0.64	0.35	0.85	0.36
0.48	0.29	0.65	0.36	0.86	0.36
0.50	0.30	0.66	0.36	0.86	0.36
0.52	0.31	0.67	0.36	0.88	0.36
0.53	0.32	0.68	0.36	0.91	0.36
0.54	0.33	0.69	0.35	0.93	0.36
0.55	0.33	0.70	0.36	0.95	0.37
0.56	0.34	0.71	0.36	0.97	0.36
0.57	0.34	0.72	0.36	0.99	0.36
0.58	0.35	0.74	0.36	1	0.36
0.59	0.35	0.75	0.36		

Table D.5: Transmittance of a Fabric Blind (Without any Sheer Facings) at Slat Angle 0 Deg and Profile Angle 30 Deg

Wavelength	Transmittance	Wavelength	Transmittance	Wavelength	Transmittance
λ, [μm]	τ(λ)	λ, [μm]	τ(λ)	λ, [μm]	τ(λ)
0.40	0.22	0.60	0.56	0.76	0.58
0.41	0.30	0.60	0.56	0.77	0.57
0.42	0.36	0.61	0.56	0.79	0.57
0.43	0.39	0.62	0.56	0.80	0.58
0.44	0.42	0.63	0.57	0.82	0.58
0.45	0.46	0.64	0.56	0.83	0.57
0.47	0.49	0.64	0.57	0.85	0.57
0.48	0.51	0.65	0.56	0.86	0.57
0.50	0.53	0.66	0.57	0.86	0.58
0.52	0.54	0.67	0.57	0.88	0.57
0.53	0.54	0.68	0.57	0.91	0.58
0.54	0.55	0.69	0.57	0.93	0.58
0.55	0.55	0.70	0.57	0.95	0.58
0.56	0.55	0.71	0.57	0.97	0.59
0.57	0.56	0.72	0.57	0.99	0.60
0.58	0.56	0.74	0.57	1	0.62
0.59	0.56	0.75	0.57		

Table D.6: Transmittance of a Fabric Blind (Without any Sheer Facings) at Slat Angle 45 Deg and Profile Angle 30 Deg

Wavelength	Transmittance	Wavelength	Transmittance	Wavelength	Transmittance
λ, [μm]	τ(λ)	λ, [μm]	τ(λ)	λ, [μm]	τ(λ)
0.40	0.23	0.60	0.34	0.76	0.35
0.41	0.23	0.60	0.34	0.77	0.35
0.42	0.24	0.61	0.34	0.79	0.36
0.43	0.24	0.62	0.35	0.80	0.36
0.44	0.23	0.63	0.34	0.82	0.36
0.45	0.25	0.64	0.35	0.83	0.36
0.47	0.27	0.64	0.35	0.85	0.36
0.48	0.29	0.65	0.35	0.86	0.36
0.50	0.30	0.66	0.35	0.86	0.36
0.52	0.31	0.67	0.35	0.88	0.36
0.53	0.34	0.68	0.35	0.91	0.36
0.54	0.32	0.69	0.35	0.93	0.36
0.55	0.33	0.70	0.35	0.95	0.36
0.56	0.32	0.71	0.35	0.97	0.36
0.57	0.34	0.72	0.35	0.99	0.36
0.58	0.33	0.74	0.35	1	0.36
0.59	0.34	0.75	0.36		

Table D.7: Transmittance of a Fabric Blind (Without any Sheer Facings) at Slat Angle 45 Deg and Profile Angle -30 Deg

Wavelength	Transmittance	Wavelength	Transmittance	Wavelength	Transmittance
λ, [μm]	τ(λ)	λ, [μm]	τ(λ)	λ, [μm]	τ(λ)
0.40	0.68	0.60	0.74	0.76	0.74
0.41	0.67	0.60	0.73	0.77	0.74
0.42	0.67	0.61	0.74	0.79	0.74
0.43	0.68	0.62	0.74	0.80	0.74
0.44	0.68	0.63	0.73	0.82	0.74
0.45	0.68	0.64	0.74	0.83	0.74
0.47	0.70	0.64	0.74	0.85	0.74
0.48	0.70	0.65	0.74	0.86	0.74
0.50	0.71	0.66	0.74	0.86	0.74
0.52	0.71	0.67	0.74	0.88	0.74
0.53	0.69	0.68	0.74	0.91	0.74
0.54	0.71	0.69	0.74	0.93	0.74
0.55	0.73	0.70	0.74	0.95	0.74
0.56	0.72	0.71	0.74	0.97	0.74
0.57	0.73	0.72	0.74	0.99	0.74
0.58	0.74	0.74	0.74	1	0.74
0.59	0.74	0.75	0.74		

Appendix E

Spectral Transmittance Measurement of a Venetian Blind Using the BAI-IS

Table E.1: Transmittance of a Venetian Blind at Slat Angle 30 Deg and Profile Angle 0 Deg

Wavelength	Transmittance	Wavelength	Transmittance	Wavelength	Transmittance
λ, [μm]	τ(λ)	λ, [μm]	τ(λ)	λ, [μm]	τ(λ)
0.40	0.45	0.70	0.51	1.28	0.51
0.41	0.48	0.71	0.51	1.31	0.52
0.42	0.50	0.72	0.51	1.34	0.52
0.43	0.51	0.74	0.51	1.36	0.51
0.44	0.51	0.75	0.51	1.39	0.53
0.45	0.52	0.76	0.51	1.42	0.53
0.47	0.52	0.77	0.50	1.45	0.54
0.48	0.52	0.79	0.51	1.48	0.54
0.50	0.52	0.80	0.51	1.51	0.56
0.52	0.52	0.82	0.51	1.54	0.57
0.53	0.52	0.83	0.51	1.57	0.59
0.54	0.52	0.85	0.51	1.59	0.58
0.55	0.52	0.86	0.51	1.62	0.58
0.56	0.52	0.86	0.52	1.65	0.60
0.57	0.52	0.88	0.51	1.68	0.60
0.58	0.52	0.91	0.52	1.70	0.45
0.59	0.52	0.93	0.52	1.73	0.46
0.60	0.52	0.95	0.53	1.76	0.47
0.60	0.52	0.97	0.53	1.79	0.48
0.61	0.52	0.99	0.54	1.81	0.46
0.62	0.52	1.01	0.55	1.84	0.47
0.63	0.52	1.04	0.51	1.86	0.44
0.64	0.51	1.07	0.50	1.89	0.50
0.64	0.51	1.10	0.51	1.92	0.47
0.65	0.51	1.13	0.51	1.94	0.42
0.66	0.51	1.16	0.51	1.97	0.41
0.67	0.51	1.19	0.51		
0.68	0.51	1.22	0.51		
0.69	0.51	1.25	0.51		

Table E.2: Transmittance of a Venetian Blind at Slat Angle 45 Deg and Profile Angle 0 Deg

Wavelength	Transmittance	Wavelength	Transmittance	Wavelength	Transmittance
λ, [μm]	τ(λ)	λ, [μm]	τ(λ)	λ, [μm]	τ(λ)
0.40	0.23	0.86	0.27	1.38	0.30
0.42	0.27	0.88	0.27	1.40	0.30
0.43	0.28	0.90	0.27	1.42	0.30
0.45	0.30	0.91	0.27	1.45	0.30
0.46	0.30	0.93	0.27	1.47	0.31
0.48	0.30	0.94	0.27	1.49	0.31
0.50	0.30	0.96	0.27	1.51	0.31
0.51	0.30	0.98	0.27	1.54	0.31
0.53	0.30	0.99	0.28	1.56	0.34
0.54	0.31	1.01	0.28	1.58	0.34
0.56	0.30	1.02	0.28	1.60	0.36
0.58	0.31	1.04	0.28	1.63	0.36
0.59	0.31	1.06	0.28	1.65	0.38
0.61	0.30	1.07	0.28	1.67	0.38
0.62	0.30	1.09	0.29	1.69	0.40
0.64	0.30	1.10	0.29	1.72	0.39
0.66	0.29	1.12	0.30	1.74	0.39
0.67	0.29	1.14	0.30	1.76	0.24
0.69	0.29	1.15	0.30	1.78	0.24
0.70	0.28	1.17	0.31	1.80	0.23
0.72	0.28	1.18	0.31	1.83	0.24
0.74	0.28	1.20	0.31	1.85	0.25
0.75	0.28	1.22	0.32	1.87	0.30
0.77	0.28	1.24	0.28	1.89	0.22
0.78	0.28	1.27	0.28	1.92	0.21
0.80	0.27	1.29	0.29	1.94	0.23
0.82	0.27	1.31	0.29	1.96	0.23
0.83	0.27	1.33	0.30	1.98	0.20
0.85	0.27	1.36	0.30		

Table E.3: Transmittance of a Venetian Blind at Slat Angle 60 Deg and Profile Angle 0 Deg

Wavelength	Transmittance	Wavelength	Transmittance	Wavelength	Transmittance
λ, [μm]	$\tau(\lambda)$	λ, [μm]	$\tau(\lambda)$	λ, [μm]	$\tau(\lambda)$
0.41	0.04	0.71	0.09	1.31	0.10
0.42	0.11	0.72	0.08	1.34	0.10
0.43	0.10	0.74	0.08	1.36	0.17
0.44	0.09	0.75	0.08	1.39	0.16
0.45	0.09	0.76	0.08	1.42	0.16
0.47	0.09	0.77	0.08	1.45	0.17
0.48	0.10	0.79	0.08	1.48	0.17
0.50	0.10	0.80	0.08	1.51	0.18
0.52	0.10	0.82	0.08	1.54	0.19
0.53	0.11	0.83	0.08	1.57	0.20
0.54	0.10	0.85	0.08	1.59	0.21
0.55	0.11	0.86	0.08	1.62	0.22
0.56	0.10	0.86	0.08	1.65	0.24
0.57	0.10	0.88	0.08	1.68	0.26
0.58	0.10	0.91	0.08	1.70	0.25
0.59	0.09	0.93	0.08	1.73	0.26
0.60	0.10	0.95	0.08	1.76	0.27
0.60	0.09	0.97	0.08	1.79	0.30
0.61	0.09	0.99	0.08	1.81	0.31
0.62	0.09	1.01	0.08	1.84	0.35
0.63	0.09	1.04	0.08	1.86	0.33
0.64	0.09	1.07	0.08	1.89	0.36
0.64	0.09	1.10	0.09	1.92	0.37
0.65	0.09	1.13	0.08	1.94	0.15
0.66	0.09	1.16	0.05	1.97	0.16
0.67	0.09	1.19	0.06	1.99	0.19
0.68	0.09	1.22	0.05		
0.69	0.09	1.25	0.05		
0.70	0.09	1.28	0.05		

Appendix F

Spectral Transmittance Measurement of a Holmium Oxide Calibration Glass Using the BAI-IS

Table F.1: Transmittance of a Holmium Oxide Calibration Glass

Wavelength	Transmittance	Wavelength	Transmittance	Wavelength	Transmittance
λ, [μm]	$\tau(\lambda)$	λ, [μm]	$\tau(\lambda)$	λ, [μm]	$\tau(\lambda)$
0.41	0.82	0.60	0.88	1.33	0.90
0.41	0.81	0.61	0.87	1.36	0.91
0.42	0.82	0.63	0.86	1.39	0.90
0.42	0.80	0.64	0.85	1.43	0.91
0.42	0.76	0.65	0.86	1.46	0.91
0.43	0.70	0.67	0.87	1.49	0.91
0.43	0.65	0.68	0.89	1.53	0.92
0.44	0.53	0.70	0.90	1.56	0.92
0.44	0.44	0.72	0.91	1.59	0.91
0.45	0.40	0.74	0.91	1.62	0.92
0.45	0.40	0.76	0.92	1.65	0.93
0.46	0.44	0.78	0.92	1.68	0.91
0.46	0.52	0.80	0.91	1.72	0.92
0.47	0.61	0.82	0.92	1.75	0.90
0.47	0.69	0.85	0.92	1.78	0.90
0.48	0.77	0.86	0.92	1.81	0.90
0.49	0.81	0.89	0.92	1.84	0.90
0.49	0.86	0.92	0.92	1.87	0.87
0.50	0.86	0.96	0.92	1.90	0.86
0.51	0.85	0.99	0.92	1.93	0.83
0.51	0.83	1.02	0.91	1.96	0.82
0.52	0.83	1.06	0.91	1.99	0.77
0.53	0.82	1.09	0.91	2	0.77
0.54	0.82	1.12	0.92		
0.55	0.84	1.16	0.90		
0.56	0.87	1.19	0.89		
0.57	0.89	1.23	0.91		
0.58	0.89	1.26	0.89		
0.59	0.89	1.29	0.90		

Appendix G

Sheer Fabric and Slat Fabric Properties Using the Cary 5000

For wavelength range $\lambda = 0.4\mu m$ to $1.0\mu m$.

Table G.1: Optical Properties of a Sheer Fabric for 0.4 to 1.0 micron

Incidence	Reflectance	Transmittance	
Angle, θ	$\rho_{f,bd}^{Sheer}(\theta) = \rho_{b,bd}^{Sheer}(\theta)$	$\tau_{f,bb}^{Sheer}(\theta) = \tau_{b,bb}^{Sheer}(\theta)$	$\tau_{f,bd}^{Sheer}(\theta) = \tau_{b,bd}^{Sheer}(\theta)$
0	0.138	0.709	0.157
15	0.143	0.697	0.161
30	0.144	0.700	0.159
45	0.157	0.672	0.171
60	0.178	0.621	0.185
90	0.584	0.354	0.077

Table G.2: Optical Properties of a Slat Fabric for 0.4 to 1.0 micron

Incidence Angle	Beam-Diffuse Reflectance	Beam-Diffuse Transmittance
θ [Deg]	$\rho_{f,bd}^{Slat}(\theta) = \rho_{b,bd}^{Slat}(\theta)$	$\tau_{f,bd}^{Slat}(\theta) = \tau_{b,bd}^{Slat}(\theta)$
0	0.641	0.325
15	0.659	0.327
30	0.663	0.319
45	0.670	0.305
60	0.694	0.260
75	0.744	0.187
90	0.822	0.165

Appendix H

Equipment Description

The photographs of the individual components of the BAI-IS is displayed in this section:

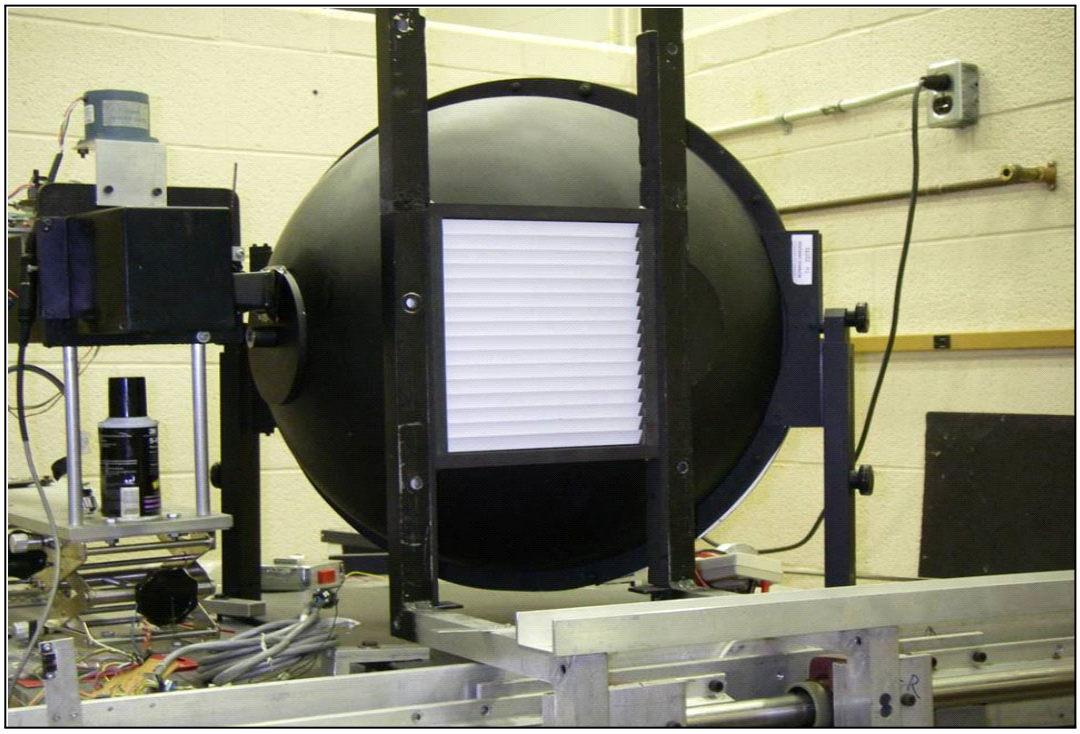

Integrating Sphere

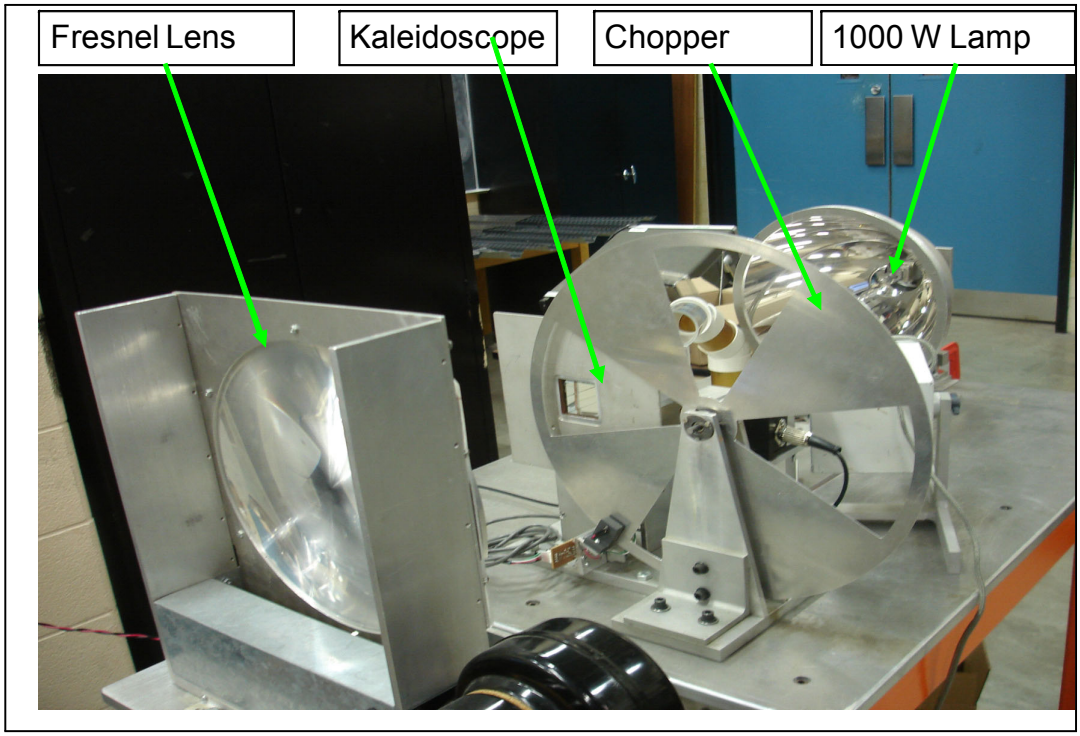

Radiant Source System

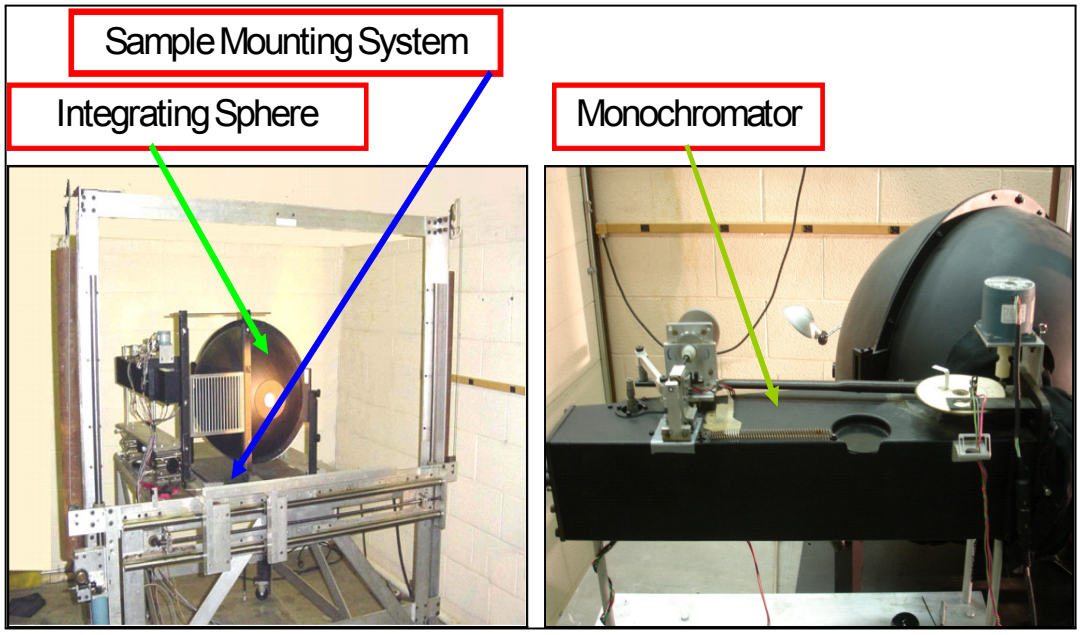

Sample Traversing System and Monochromator

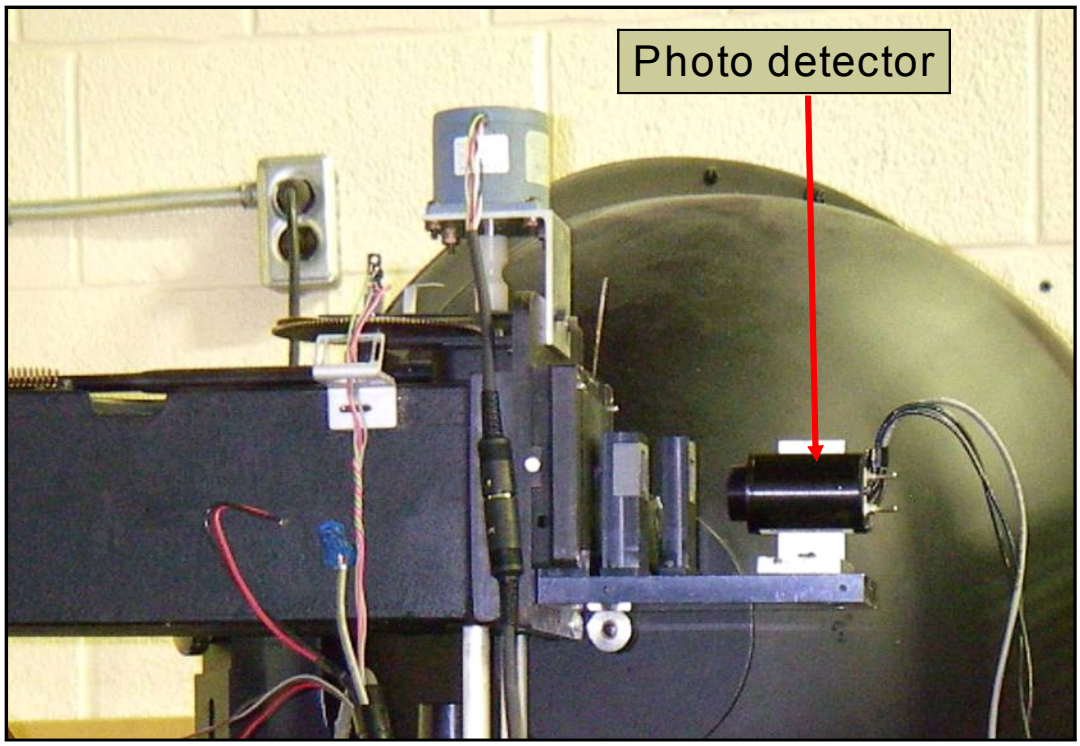

Photo-Detector System

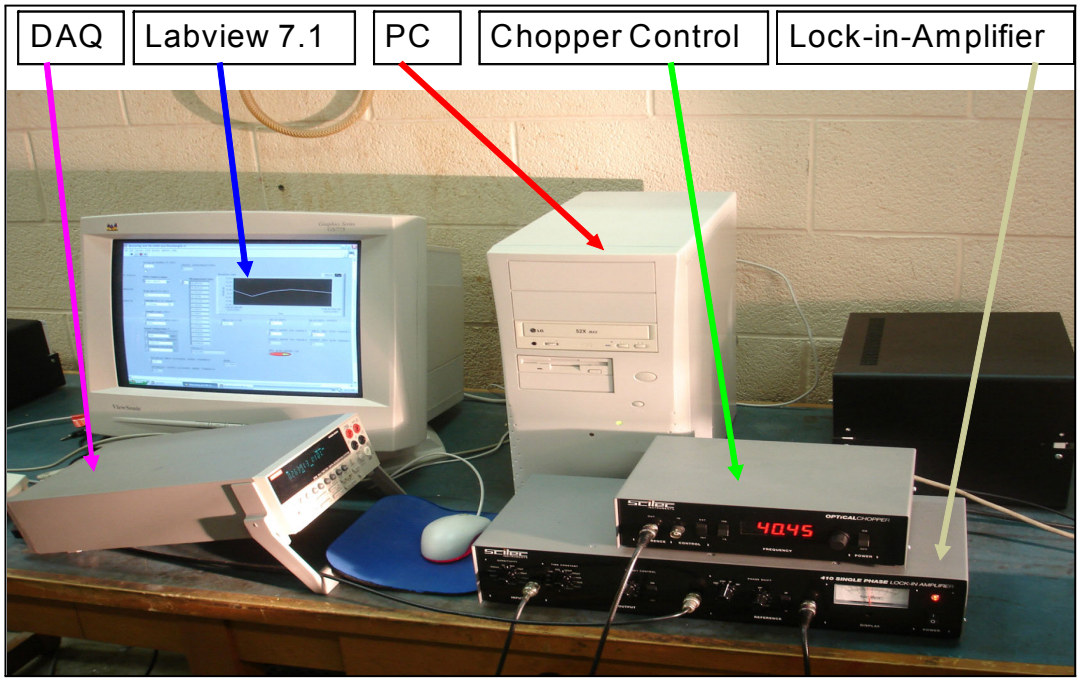

Control and Measurement System

Low Noise Power Supply for Photo-detector

Power Supply Cabinet for Lamp Feedback Mechanism

Power Supply Cabinet for Stepper Motor Drives

Appendix I

Uncertainty Analysis

The uncertainties in the measurement of spectral transmittance and in setting the wavelength scale are the consequences of errors in the measurement of voltage and wavelength.

The transmittance measurement is obtained as the ratio of the sample reading to the reference reading.

$$\tau(\lambda) = \frac{\text{Sample reading}}{\text{Reference reading}}$$

The primary data comprises voltage measurement for sample and reference readings. Let the voltage reading with the sample be V_S and let the reference reading be $V_{R.}$ Therefore, at any wavelength, λ,

$$\tau(\lambda) = \frac{V_S(\lambda)}{V_R(\lambda)} \tag{I.1}$$

The sample and reference readings are taken from a series of instruments, i.e., the photo detector, lock-in-amplifier and data acquisition system (DAQ). These raw data were processed to obtain the transmittance of the sheer blind. The errors associated with all the instruments propagate through the data processing phase and constitute uncertainty in the final result. Let it be assumed that at any wavelength,

Voltages from the detector for sample and reference readings are $V_{Detector,S}$ and

$V_{Detector,R}$

Voltages from the lock-in-amplifier for sample and reference readings are $V_{Lock,S}$ and $V_{Lock,R}$

Voltages from the DAQ for sample and reference readings are $V_{DAQ,S}$ and $V_{DAQ,R}$

$$\begin{aligned} V_S &= V_S(V_{Detector,S,}V_{Lock,S,}V_{DAQ,S}) \\ V_R &= V_R(V_{Detector,R,}V_{Lock,R,}V_{DAQ,R}) \end{aligned}$$

To estimate the uncertainty in $\tau(\lambda)$ both bias and random errors need to be incorporated. The bias error is a fixed or systematic error which can occur due to gross design or operational fault in apparatus or instrument construction. Bias error causes the repeated readings to deviate from the true reading by the same amount.

Ideally, a measurement device is expected to be free of bias with measurements all tightly centred about the true value. Since the BAI-IS apparatus comprises well designed and calibrated instruments and control devices it was assumed to be free of bias error. No sign of bias error was observed once the instruments were calibrated. Moreover, since the transmission is obtained from the ratio of two voltage readings the effect of bias error will be cancelled. Therefore, for transmittance measurement of the sheer blind, it was assumed that the overall uncertainty arises from random errors only.

I.1 Single-Sample Voltage Measurement

The measurement uncertainty can be estimated by using a single sample measurement approach considering the accuracy of each instrument. The instrument accuracy is generally supplied by the manufacturer and the bias of each instrument was also taken as zero. Using the standard root sum square technique the single sample measurement uncertainty can be estimated as follows:

The uncertainty related to random error for an experimental procedure can be estimated for a set of primary measurements (Holman 1994 and Moffat 1988). The uncertainty in the final result is estimated on the basis of individual uncertainties in the primary measurements and the knowledge of the way in which these errors propagate.

Let us assume, the measured quantity is R, which is a function of "n" primary measurements, $x_1, x_2, x_3, x_4, ..., x_n$.

$$R = R(x_1, x_2, x_3, x_4, ..., x_n) \tag{I.2}$$

Each measurement, x_i, has an uncertainty, δx_i. Propagation of the various δx_i to uncertainty in R, δR, can be quantified using to root-mean-square method of Kline and McClintock (1953).

$$\delta R = \pm\sqrt{\left(\frac{\partial R}{\partial x_1}\delta x_1\right)^2 + \left(\frac{\partial R}{\partial x_2}\delta x_2\right)^2 + \left(\frac{\partial R}{\partial x_3}\delta x_3\right)^2 + ... \left(\frac{\partial R}{\partial x_n}\delta x_n\right)^2} \tag{I.3}$$

Say R represents V_S or V_R. The independent variables, $x_1, x_2 ... x_n$, are the voltage readings from different instruments (e.g., detector, lock-in-amplifier and DAQ). The uncertainty in voltage measurement, V_S or V_R, (say V_j) can be expressed as:

$$\delta V_j = \pm\sqrt{\left(\frac{\partial V_j}{\partial V_{Detector}}\delta V_{Detector}\right)^2 + \left(\frac{\partial V_j}{\partial V_{Lock}}\delta V_{Lock}\right)^2 + \left(\frac{\partial V_j}{\partial V_{DAQ}}\delta V_{DAQ}\right)^2} \tag{I.4}$$

Replacing the values of derivatives and simplifying, Equation I.4 can be re-written as:

$$\frac{\delta V}{V} = \pm\sqrt{\left(\frac{\delta V_{Detector}}{V_{Full}} \times \frac{V_{Full}}{V_{Detector}}\right)^2 + \left(\frac{\delta V_{Lock}}{V_{Lock}}\right)^2 + \left(\frac{\delta V_{DAQ}}{V_{DAQ}}\right)^2} \tag{I.5}$$

$\frac{\delta V_{Detector}}{V_{Full}}$ = Relative error with respect to full scale reading from photo-detector

$\frac{\delta V_{Lock}}{V_{Lock}}$ = Relative error with respect to output voltage reading from lock-in-amplifier

$\frac{\delta V_{DAQ}}{V_{DAQ}}$ = Relative error with respect to output voltage reading from DAQ

Table I.1: Instrument Accuracy of Keithley DAQ System

Range	δV_{DAQ}
100mV	$\delta V_{DAQ,1} = \pm(30 \times V_{DAQ,\,j} + 35 \times Range) \times 10^{-6}$
1 V	$\delta V_{DAQ,2} = \pm(30 \times V_{DAQ,\,j} + 7 \times Range) \times 10^{-6}$
10 V	$\delta V_{DAQ,3} = \pm(30 \times V_{DAQ,\,j} + 5 \times Range) \times 10^{-6}$

I.1.1 The DAQ System

The DC voltage outputs from the lock-in-amplifier were measured by using a Keithley 2700 DAQ system. Three sets of voltage ranges were used to measure these voltages: 100 mV, 1 V and 10 V. The corresponding accuracy of data are listed in Table I.1 (Specs-2700 Rev_G, 2005):

These data correspond to $\frac{\delta V_{DAQ}}{V_{DAQ}}$ ranging from ± 0.001 to ± 0.0001. For all calculations in this uncertainty analysis $\frac{\delta V_{DAQ}}{V_{DAQ}} = \pm 0.001$ was used.

I.1.2 The Lock-in-Amplifier

The uncertainty of the lock-in-amplifier is $\pm 1\%$ of actual voltage output (Bathe 2007). Therefore,

$$\frac{\delta V_{Lock}}{V_{Lock}} = \pm 0.01 \tag{I.6}$$

I.1.3 The Photo Detector

The uncertainty of photo detector is $\pm 1\%$ of full scale reading (Maddox 2007)

$$\frac{\delta V_{Detector}}{V_{Full}} = \pm 0.01 \tag{I.7}$$

Using $\frac{V_{Full}}{V_{Detector}} = 1$ in Equation I.5

$$\left[\frac{\delta V}{V}\right]_S = \left[\frac{\delta V}{V}\right]_R = \pm 0.0142$$

This result is then used with Equation I.1 and I.3 to obtain

$$\frac{\delta \tau}{\tau} = 0.02$$

If the input to the detector is not as strong, say $\frac{V_{Full}}{V_{Detector}} = 2$, the uncertainty in measurement becomes

$$\frac{\delta \tau}{\tau} = 0.032$$

It was observed at higher wavelengths ($\lambda \geq 1.0\ \mu m$), due to low radiant flux from the lamp and low reflectance of integrating sphere coating, the S/N ratio of the lead-sulphide photo-detector reduces significantly (i.e., $\frac{V_{Full}}{V_{Detector}}$ increases) and hence the $\delta\tau$ increases appreciably. In this scenario, the $\frac{\delta \tau}{\tau} = 0.02$ value is far too optimistic. To reduce uncertainty in τ, it was necessary to use a multiple-sample measurements scheme.

I.2 Multiple-Sample Voltage Measurement

If a voltage is sampled many times, the uncertainty can be estimated using statistical methods. Consider the measurement of V_S by taking N samples, $V_{S,i}$. The standard deviation will measure the spread of the data with respect to the mean.

$$S_S = \pm \sqrt{\frac{1}{N-1} \sum_{i=1}^{N} (V_{S,k} - \overline{V_S})^2} \tag{I.8}$$

$\overline{V_S}$ = sample mean for "N" readings.

$$\overline{V_S} = \sum_{k=1}^{N} V_{S,k} \tag{I.9}$$

The voltage of interest, and its uncertainty, can then be expressed as

$$V_S = \overline{V_S} \pm \delta V_S = \overline{V_S} \pm t \times \frac{S_S}{\sqrt{N}}$$

Here, the Student t value is a function of N for a chosen confidence level. For $N \geq 30$ and a 95% confidence level $t = t_{95} = 2$ is obtained.

In each measurement, V_S or V_R, a sufficient number of samples were taken such that $\frac{S}{\sqrt{N}} < 0.007$. Having done this

$$V_j = \overline{V}_j \pm \delta V_j = \overline{V}_j \pm 0.014$$

It was found that $N \simeq 200$ for measurements at $\lambda < 1.0$ μm and $N \simeq 400$ at longer wavelengths.

I.3 Uncertainty in $\tau(\lambda)$ and τ_{Solar}

The uncertainty in $\tau(\lambda)$ can be derived from Equation I.3 by using the relationship as shown in Equation I.1.

$$\frac{\delta\tau(\lambda)}{\tau(\lambda)} = \pm\sqrt{\left((1) \times \frac{\delta V_S}{V_S}\right)^2 + \left((-1)\frac{\delta V_R}{V_R}\right)^2} \tag{I.10}$$

Let us consider,

$$\frac{\delta\tau(\lambda)}{\tau(\lambda)} \simeq 0.001$$

Measuring $\tau(\lambda)$ at many wavelengths, a set of $\tau(\lambda_i)$ can be obtained (or interpolated to obtain $\tau(\lambda_i)$). In each case $\frac{\delta\tau(\lambda_i)}{\tau(\lambda_i)} \simeq 0.001$. The total solar transmittance is obtained by averaging 50 values of $\tau(\lambda)$ for 50 specific (equal energy) values of λ (ASTM 891-87).

$$\tau_{Solar} = \frac{1}{50}\left[\tau(\lambda_1) + \tau(\lambda_2) + ... + \tau(\lambda_{50})\right]$$

Applying Equation I.3

$$
\begin{aligned}
(\delta\tau_{Solar})^2 &= \sum_{i=1}^{50}\left(\frac{1}{50}\frac{\partial\tau_{Solar}}{\partial\tau(\lambda_i)}\delta\tau(\lambda_i)\right)^2 \\
\frac{\delta\tau_{Solar}}{\sum_{i=1}^{50}\tau(\lambda_i)} &= \pm\sqrt{\left[\left(\frac{1}{50}\frac{\delta\tau(\lambda_1)}{\tau(\lambda_1)}\right)^2+\left(\frac{1}{50}\frac{\delta\tau(\lambda_2)}{\tau(\lambda_2)}\right)^2+...+\left(\frac{1}{50}\frac{\delta\tau(\lambda_{50})}{\tau(\lambda_{50})}\right)^2\right]} \\
\frac{\delta\tau_{Solar}}{\tau_{Solar}} &= \pm\frac{1}{50}\sqrt{\left[\sum_{i=1}^{50}\left(\frac{\delta\tau(\lambda_i)}{\tau(\lambda_i)}\right)^2\right]}
\end{aligned}
$$

If for instance the same relative uncertainty is associated with each $\tau(\lambda_i)$, say $\frac{\delta\tau(\lambda_i)}{\tau(\lambda_i)} = 0.001$, then the same relative uncertainty is associated with the solar transmittance.

$$\frac{\delta\tau_{Solar}}{\tau_{Solar}} \approx \pm 0.001$$

The uncertainty in solar transmittance for the sheer blind measurement was found to be lower than $\pm 1.0\%$.

I.4 Wavelength Setting

The wavelength sampled by the BAI-IS is adjusted by changing the prism angle via linkages and a lead screw, which are driven by a stepper motor. When the BAI-IS is turned on, the stepper motor cannot determine the initial position. Before starting any measurement it is necessary to ascertain the reference position of the wavelength scale. To begin the experiment, the wavelength scale needs to be reset to its reference position at $\lambda = 0.4\mu m$. Due to backlash in the mechanical linkages, drive motor, gears and lead screws, the certainty of getting the same initial reference position is not guaranteed.

For spectral measurements the wavelength scale was adjusted from $\lambda_i = 0.4\mu m$ to $\lambda_i = 2.0\mu m$. The prism splits the radiation into different wavelength due to change in index of refraction, N, of the prism material with the change in prism

angle. The relation between stepper motor position and wavelength is estimated using a six-degree spline curve-fit as shown in Equation I.11 and Figure I.1 and I.2.

$$Position = \frac{\sin^{-1}(0.5N) - 0.83485461}{0.90422 \times 10^{-5}} + 0.00001 \tag{I.11}$$

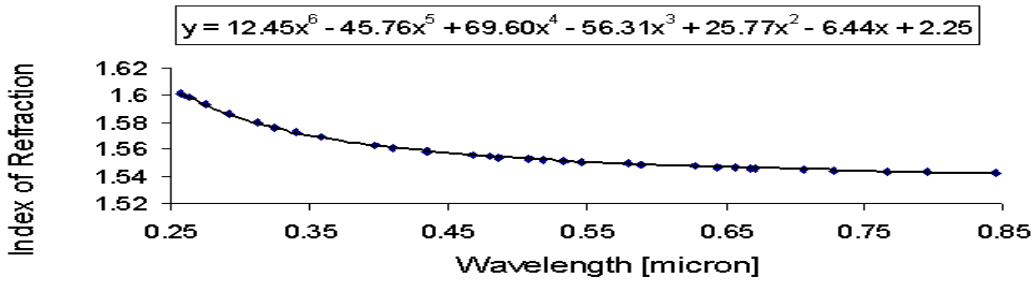

Figure I.1: Index of Refraction Vs Wavelength when $\lambda \leq 0.85\mu m$

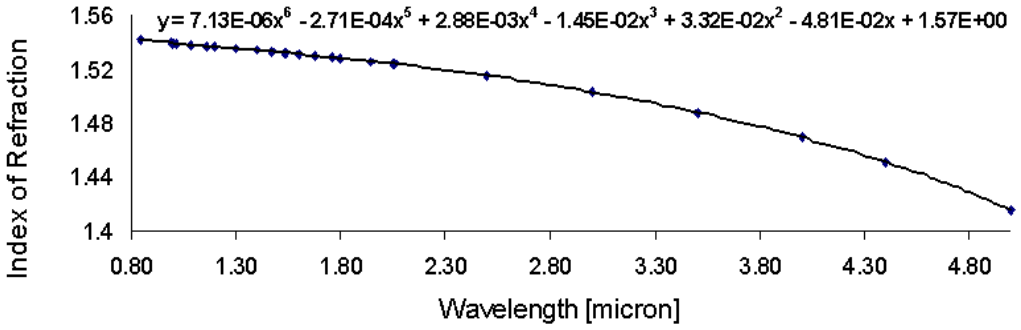

Figure I.2: Index of Refraction Vs Wavelength when $\lambda > 0.85\mu m$

Therefore, the reading from this wavelength scale is influenced by the following two factors:

(1) the repeatability of the reference position and (2) the accuracy of the spline curve-fit used to convert wavelength to stepper motor position.

The spectral transmittance of the holmium oxide glass, obtained from the Cary 5000, was used to set the reference position at $\lambda = 0.4\ \mu m$ on the wavelength scale of the BAI-IS. After setting the reference position at $\lambda = 0.4\ \mu m$ it was observed that the distance between the bracket attached to the lead screw, B, and a reference fixed block, A, as shown in Figure I.3 was 20.75 mm. This calibration process was repeated several times to check if this distance always remained the same. For convenience the reference was set by adjusting the distance between 'A' and 'B' to 20.75 mm thus overcoming the uncertainty caused by backlash.

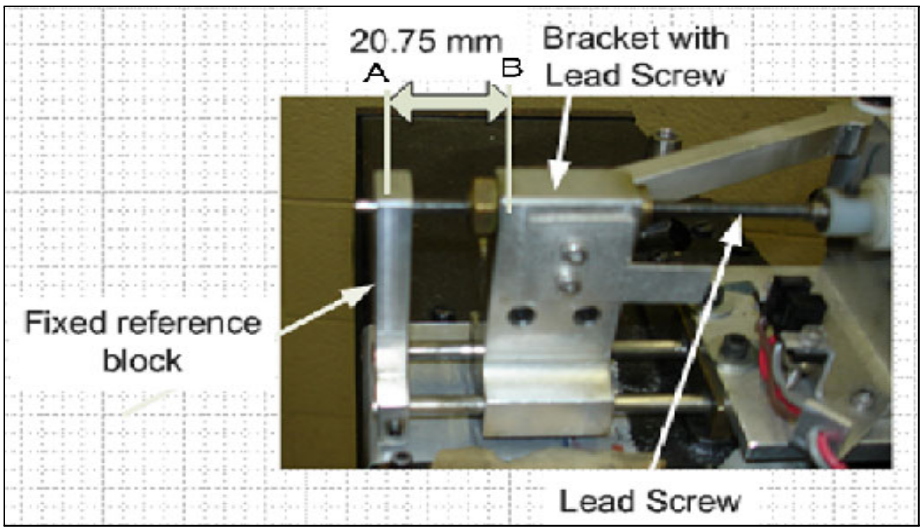

Figure I.3: Bracket position for reference wavelength.

The monochromator manufacturer has set the wavelength scale by tracing stepper motor rotation according to the spline the curve-fit. It was observed that after calibration with the holmium oxide glass, the actual wavelength scale with respect to the curve-fit has some differences. The uncertainty regarding actual wavelength scale and the wavelength scale obtained from the curve-fit was estimated to be:

$$\delta\lambda = \pm 0.02 \quad \mu m$$

Appendix J

Measurement Procedure

J.1 Introduction

BAI-IS apparatus is a spectrophotometer to measure spectral optical properties of light scattering and spatially non-uniform samples. A single beam of light from the 1000 watt lamp passes through a kaleidoscope and fresnel lens. Kaleidoscope makes the beam collimated and fresnel lens magnifies it. This incident beam of light illuminates a broad area on the sample, which is sufficient enough to represent the entire sample properties. At the back of the sample, the integrating sphere is installed whose inlet port is aligned in such a way, so that the center of the inlet port and the sphere, the lamp axis, center of fresnel lens and the axis of square kaleidoscope all lie on the same straight line at 0^0 setting of the swiveling table.

J.2 Procedure

The operating procedure involves instrument calibration and running the lab-view program to adjust wavelength, change sample position and record signal responses. The signal responses from the photo-detectors are proportional to the radiant flux transmitted through the sample.

J.2.1 Cleaning

1. Clean dust from concentrating reflector, kaleidoscope interior surface, fresnel lens with a clean, lint-free cloth. Make sure, lamp is not operated more than 300 hours. If so, replace lamp with a new one and keep the record.

2. Check the integrating sphere inlet. If dust is seen, then clean the interior after opening the faceplate at the inlet or sample port. Use a small vacuum cleaner or compressed air to drive out the dust. Note: care should be taken not to touch the white coating.

J.2.2 Preparation

1. Make sure all instruments are switched-off to avoid electrical surge as soon as the electrical connections are established. The electrical surge is harmful for sensitive devices, such as the lock-in-amplifier, Keithley 2700 multimeter, Keithley 7706 DAQ card, photo-detector and optical chopper control unit.

2. Check if the swivelling table is set at the correct angular position as desired. Position the table at the correct profile angle and set the pointer on the scale located at the right hand corner on the floor.

3. Check that the sample is mounted correctly on the sample traversing rig.

4. Bring the wavelength setting lead screw to its reference position, where the scale starts from 0.4 μm, which measures 20.75 mm distance between outer and inner face of fixed reference block and the bracket attached to lead-screw respectively.

5. On the circular dial of slit-width adjusting sub-assembly, confirm that the pointer is set at 2 mm graduation. This ensures maximum slit width and large signal-to noise ratio.

J.2.3 Establish Electrical And Control Cable Connections.

Connection to Lamp Feedback Control Cabinet

1. Plug-in control cable from the light feedback unit
2. Plug in the power cable of the kaleidoscope cooling fan.
3. Plug-in power cable from the lamp.

Note: This is a high voltage (110 V DC) and high current (10 ampere) device. Care must be taken during operation that, accidental personal contact is always prevented. Never operate with its cover open, make sure the cooling fan is operating. The box has floating ground, so no other instruments should be connected to this control cabinet.

Connection For Lamp Feedback Control Cabinet

1. Plug in lamp power supply from the lamp-feedback box into the stabilizing transformer.
2. Plug in main power cable.

Connection For Stepper Motor Control Cabinet

1. Plug in main power supply to a separate extension chord unit. Note: This power supply should not come from the same power outlet, which is supplying power to the photo-sensor unit. This is a precaution to avoid additional noise, electrical interference that may transfer to sensor, from stepper motor drive.
2. Connect three stepper motor power supply plugs into the control cabinet, which will provide pulse signals from drivers to respective stepper motors.
3. Connect the control cable from this box to the Keithley DAQ card 7706. This provides digital signal output from the DAQ card to generate electrical pulses to drive the stepper motors.

Low Noise Power Supply Unit (Model: PS-1)
For Photo-Detector

1. Plug in the 9-pin D connector (DB-9) to PS-1, which will supply 15 VDC excitation power to photo-detector.

Lock-in-Amplifier Connection

1. Signal output cables from photo-detector has BNC terminal which is connected as signal input into the lock-in-amplifier. This BNC connector can be switched manually between Si photodiode and PbS photo-conductor depending on the wavelength range.

2. Lock-in-amplifier has reference input connection coming from chopper control unit.

3. The filtered output signal from lock-in-amplifier is connected to the analog input channel 101 on the Keithley DAQ card 7706.

Chopper Control Unit Connections

1. The signal input is connected at the back of the unit through the 9-pin D-type connector which connects the 300H chopper head. This chopper head serves three purposes. (1) The chopper head provides power to the opto-switch. (2) The opto-switch picks up signal from chopper blade and provides reference signal to the chopper control unit and (3) The chopper head provides 12 VDC supply power to drive the rotating chopper motor (12 VDC$\times$ 0.25 A $\times$4Watt). The chopper head 300H connection and D-type connection layout is described in Figure J.1.

Keithley 2700 Multimeter Connections

1. At the back of 2700 multimeter, in slot 1 the 7706 DAQ card is installed. On the card two sets of channels are used. (1) Digital signal out put channels 121

9 Way D-Type Connection	300H Connection
Pin 6 – Motor Positive	Pin 2 – Motor Positive
Pin 9 – Motor Negative	Pin 4 – Motor Negative
Pin 8 – 0V	Screen – 0V
Pin 4 - +15V	Pin 3 - +15V
Pin 5 – LED Cathode	Pin 5 – LED Cathode
Pin 2 – Reference Input	Pin 1 – Reference Output

Figure J.1: Connection Layout for Chopper Head

and 122 are connected to the three stepper motor drivers. The digital pulses are used to drive the stepper motors. (2) The analog input channel (101) is connected to signal output channel of the lock-in-amplifier. Through channel 101 the data are recorded into labview program files.

Establish Electrical Connections

- Ensure electrical power supply for wall mounted outlets.
- Plug in power stabilizing transformer and extension cable units to the wall mounted power outlets.
- Connect the power cable of the cooling fan for Fresnel lens, lock-in-amplifier, chopper control unit and the lamp feedback control cabinet into one extension chord unit.
- Plug in the computer, monitor and the low noise power supply unit for the photo-detector into the second extension chord unit.
- The third extension cable unit provides power supply to the stepper motor driver cabinet and keithley 2700 multimeter.

J.2.4 Energizing Instruments

- Switch on all three extension cable units.

Lamp

- Energize lamp-feedback control cabinet by turning on the control power switch.
- Tun-on the lamp toggle switch on the same cabinet. Keep the lamp turned on for atleast 15 minutes to warm-up.

Optical Chopper

- Make sure the chopper wheel and the coupling are free of any visible signs of damage or deformation and can rotate without any abnormal noise or rubbing. Confirm that all screws, nut and bolts are tight.

- Turn on the chopper control unit. If the opto-switch is properly connected at the base of the chopper blade to pick-up reference signal, then the LED display will start showing change in frequency readings. If the display does not change then stop the machine and see if the signal pick-up circuit assembly is properly installed on the chopper base. If the circuit assembly is found loose or out of place, then fix it tight in place and re-start the chopper wheel.

- Set the chopping frequency by turning the control knob at the front panel of the control unit which regulate the voltage input to the chopper motor via 9-pin D-connector. For this experiment, the disc rotating frequency is kept between 51 and 52 Hz. Ensure that this rotating frequency does not match with the alternating current (AC) cycle frequency of 60 Hz or any of its multiples. The frequency is found to be fairly constant with a variation of ± 0.1 Hz. If frequency changes abruptly then stop the machine, investigate for rubbing, vibration, loose foundation,disc deformation, damaged or loose coupling disc or possible misalignment in any of the elements in this mechanical sub-system. Once the frequency is set, it is observed that, the knob does not need to be changed at anytime. In all future attempts, the rotating frequency reaches almost the same value. NOTE: While shutting down the machine, only turn-off the switch, do not change frequency control knob. At the beginning of rotation, at around 35 to 45 Hz, when the chopper wheel crosses its critical speed, it experiences some chattering noise and vibration due to resonance. However, within a few seconds everything gets stabilized and continues running smoothly and steadily without any noise and vibration.

Photo-Detector

- Once the chopper unit reaches it maximum frequency confirm whether the BNC connector of Si photo-diode is connected to the input port of the lock-in-amplifier.
- Turn-on the low noise power supply unit (PS-2).

Lock-in-Amplifier

- Switch the offset control to 'OFF', Switch 1F/2F selector to the '1F' setting. Note: On the 1F setting, the amplified input signal (known as the recovered signal) is at the same frequency as the original input. On the 2F setting, the recovered signal is at twice the frequency of the original input.
- Switch the input sensitivity to 1 V.
- Switch the time constant to 100 ms.
- Switch both phase controls to 0°.
- Now turn on the switch for lock-in-amplifier.
- Keep this running for about 10 minutes to warm it up.

J.2.5 Computer Set-up

- Turn the computer and the monitor on.
- Open Labview 7.1.
- Open the "SCAN" virtual instrument program (VI) from desktop for automatic scanning and controlling the wavelength sample position. VI represents graphical program in Labview 7.1 that models the appearance and function of a physical instrument.

- On the SCAN VI, open the graphical input screen, also known as front panel (FP), where input parameters are set. The FP is the interactive user interface of a VI. The appearance of the FP imitates physical instruments, such as oscilloscopes and multimeters. On the FP interface the parameters A1, A2, B1, B2, C, D, E1 and E2 are typed depending on the wavelength and profile angle as shown in Figure J.3 and Table J.1. As shown in figure J.2, the parameters on the FP are never required to change.

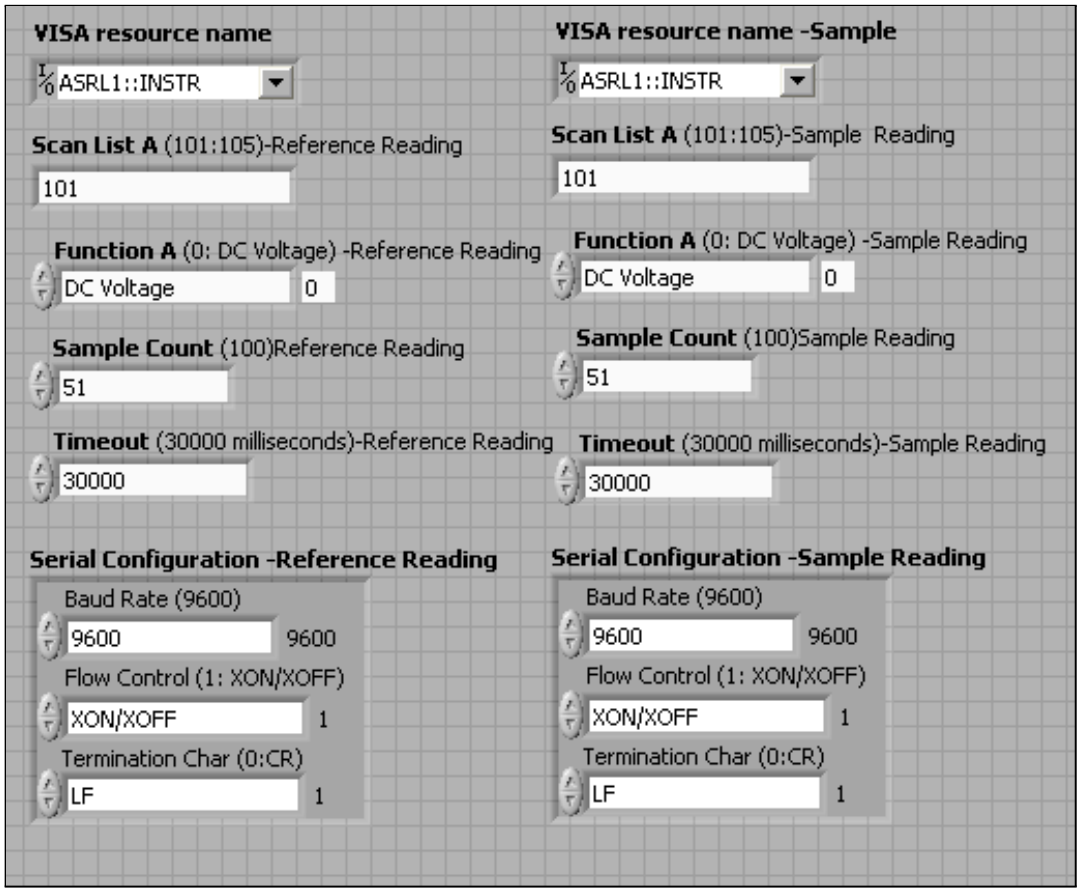

Figure J.2: Front Panel

Table J.1: Front Panel Input

PD	λ	Ω	A1	A2	B1	B2	C	D	E1/E2
Si	0.4∼0.52	**0**	*5*	*75000*	*5*	*90000*	10	100	**2500**
Si	0.53∼0.57	**0**	*5*	*75000*	*5*	*90000*	5	50	**2500**
Si	0.59∼1.0	**0**	*5*	*75000*	*5*	*90000*	35	25	**2500**
PbS	1.04∼1.99	**0**	*8*	*90000*	*8*	*120000*	35	35	**2500**
Si	0.4∼0.52	±30	5	75000	5	75000	10	100	2800
Si	0.53∼0.57	±30	5	75000	5	75000	5	50	2800
Si	0.59∼1.0	±30	5	75000	5	75000	35	25	2800
PbS	1.04∼1.99	±30	8	90000	8	120000	35	35	2800
Si	0.4∼0.52	±45	5	75000	5	90000	10	100	3200
Si	0.53∼0.57	±45	5	75000	5	90000	50	50	3200
Si	0.59∼1.0	±45	5	75000	5	90000	35	25	3200
PbS	1.04∼1.99	±45	8	90000	8	120000	35	35	3200
Si	0.4∼0.52	±60	5	75000	5	90000	10	100	3500
Si	0.53∼0.57	±60	5	75000	5	90000	5	50	3500
Si	0.59∼1.0	±60	5	75000	5	90000	35	25	3500
PbS	1.04∼1.99	±60	8	90000	8	120000	35	35	3500

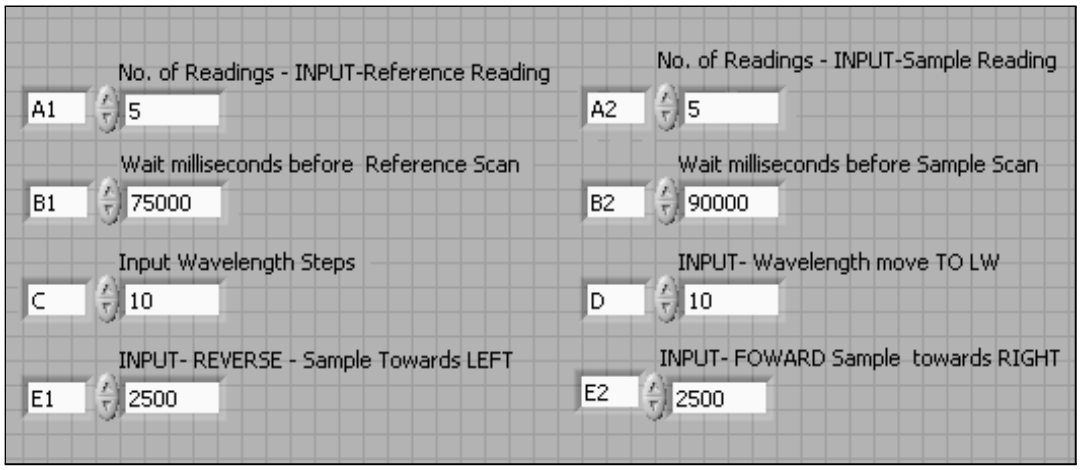

Figure J.3: Front Panel Input

J.2.6 Tuning Lock-in-Amplifier

Keeping the sample away from the integrating sphere, when the wavelength is set at 0.4 μm start tuning the lock-in-amplifier for accurate measurement as follows:

- 1. Increase the input sensitivity until a signal is seen on the output dial of the lock-in amplifier.
  2. If the output needle does not remain still, increase the time constant setting until the noise is removed.
  3. Adjust the phase control dials until a maximum output is seen.
  4. Subtract 90° from the phase shift by turning the coarse phase control by one position counter-clockwise (or three positions clockwise).
  5. Take a measurement of the output.
  6. Add 180° to the phase shift by turning the coarse phase control by two positions.
  7. Take a measurement of the output.
  8. Using the fine phase control adjust the outputs seen in steps 5 and 7 so that they are the same.
  9. If the signals seen in steps 5 and 7 are not both 0 V switch on the offset control and adjust until both signals are 0 V.
  10. Note: Fine phase control is used to remove a positive voltage from one output while removing a negative voltage from the other. Offset control is used to remove either a positive or negative voltage from both outputs.
  11. When the fine phase control and offset controls are correctly set, the four positions of the coarse phase control knob should give two readings of 0 V, one negative reading and one positive reading (of the same amplitude). The instrument is now correctly set up and readings can be made.

J.2.7 Reset Wavelength Scale

- Open the VI to control the wavelength.
- Go to block diagram for this VI and type in *"100"* to move the wavelength scale in backward towards shortwave. This way, the distance between the fixed reference block and the bracket attached to lead screw will decrease. Hit the toggle switch button into "Green" to ensure Boolean command to choose reverse direction for stepper motor, so that the leadscrew turns towards shorter wavelength by 100 steps. See Figure J.4. Hit the run button on the FP interface to adjust the wavelength scale 100 units in backward direction. So the wavelength scale is positioned at 0.39 μm. The SCAN program always starts by changing the wavelength, so this 100 unit shift in wavelength scale ensures that while the scan program is started the reading begins from 0.4 μm.

J.2.8 Scan Operation

When everything is ready hit the RUN button with the cursor. The RUN button is shown as white arrow located in the extreme top left hand corner in the front panel as shown in Figure J.5. Then the program will start executing all necessary actions as follows:

(a) Rotate wavelength adjusting stepper motor by 100 units

(b) Wait for 75 seconds to stabilize Si photo diode signal output and lock-in-amplifier reading.

(c) Scan 50 times and record the average of these 50 scan.

(d) At every 15 seconds the program will take 50 readings and record the average for 4 more times.

(e) Then the sample traversing stepper motor will start rotating and move the sample towards left and position it in front of the inlet port of the integrating sphere.

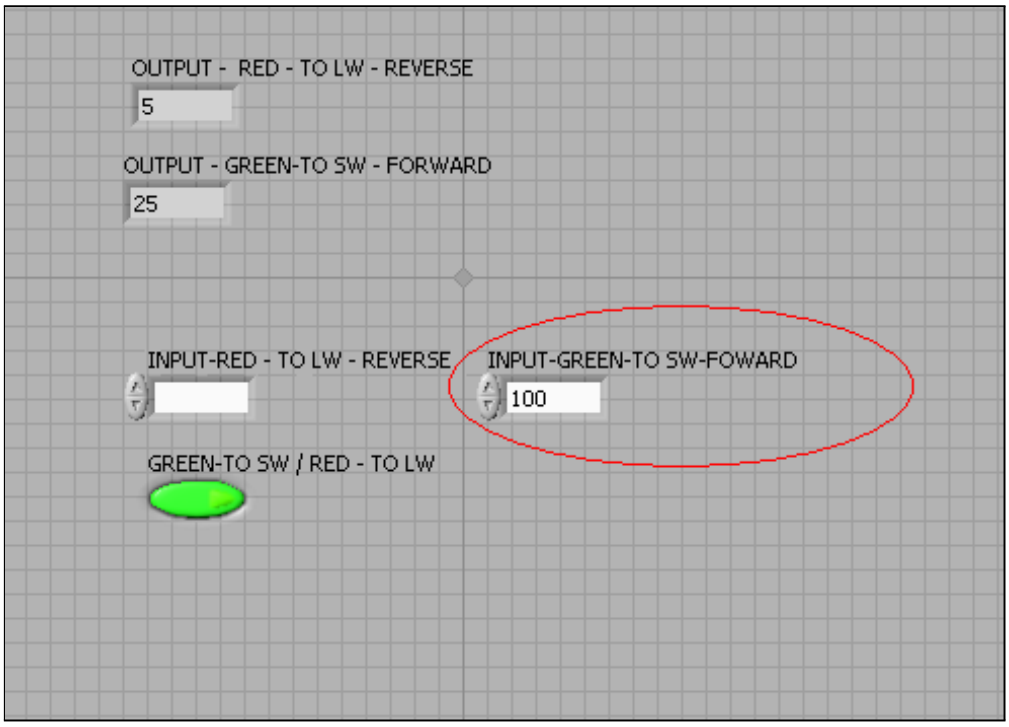

Figure J.4: Wavelength Adjustment VI

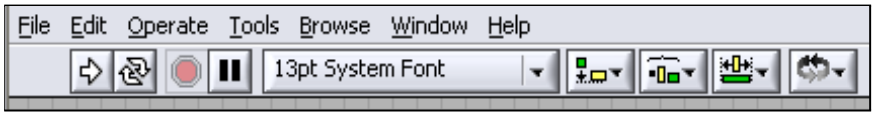

Figure J.5: Run Button in Front Panel Interface

(f) Wait for another 90 seconds to stabilize the silicon photo diode signal output and lock-in-amplifier reading.

(g) Repeat step (c) and (d). In this case the five average readings and all 50x5 scans will be recorded in a separate data file as sample reading

(h) The sample traversing stepper motor will start rotating in reverse direction, thus moving the sample towards right and position it further away from the inlet port opening to avoid reflection from the frame and rig which may get into the integrating sphere. This may happen only when the rig is close to the port while taking reference reading. It is found that this may cause about 1 to 2 % drop in measured transmittance value for different profile angle, since the additional reflected radiation cause increase in the reference reading thus dropping the transmittance ratio. This step completes one complete set of readings at wavelength, $\lambda = 0.4\ \mu m$.

(i) For the next set of readings the stepper motor for adjusting wavelength moves to another 100 units in forward direction toward the longer wavelength to $\lambda = 0.41$ μm.

(j) the cycles repeats until the 10 steps as indicated in the box "input wavelength steps" are completed as shown in the Figure J.3 on the FP interface. At the end of 10 steps, 10 intervals of wavelength readings will be completed and the wavelength scale will reach at $\lambda = 0.52$ μm.

(k) From experience, it is found that, the sensitivity knob set at 3 mV and time constant knob set at 3 S, provide good input signal amplification on lock-in-amplifier for this first 10 sets of readings.

NOTE:

It is very important, to have an additional connection from lock-in-amplifier output to which a voltmeter is kept connected all through the experiment. This provides a good display of instantaneous output voltage, for tuning the lock-in-amplifier or to verify if the readings are OK.

The lock-in-amplifier front panel layout can be divided into 4 parts as shown in Figures J.6, J.7, J.8 and J.9. These four parts are: (1) Input with a BNC connector to receive raw sensor input signal(2) Output with a BNC connector to

provide processed signal output to DAQ board for recording (3) Reference with another BNC connector to collect reference signal from optical chopper (4) Display provides signal output on a dial gauge.

Figure J.6: Input Section of Lock-in-Amplifier

It is important to mention here, that this instrument provides accurate measurement within ± 1% variation, provided a stable environment is kept in the surrounding. The largest source of error is its output offset drift, which is temperature dependant, so keeping the internal circuitry temperature constant is the most important thing to do. Physically it is observed that with all the cooling fans around the lamp and instruments, the temperature remains almost constant and does not affect the integrity of measurement. This is also reflected in the readings while the standard deviation of repeated readings are found negligible (Personal communication 2007).

Once the first 10 readings are complete the Labview program will cease to execute. Then change the sensitivity to 100mV; time constant to 3 S on the lock-in-amplifier panel. Change "input wavelength steps" to 35 units and "input wave-

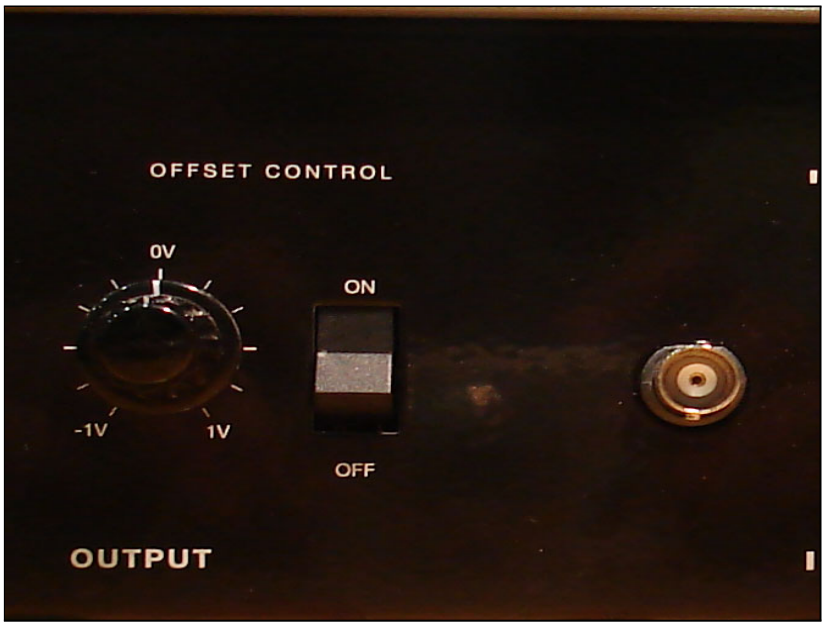

Figure J.7: Output Section of Lock-in-Amplifier

Figure J.8: Reference Section of Lock-in-Amplifier

Figure J.9: Display Section of Lock-in-Amplifier

length move to LW" to 25 units on the front panel of Scan VI. Keeping the sample away from the integrating sphere when the wavelength is set to $\lambda = 0.52$ μm repeat the step "Tuning Lock-in-Amplifier". If everything is found satisfactory then hit the arrow button with the cursor on the front panel of Labview SCAN program to execute the scan operation.

After 5 wavelength reading the program will stop and the wavelength will reach at $\lambda = 0.57$ μm.

Change the sensitivity to 300mV; time constant to 3 S on the lock-in-amplifier panel. Change "input wavelength steps" to 5 units and "input wavelength move to LW" to 50 units on the front panel of SCAN VI. Keeping the sample away from the integrating sphere when the wavelength is set to $\lambda = 0.57$ μm repeat the step "Tuning Lock-in-Amplifier". If everything is found satisfactory then hit the arrow button with the cursor on the front panel of Labview SCAN program to execute the scan operation.

After 35 wavelength reading the program will stop and the wavelength will

reach at 1.0 μm mark. Now it is time to change the photo-detector to PbS photo-conductor. Due to weaker signal response at longer wavelength, change the sensitivity to 3mV; time constant to 30S on the lock-in-amplifier panel. Change "input wavelength steps" to 35 units and "input wavelength move to LW" to 35 units on the front panel of SCAN VI. At this point, the signal variation is more frequent so the scan time and the scan frequency are increased by increasing number of readings to 8 for each sample and reference readings. Moreover to allow more time to get steady state after change in wavelength and sample position, the wait times for sample and reference signals need to change to 90,000 mS and 120,000 mS. Keeping the sample away from the integrating sphere when the wavelength is set to $\lambda = 0.57$ μm repeat the step "Tuning Lock-in-Amplifier". If everything is found satisfactory then hit the arrow button with the cursor on the front panel of Labview "SCAN" program to execute the scan operation.

NOTE: It is very important to make sure, the longwave measurements are continued without any disruption. If it is stopped in between then it is very hard to tune the lock-in-amplifier and get reliable reading. It is observed that in the beginning of longwave readings at high slat angle and high profile angle, the signal is too weak, hence provides negative readings which are not considered for transmittance calculation. This is caused because, the lamp produces insufficient radiant energy at longer wavelength and at deeper profile angle the inlet port opening area gets smaller since the projected area exposed to radiant source assumes an ellipse. So the total energy which enters the integrating sphere is not sufficient enough to overcome the detector noise at higher wavelengths, deeper profile angles and greater slat angles.

Once the complete set of readings are complete for a certain slat and profile angle, then change the profile angle by swivelling the table, reset the wavelength scale by bringing the lead screw to the reference position which represents $\lambda = 0.4$ μm, change the BNC connector to Si photo-diode for short wavelength reading. Repeat the same procedure and record data.

The above is repeated for a single sample with one slat angle at 0^0, $\pm 30^0$, $\pm 45^0$, and $\pm 60^0$ profile angle. When 7 sets of readings are taken then change the sample with a different slat angle and repeat the above procedure to take another 7 sets of

readings.

Repeat the complete 7 sets of reading with 4 different samples having slat angles 0^0, 30^0, 45^0 and 60^0.

In all cases, the output data are saved in 2 different data files: one for sample readings and the other one for reference readings. The main files contain 85 sets of readings to cover total wavelength range, which are averages of 5 sets of readings for wavelength 0.4 μm to 1.0 μm and 8 sets of readings for wavelength 1.0 μm to 2.0 μm.

References

[1] Abernathy, R. B. et al., Thompson, J. W. Jr. 1980. Handbook , Uncertainty in Gas Turbine Measurements. National Technical Information Service. Springfield, VA. USA.

[2] Abernethy, R.B., Benedict, R. P., Dowdell, R. B. 1985. ASME Measurement Uncertainty. Journal of Fluids Engineering. 107 (161-164)

[3] Agenda 21 on Sustainable Construction, CIB Report Publication 237, July 1999.

[4] ANSI/ASHRAE 74-1988. 1988. ASHRAE Standard. Method of Measuring Solar-Optical Properties of Materials. ASHRAE Engineers, Inc. Atlanta, GA. USA.

[5] ANSI/ASME PTC 19.1. 1983. Measurement Uncertainty.

[6] ASHRAE Handbook; Fundamentals.1989. Chapter 27, Fenestration.

[7] ASTM E 424. 1971. (Reapproved 2001) Standard Test Method for Solar Energy Transmittance and Reflectance (Terrestrial) of Sheet Materials. Annual Book of ASTM Standards, Section 12.02.

[8] ASTM E 891. 1987. Standard Tables for Terrestrial Direct Normal Solar Spectral Irradiance for Air Mass 1.5. Annual Book of ASTM Standards.

[9] ASTM E 903. 1996. Standard Test Method for Solar Absorptance, Reflectance, and Transmittance of Materials Using Integrating Spheres. Annual Book of ASTM Standards, Section 12.02.

[10] ASTM E 972-96. 1996. (Re-approved 2002). Standard Test Method for Solar Photometric Transmittance of Sheet Materials Using Sunlight. Annual Book of ASTM Standards, Section 12.02.

[11] ASTM E 1175. 1987. (Reapproved 2003) Standard Test Method for Determining Solar or Photopic Reflectance, Transmittance and Absorptance of Materials Using Large Diameter Integrating Sphere. Annual Book of ASTM Standards, Section 12.02.

[12] AstroSurf. 2001. The Littrow Spectrograph. Retrieved November 2007 from www.astrosurf.com.

[13] Bathe, C. 2007. Personal Communication. Scitec Instruments Ltd., UK. 25 September 2007.

[14] Beckman Instruction Manual. 1950. The Beckman Model DU Spectrophotometer and Accessories. Beckman Instruments Inc., CA., USA.

[15] Boston Electronics Corporation. 2006.Model 410 Single Phase Lock-In Amplifier. Retrieved on May 2006 from www.boselec.com

[16] Breitenbach, J., Lart, S., Längle, I., Rosenfeld, J.L.J. 2001. Optical and thermal performance of glazing with integral venetian blinds Energy and Buildings. 33 (5). 433-442.

[17] Broeke, M.R.V D and Reijmer, C. H. T 2006. Downloaded on May 2006 from www.phys.uu.nl/˜broeke/

[18] Budde, W. 1983. Optical Radiation Measurements. Volume 4; Physical Detectors of Optical Radiation Academic Press, Inc., London.

[19] Canada Green Building Council. 2007. Business Plan 2007. Retrieved December 2007 from www.cagbc.org

[20] Cary, H. H., Beckman, A. O. 1941. Journal of The Optical Society of America. 31 (11), 682-689.

[21] Clarke, F. J. J., Compton, J. A. 1986. Correction Methods for Integrating-Sphere Measurement of Hemispherical Reflectance. COLOR Research and Application. 11 (4), 253-262.

[22] Colson, W., B., Swiszcz, P. G. 1992. Fabric light control window covering. Patent number: 5394922

[23] Duffie, J. A. Beckman, W. A. 1991. Solar Engineering of Thermal Processes. John Wiley & Sons, Inc., USA.

[24] Energy Plus. 2007. EnergyPlus Engineering Reference. Daylighting and Window Calculations. Window Calculation Module.155-176. Downloaded on December 2007 from www.eere.energy.gov/buildings/energyplus/documentation.

[25] Edwards, D. K., Nelson, Roddick, R. D. 1961. Integrating Sphere for Imperfectly Diffuse Sample. Applied Optics. 51 (11), 1279-1288.

[26] Edwards, D. K. 1977. Solar absorption by each element in an absorber-coverglass array. Technical note. Solar Energy. 19: 401-402.

[27] Elmahdy, A. H., Cornick, S. M. 1990. Emerging Window Technology. Construction Canada. 32(1). 46-48. Retrieved on November 2007 from http://irc.nrc-cnrc.gc.ca.

[28] Fendley, J. 1985. An Analysis of the Measuring Procedure for the Integrating Sphere Spectrophotometer. Solar Energy. 35 (3), 281-282.

[29] Goebel, D. G. 1967. Generalized Integrating-Sphere Theory. Applied Optics. 6 (1), 125-128.

[30] Hanssen, L. M. 1989. Effects of Restricting the Detector Field of View when using Integrating Spheres. Applied Optics. 28 (11). 2097-2103.

[31] Hisdal, B. J. 1965a. Reflectance of Perfect Diffuse and Specular Samples in Integrating Sphere. Journal of the Optical Society of America. 55(9), 1122-1128.

[32] Hisdal, B. J. 1965b. Reflectance of Non-perfect surfaces in the Integrating Sphere. Journal of the Optical Society of America. 55(10), 1255-1260.

[33] Hollands, K. G. T. 2004. Thermal Radiation Fundamentals. Begell House Inc., USA.

[34] Hollands, K.G. T., Wright, J. L., Granqvist, C. G. 2001. Solar Energy - The State of The Art - ISES Position Papers. James and James Ltd. Chapter 2. Glazing and Coatings. 29-50.

[35] Holman, J. P. 1994. Experimental Methods For Engineers. 6th Edition. McGraw Hill, Inc.

[36] Hunn, B.D., Jones, J.W., Grasso, M. M., Hitzfelder, J., D. 1993. Effectiveness of Shading Devices on Buildings in Heating-Dominated Climates. ASHRAE Transaction 99 (1). 207-222.

[37] Hunter Douglas 2007. Custom Window Shadings, Sheers, Louvers and Panels. Downloaded on September 2007 from www.hunterdouglas.com

[38] ISO/FDIS 15099. 2003. Thermal Performance of Windows, Doors and Shading Devices - Detailed Calculations. The International Organization for Standardization.

[39] Jacquez, J.A., Kuppenheim, H.F. 1955. Theory of integrating sphere. Journal of the Optical Society of America. 45 (6).

[40] Jacobs, G., Kreis, O. 1964. Slit Width Adjustment Means for Optical Instruments. United States Patent Office. Patent No. 3.160.697. December 1964.

[41] Jiang, T. 2005. Transmittance Measurements of Louvered Blinds Using a Broad Area Illumination Integrating Sphere. MASc. Thesis. University of Waterloo, Waterloo, Ontario.

[42] Jiang, T., Collins, M.R. 2007. Validation of Solar/Optical Models for Louvered Shades Using a Broad Area Illumination Integrating Sphere. Submitted to ASHRAE Transactions.

[43] Kessel, J., Selkowitz, S. 1984. Integrating sphere measurements of directional-hemispherical transmittance of window systems. Journal of IES. 14 (1), 136-150.

[44] Klems, J.H. 1994a. A New Method for Predicting the Solar Heat Gain of Complex Fenestration System – 1. Overview and Derivation of the Matrix Layer Calculation. ASHRAE Transactions. 100 (1). 1065-1072.

[45] Klems, J.H. 1994b. A New Method for Predicting the Solar Heat Gain of Complex Fenestration System – 2. Detailed Description of the Matrix Layer Calculation. ASHRAE Transactions. 100 (1). 1073-1086.

[46] Kline, S. J., McClintock, F. A. 1953. Describing Uncertainties in Single-Sample Experiments. Mechanical Engineering by ASME. 75 (1).

[47] Kotey, N. A., Wright, J. L. 2006. Simplified Solar Optical Calculations For Windows With Venetian Blinds. In Proceedings of the 31st Conference of the Solar Energy Society of Canada Inc. (SESCI) and 1st Conference of the Solar Building Research Network (SBRN), Montreal, Quebec, Canada, August 20-24, 2006.

[48] Kotey, N. A., Collins, M. R., Wright, J. L., Jiang, T. 2007. A Simplified Method for Calculating the Effective Solar Optical Properties of a Venetian Blind Layer for Building Energy Simulation. Submitted to ASHRAE Transactions.

[49] Kotey, N. A., Wright, J. L., Collins, M. R. 2008. Measurement of Angle-Dependent Solar Optical Property of Drapery Fabrics. To be Submitted for review.

[50] Krochmann, J. 1979. On the Measurement of reflectance and transmittance with Directional and Diffuse Incidence of Light. Proceedings of the CIE Session 1979 in Kyoto, 19th Session.

[51] Krochmann, E., Krochmann, J. 1983. On the Measurement of Photometric Characteristic of Diffusing Materials. Proceedings of the CIE Session 1983, 20th Session.

[52] Labsphere Inc. 2005. A Guide to integrating spheres Radiometry and Photometry. Technical Guide : Labsphere. Downloaded on October 2005 from www.labsphere.com.

[53] Labsphere Inc. 2007. Materials and Coatings: Comparison Chart. Typical Reflectance Data of Labsphere Reflective Coatings.

[54] Lavalle, T. personal communication, April 2007.

[55] Li, D. H. W., Lam, J. C. 2000. Solar heat gain factors and the implications to building designs in subtropical regions. Energy and Buildings. 32 (1). 47-55.

[56] Light House Sustainable Building Centre. 2007. Downloaded on December 2007 from www.sustainablebuildingcentre.com.

[57] LOT-Oriel Group. 2007. Oriel Quartz Tungsten Halogen Lamps. Downloaded on December 2007 from www.newport.com.

[58] Lovell, D. J. 1984. Theory and Applications of Integrating Sphere Technology. Laser Focus / Electro-Optics. May 1984. 86-96

[59] Maddox, J. 2007. Personal Communications. Electro-Optical Systems Inc, PA. USA. 21 September 2007

[60] Merriam-Webster Inc. 2005. Merriam-Webster Online Dictionary Retrieved February 2008 from www.Merriam-Webster.com.

[61] Milburn, D. I. 1994. Measurement of Solar Transmittance of Advanced Glazing Materials. Phd Dissertation, University of Waterloo, Waterloo, Canada.

[62] Milburn, D. I., Hollands, K. G. T. 1994. Solar Transmittance Measurements using an Integrating Sphere with Broad Area Irradiation. Solar Energy. 52(6), 497-507.

[63] Milburn, D. I., Hollands, K. G. T. 1995. An analysis of thick-sample effects in the measurement of directional-hemispherical transmittance. Optics Communications. 118, 1-8.

[64] Milburn, D. I., Hollands, K. G. T. 1995. The Directional Response Error in Integrating Sphere Transmittance Measurements at Solar Wavelengths. Solar Energy. 55 (2), 85-91.

[65] Milburn, D. I., Hollands, K. G. T. 1995. The Directional Response of an Integrating Sphere Detector System. Optics Communications. 115, 158-169.

[66] Milburn, D. I., Hollands, K. G. T. 1996. An Experimental Investigation of Thick-Sample Effects in The Measurement of Directional-Hemispherical Transmittance of Advanced Glazing Materials. Solar Energy. 57 (4), 261-275.

[67] Moffat, R. J. 1982. Contributions to the Theory of Single-Sample Uncertainty Analysis. Transactions of the ASME. 104 (6)

[68] Moffat, R. J. 1985. Using Uncertainty Analysis in the Planning of an Experiment. Journal of Fluids Engineering. 1985 (6) (173-178

[69] Moffat, R. J. 1988. Describing the Uncertainties in Experimental Results. Experimental Thermal and Fluid Science. 1 (3-17)

[70] Moffat, R. J. 1997. Uncertainty Analysis. Chapter 2. Thermal Measurements in Electronics Cooling. Edited by Azar, K. CRC Press LLC.

[71] NFRC 300 standard. 2001. Standard Test Method for Determining the Solar Optical Properties of Glazing Materials and Systems.

[72] NZEH Coalition. 2005. Net Zero Energy Home: Powering Canadian Homes Through Conservation, Supply and Innovation. Retrieved December 2007 from www.netzeroenergyhome.ca.

[73] Papamichael, K. M., Selkowitz, S. E. 1987. Simulating the luminous and thermal performance of fenestration systems. Applied Science Division. Lawrence Berkeley Laboratory, University of California. LBL-24243 (DA-244).

[74] Parmelee, G. V., Aubele, W. W. 1952. The Shading of Sunlit Glass - an Analysis of The Effect of Uniformly Spaced Flat Opaque Slats. ASHVE Transactions. 58, 377-398.

[75] Parmelee, G. V., Aubele, W. W., Vild, D. J. 1953. The Shading of Sunlit Glass - an Experimental Study of Slat-Type Sun Shades. ASHVE Transactions. 59, 221-240.

[76] Pettit, R. B. 1979. Hemispherical Transmittance Properties of Solar Glazing as a function of Averaging Procedure and Incident Angle. Solar Energy Materials. 1, 125-140.

[77] Pfrommer, P., Lomas, K.J., Kupke, C. 1996. Solar radiation transport through slat-type blinds: A new model and its application for thermal simulation of buildings. Solar Energy. 57 (2), 77-9.

[78] Platzer, W. J. 1992. Directional-Hemispherical Solar Transmittance data for Plastic Honeycomb- Type Structures. Solar Energy. 49 (5), 359-369.

[79] Pini, R. 2003. Resolving Resolution: Achieving accurate results for your spectroscopy application requires a clear understanding of instrument resolution. SPIE Optical Engineering Magazine. July 2003.

[80] Reilly, S., Hawthorne, W. 1998. The Impact of Windows on Residential Energy Use. ASHRAE Transactions. 104 (2). 1998 Winter Meeting, San Francisco, CA.

[81] Rosa, E. B., Taylor, A. H. 1922. Theory, Construction and use of the Photometric Integrating Sphere. Scientific Papers of the Bureau of Standards. No. 447. Part of Volume 18. Department of Commerce. USA.

[82] Roos, A., Ribbing, C. G., Bergkvist, M. 1988. Anomalies in Integrating Sphere Measurements on Structured Samples. Applied Optics. 27 (18). 3828-3832.

[83] Rosenfeld, J. L. J., Platzer, W. J., Dijk, H., Maccari, A. 2000. Modelling The Optical And Thermal Properties of Complex Glazing: Overview of Recent Developments. Solar Energy. 69 Supplement. 1-13.

[84] William E. Schneider, W. E., Young, R. 1998. Spectroradiometry Methods: A Guide to Photometry and Visible Spectroradiometry. Application Note (A14). Optronic Laboratories Inc. Orlando, FL, USA.

[85] Shurcliff, W. A. 1980. Thermal Shutters and Shades. Brick House Publishing Co., Inc.MA, USA.

[86] Smith, J.W. 2005. 410 Lock-in Amplifier Health Check Issue 1.0. Scitec Instruments Limited, UK.

[87] Sphere Optics. 2005. Integrating Sphere Design and Application: Technical information. Retrieved September 2005 from www.spheroptics.com.

[88] Sumpner, W.E. 1892. Proceedings of the Physical Society of London. 12.

[89] Symons, J. G. 1982. The Solar Transmittance of some Convection Suppression Devices for Solar Energy Applications: An Experimental Study. Journal of Solar Energy Engineering. 104. 251-256.

[90] Symons, J. G., Christie, E. A., Peck, M. K. 1982. Integrating Sphere for Solar Transmittance Measurement of Planar and Nonplanar Samples. Applied Optics. 21 (15), 2827-2832.

[91] Tardy, H. L. 1991. Matrix method for integrating-sphere calculations. Journal of the Optical Society of America. 8 (9). 1411-1418.

[92] U.S Green Building Council. 2007. Green Homes. Retrieved December 2007 from www.usgbc.org.

[93] U.S Green Building Council. 2008. Leed Rating Systems. Retrieved February 2008 from www.usgbc.org.

[94] Van Dijk, D., Goulding, J. 1996. Advanced Windows Information System: WIS Reference Manual. TNO Building and Construction Research. University College Dublin.

[95] Varian Inc. 2002. Internal Diffuse Reflectance Accessory. Cary 5000: Operation Manual. Varian Inc., USA.

[96] Varian Inc. 2004. UV-Vis-NIR brochures. Cary 4000, 5000 and 6000i Spectrophotometers. Retrieved on February 2008 from www.varianinc.com.

[97] Varian Inc. 2005. Cary 5000 UV-Vis-NIR spectrophotometer. Downloaded on December 2007 from www.varianinc.com.

[98] Wright, J. L. 1998. Calculating Center-Glass Performance Indices of Windows. ASHRAE Transactions. 104 (1) 1230-1241.

[99] Wight, J. L., Kotey, N. A. 2006. Solar Absorption by Each Element in a Glazing/shading Layer Array. ASHRAE Transactions. 112(2).

[100] Your Blinds Inc. 2005. Sheer Horizontal Shades. Downloaded on October 2005 from www.yourblinds.com.

[101] Yahoda, D. S. 202. Calculating Effective Longwave and Solar Optical Properties of a Venetian Blind. MASc Thesis. University of Waterloo. Waterloo. Ontario.

[102] Yahoda, D. S., Wright, J. L. 2005. Methods for Calculating the Effective Solar Optical Properties of a Venetian Blind Layer. ASHRAE Transactions. 111 (1). 572-586

[103] Youngberg, J. E. 2000. Solar Transmittance and Heat Transfer Through Polypropylene Honeycombs in a Greenhouse. MASc Thesis. University of Waterloo. Waterloo. Ontario.

[104] Zerlaut, G. A., Anderson, T.E. 1981. Multiple-Integrating Sphere Spectrophotometer for Measuring Absolute Spectral Reflectance and Transmittance. Applied Optics. 20 (21), 3797-3804.

[105] Zerlaut, G. A., Anderson, T. E. 1984. A Large, Multipurpose, Solar-Illuminated 8-ft Integrating Sphere. Proceedings of SPIE. 502. Optical Materials Technology for Energy Efficiency and Solar Energy Conversion III.